Engineering Journal

Smarter.
Stronger.
Steel.

Engineering Journal

American Institute of Steel Construction

Dedicated to the development and improvement of steel construction, through the interchange of ideas, experiences, and data.

Torsional Design of Round HSS Members—
A Critical Review

BO DOWSWELL

ABSTRACT

Shear yielding is the controlling limit state for most round HSS members subjected to torsion; however, buckling is a limit state that can reduce the torsional strength of members with high diameter-to-wall thickness (D/t) ratios. The purposes of this paper are to summarize the available research on the torsional performance of round HSS members and evaluate the applicable provisions in the AISC *Specification*. A historical review of the available research revealed 125 experimental tests from seven projects, leading to evolving design methods over the last century. An evaluation of the AISC *Specification* provisions indicated an appropriate reliability level for the yielding limit state; however, the target reliability for buckling is met only for long specimens. A new equation is proposed to predict the buckling strength of intermediate-length members.

Keywords: round HSS, torsion, D/t ratio, shear yielding, buckling.

INTRODUCTION

For most round HSS members subjected to torsion, shear yielding is the controlling limit state; however, buckling is a limit state that can reduce the torsional strength of members with high diameter-to-wall thickness, D/t, ratios. Many of the available design equations for the buckling strength of round hollow structural members are based on research related to thin-walled cylindrical shells such as tanks, silos and airplane components. The geometries, fabrication methods, and imperfections for these structures can be dramatically different from those of round HSS members. Also, much of the experimental research used materials such as aluminum, brass, and rubber, which have different material behaviors compared to steel. The purposes of this paper are to summarize the research on the torsional performance of round HSS members and compare the available experimental results to the applicable provisions in the AISC *Specification for Structural Steel Buildings* (2022), hereafter referred to as the AISC *Specification*.

AISC *SPECIFICATION* SECTION H3

The nominal torsional strength of an HSS member is calculated using Equation H3-1 from AISC *Specification* Section H3.1.

$$T_n = F_{cr}C \tag{H3-1}$$

Bo Dowswell, PhD, PE, Principal, ARC International, LLC, Birmingham, Ala. Email: bo@arcstructural.com

The available torsional strength is $\phi_T T_n$ (LRFD) or T_n/Ω_T (ASD), as applicable. For round HSS members, the critical shear stress is the largest value from Equations H3-2a and H3-2b but not exceeding the shear yield stress, $0.6F_y$.

$$F_{cr} = \frac{1.23E}{\sqrt{\frac{L}{D}}\left(\frac{D}{t}\right)^{5/4}} \tag{H3-2a}$$

$$F_{cr} = \frac{0.60E}{\left(\frac{D}{t}\right)^{3/2}} \tag{H3-2b}$$

where

C = torsional constant, in.^{3}
D = outside diameter, in.
L = member length, in.
t = design wall thickness, in.
ϕ_T = 0.90 (LRFD)
Ω_T = 1.67 (ASD)

SECTION PROPERTIES

The polar moment of inertia of a round cross section is (Holland, 1970; Seaburg and Carter, 1997)

$$J = \frac{\pi}{2}(R^4 - R_i^4) \tag{1}$$

$$= \frac{\pi}{32}(D^4 - D_i^4)$$

$$= \frac{\pi}{4}(D - t)^3 t$$

Table 1. Ovalization Tolerances and Imperfection Reduction Factors in Eurocode 3, Part 1-6 (CEN, 2007).					
			ρ_{max}		
Quality Class	Description	α_τ	$D \le 20$ in.	20 in. < D < 49 in.	$D \ge 49$ in.
Class A	Excellent	0.75	0.014	$0.007 + (49 - D)/4143$	0.007
Class B	High	0.65	0.020	$0.010 + (49 - D)/2900$	0.010
Class C	Normal	0.50	0.030	$0.015 + (49 - D)/1933$	0.015

As discussed in AISC *Specification* Section H3.1 Commentary, the torsional constant can be defined as the polar moment of inertia divided by the radius at the mid-thickness.

$$C = \frac{2J}{D - t} \tag{2}$$

$$= \frac{\pi}{2}(D - t)^2 t$$

$$= \frac{\pi}{2} D_m^2 t$$

where
D_i = inside diameter, in.
D_m = mean diameter, in.
R = outside radius, in.
R_i = inside radius, in.

EUROCODE 3, PART 1-6

The design equations in Eurocode 3, Part 1-6 (CEN, 2007), are applicable to both clamped and pinned end conditions. The effects of both inelastic buckling in the transition zone and geometric imperfections are considered explicitly. The nominal stress is:

$$\tau_n = \chi \tau_y \tag{3}$$

When $\lambda \le \lambda_p$

$$\chi = 1.0 \tag{4}$$

When $\lambda_p < \lambda \le \lambda_r$

$$\chi = 1.0 - 0.6 \frac{\lambda - \lambda_p}{\lambda_r - \lambda_p} \tag{5}$$

When $\lambda > \lambda_r$

$$\chi = \frac{\alpha_\tau}{\lambda^2} \tag{6}$$

Where the shear yield stress is:

$$\tau_y = \frac{F_y}{\sqrt{3}} \tag{7}$$

the nondimensional slenderness is:

$$\lambda = \sqrt{\frac{\tau_y}{\tau_{cr}}} \tag{8}$$

The limiting slenderness parameter for compact elements is:

$$\lambda_p = 0.4 \tag{9}$$

and the limiting slenderness parameter for noncompact elements is:

$$\lambda_r = \sqrt{2.5\alpha_\tau} \tag{10}$$

where the imperfection reduction factor, α_τ, is selected from Table 1 based on the fabrication quality class.

The critical buckling stress is:

$$\tau_{cr} = 0.75 E C_\tau \frac{t}{R\sqrt{\omega}} \tag{11}$$

The dimensionless length parameter is:

$$\omega = \frac{L}{\sqrt{Rt}} \tag{12}$$

For medium-length cylinders, which are defined by $10 \le \omega \le 8.7R/t$,

$$C_\tau = 1.0 \tag{13}$$

For long cylinders, which are defined by $\omega > 8.7R/t$,

$$C_\tau = \frac{1}{3}\sqrt{\omega \frac{t}{R}} \tag{14}$$

HISTORICAL REVIEW

The *Specification* requirements are based on the theoretical equations that were derived for the elastic critical buckling stresses by various researchers. The equations were derived for tubular sections with length-to-diameter ratios that are categorized as short, moderate-length, and long cylinders.

Schwerin (1924)

Schwerin (1924) developed Equation 15 to predict the critical stress of round HSS members in torsion.

$$\tau_{cr} = 0.248E\left(\frac{t}{R}\right)^{3/2}\left(1+0.45\frac{t}{R}\right) \qquad (15)$$

Donnell (1935) showed that Equation 15 is accurate only for longer members and noted that the value in the second parenthesis is approximately unity, resulting in Equation 16.

$$\tau_{cr} = 0.248E\left(\frac{t}{R}\right)^{3/2} \qquad (16)$$
$$= \frac{0.701E}{\left(\frac{D}{t}\right)^{3/2}}$$

Sezawa and Kubo (1931)

Sezawa and Kubo (1931) believed that the equations developed by Schwerin (1924) were incorrect due to "certain misconceptions." Sezawa and Kubo derived theoretical equations for long cylinders, which showed that the end conditions have a negligible influence on the critical buckling stress. The buckled shapes were characterized by two waves that formed a helical curve with a 27.5° angle from the longitudinal axis of the cylinder as shown in Figure 1. With $n = 2$ (two circumferential buckling waves), the load was minimized to determine the critical stress according to Equation 17, which is applicable only when $L/D \geq 2$. For steel, Poisson's ratio, ν, is 0.3.

$$\tau_{cr} = \frac{0.563E}{1-\nu^2}\left(\frac{t}{R}\right)^2 \qquad (17)$$
$$= \frac{2.47E}{\left(\frac{D}{t}\right)^2}$$

Lunquist (1932)

Based on experimental tests on duralumin cylinders, Lunquist (1932) proposed a critical buckling stress of

$$\tau_{cr} = \frac{k_s E}{\left(\frac{R}{t}\right)^c} \qquad (18)$$

where
c = constant that was determined empirically to be 1.35
k_s = coefficient that varies with the L/R ratio

The research showed that the number of buckling waves increases with an increase in the R/t ratio and decreases with increase in the L/R ratio. The specimens in Figure 2 show the effect of the L/R ratio. Small geometric imperfections caused minor buckling distortions below the buckling failure load without significantly affecting the strength. Although the short cylinders had a significant post-buckling strength increase, long cylinders had negative post-buckling strength.

Donnell (1935)

Donnell (1935) derived the differential equations of equilibrium in a simpler form than previous researchers by neglecting several items that would be included in an exact analysis. Many terms in the equilibrium conditions and the term relating the change in curvature to the change in the radius of the buckled shape were neglected. Additionally, the variation in length of the circumferential fibers along the thickness was neglected. For long cylinders where $n = 2$, many studies have shown that Donnell's approximate solution is about 10% higher than that of an exact analysis (Chen, 2016) and the experimental buckling stresses averaged about 75% of those calculated with the proposed

Fig. 1. Buckled shape for n = 2.

design equation. For short and moderately long cylinders with simply supported edges Donnell's theoretical approximation of the critical buckling stress is 7:

$$\tau_{cr} = \frac{E}{1-v^2}\left(\frac{t}{L}\right)^2\left[2.8 + \sqrt{2.6 + 1.40\frac{L^3}{(tD)^{3/2}}(1-v^2)^{3/4}}\right]$$

(19)

Substituting $v = 0.3$ into Equation 20 and multiplying by 0.6 to get a lower-bound curve results in Donnell's proposed design equation:

$$\tau_{cr} = E\left(\frac{t}{L}\right)^2\left[1.8 + \sqrt{1.2 + 0.57\frac{L^3}{(tD)^{3/2}}}\right] \qquad (20)$$

L/R = 0.87
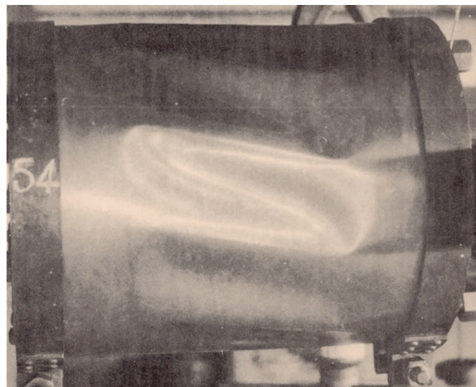
L/R = 2.0

L/R = 3.0

Fig. 2. Buckled specimens from Lundquist (1932).

Batdorf, Schildcrout, and Stein (1947)

According to the theoretical derivation by Batdorf et al. (1947), the elastic critical stress of a thin-walled cylinder loaded in torsion is:

$$\tau_c = k_s \frac{\pi^2 E}{12(1-\nu^2)\left(\dfrac{L}{t}\right)^2} \tag{21}$$

The value for k_s was determined by successive calculations to minimize the critical stress. For simply supported intermediate-length cylinders, k_s is calculated with Equation 22.

$$k_s = 0.85 Z^{3/4} \tag{22}$$

The length ratio, now known as Batdorf's parameter, is:

$$Z = \frac{L^2}{Rt}\sqrt{1-\nu^2} \tag{23}$$

$$= 2\left(\frac{L}{D}\right)^2\left(\frac{D}{t}\right)\sqrt{1-\nu^2}$$

When $\nu = 0.3$, Equation 23 simplifies to:

$$Z = 1.91\left(\frac{L}{D}\right)^2\left(\frac{D}{t}\right) \tag{24}$$

Substituting Equations 22 and 23 into Equation 21 results in Equation 25.

$$\tau_c = \frac{0.85\pi^2 E}{12(1-\nu^2)^{5/8}}\left(\frac{t}{R}\right)^{5/4}\sqrt{\frac{R}{L}} \tag{25}$$

$$= \frac{1.43\pi^2 E}{12(1-\nu^2)^{5/8}}\left(\frac{t}{D}\right)^{5/4}\sqrt{\frac{D}{L}}$$

When $\nu = 0.3$, Equation 25 simplifies to:

$$F_{cr} = \frac{1.25E}{\sqrt{\dfrac{L}{D}}\left(\dfrac{D}{t}\right)^{5/4}} \tag{26}$$

For long cylinders, the buckled configuration was the same as that described by Sezawa and Kubo (1931), where two circumferential waves formed a helical curve along the cylinder. The critical stress of long cylinders, which was found to be dependent on the R/t ratio, deviated from that of short cylinders at approximately $Z = 10(R/t)^2$. Due to simplifications in the derivation based on the assumption that n^2 is much greater than 1, Batdorf et al. (1947) noted that Equation 26 may be accurate only in the approximate range, $100 \leq Z \leq 10(R/t)^2$.

Sturm (1948)

Sturm (1948) simplified a theoretical solution for graphical representation according to Equation 27. Coefficient K_D is plotted against the L/D ratio in Figure 3. The family of curves, which are based on the D/t ratio, show that the number of buckling waves (labeled N in Figure 3) is dependent on both the L/D and D/t ratio. However, for practical geometries of HSS members used in steel structures, the buckled shape is characterized by only two waves.

$$\tau_{cr} = \frac{K_D E}{\left(\dfrac{D}{t}\right)^2} \tag{27}$$

where
K_D = coefficient that varies with the L/D and D/t ratios

Sturm (1948) also derived a theoretical solution for the circumferential stress caused by initial geometric imperfections, which were assumed to be identical to the buckled shape. For typical round HSS member geometries, the geometric imperfections caused only a 6% stress increase compared to a perfectly round section.

Timoshenko and Gere (1961) and Flugge (1973)

Timoshenko and Gere (1961) and Flugge (1973) developed Equation 28 for the elastic shear buckling stress of infinitely long cylinders by solving the differential equations of equilibrium of the buckled shape.

$$\tau_{cr} = \frac{E}{3\sqrt{2}\,(1-\nu^2)^{3/4}}\left(\frac{t}{R}\right)^{3/2} \tag{28}$$

When $\nu = 0.3$, Equation 28 simplifies to:

$$\tau_{cr} = \frac{0.716E}{\left(\dfrac{D}{t}\right)^{3/2}} \tag{29}$$

Gerard (1962) and Schilling (1965)

Based on the experimental results summarized by Batdorf et al. (1947), Gerard (1962) recommended a reduction factor of 0.85 to account for the lower strength caused by imperfections in intermediate-length shells. Schilling (1965) applied this reduction to Equation 26, resulting in Equation 30.

$$\tau_c = \frac{1.06E}{\sqrt{\dfrac{L}{D}}\left(\dfrac{D}{t}\right)^{5/4}} \tag{30}$$

By setting Equation 30 equal to the shear yield stress, τ_y, Schilling (1965) determined the transition point between

buckling and yielding. He noted that the shear yielding limit state is applicable when

$$\frac{\tau_y}{E}\sqrt{\frac{L}{D}}\left(\frac{D}{t}\right)^{5/4} \leq 1.06 \qquad (31)$$

and shear buckling is applicable when

$$\frac{\tau_y}{E}\sqrt{\frac{L}{D}}\left(\frac{D}{t}\right)^{5/4} > 1.06 \qquad (32)$$

Sherman (1975)

Sherman (1975) recommended using Equations H3-2a and H3-2b for hot-formed intermediate-length and long members, respectively. Due to the rounded stress-strain curves for cold-formed members, equations defining an inelastic transition region were developed. The equations were based on recommendations by Felton and Dobbs (1967) for aluminum members. For intermediate-length members, elastic buckling is defined by the range

$$\frac{D}{t} > \frac{3.09}{\left(\frac{L}{D}\right)^{2/5}}\left(\frac{E}{F_y}\right)^{4/5} \qquad (33)$$

The elastic critical buckling stress is calculated with Equation H3-2a. The inelastic transition zone is defined by the range

$$0.530\left(\frac{E}{F_y}\right)^{2/3} < \frac{D}{t} \leq \frac{3.09}{\left(\frac{L}{D}\right)^{2/5}}\left(\frac{E}{F_y}\right)^{4/5} \qquad (34)$$
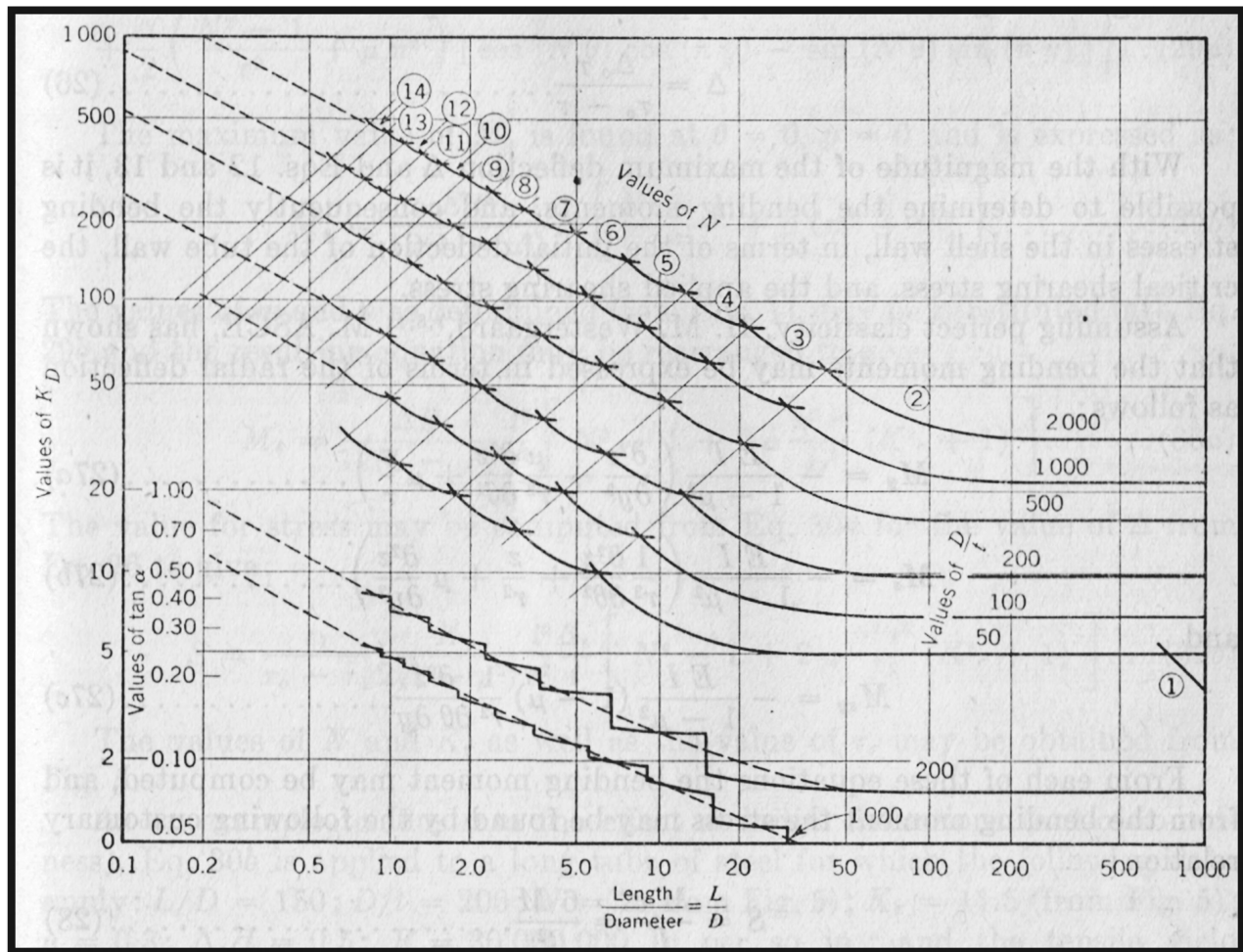

Fig. 3. K_D *versus* L/D *for various* D/t *ratios (Sturm, 1948).*

The inelastic buckling stress in the transition zone is:

$$\tau_c = \tau_y \left[\frac{1 - 0.363\left(\dfrac{L}{D}\right)^{2/5}}{1 - 0.0727\left(\dfrac{L}{D}\right)^{2/5}} \right]\left[1 + \frac{1.89}{\left(\dfrac{E}{F_y}\right)^{2/3}}\left(\dfrac{D}{t}\right) \right] \quad (35)$$

The limit state is shear yielding when

$$\frac{D}{t} \leq 0.530\left(\frac{E}{F_y}\right)^{2/3} \quad (36)$$

For long members, elastic buckling is defined by the range

$$\frac{D}{t} > 1.59\left(\frac{E}{F_y}\right)^{2/3} \quad (37)$$

The elastic critical buckling stress is calculated with Equation H3-2b. The inelastic transition zone is defined by the range

$$0.530\left(\frac{E}{F_y}\right)^{2/3} < \frac{D}{t} \leq 1.59\left(\frac{E}{F_y}\right)^{2/3} \quad (38)$$

The inelastic buckling stress in the transition zone is:

$$\tau_c = \tau_y \left[1 - \frac{0.378}{\left(\dfrac{E}{F_y}\right)^{2/3}}\left(\dfrac{D}{t}\right) \right] \quad (39)$$

The limit state is shear yielding when

$$\frac{D}{t} \leq 0.530\left(\frac{E}{F_y}\right)^{2/3} \quad (40)$$

Ellinas, Supple, and Walker (1984)

For elastic buckling, Ellinas et al. (1984) recommended Equation 30 for intermediate-length cylindrical members, which have length-to-diameter ratios in the range

$$\frac{5.12}{\sqrt{\dfrac{D}{t}}} \leq \frac{L}{D} \leq 1.09\sqrt{\frac{D}{t}} \quad (41)$$

Equation 42, which was developed by multiplying Equation 29 by a reduction factor of 0.73 to account for imperfections, was recommended for long cylinders.

$$\tau_{cr} = \frac{0.524E}{\left(\dfrac{D}{t}\right)^{3/2}} \quad (42)$$

where long cylinders are defined by the range

$$\frac{L}{D} > 1.09\sqrt{\frac{D}{t}} \quad (43)$$

To account for inelastic effects in long cylinders, a torsional parameter, α_t, was introduced.

$$\alpha_t = \frac{E}{\tau_y}\left(\frac{t}{D}\right)^{3/2} \quad (44)$$

For elastic buckling, which is defined by the range $\alpha_t \leq 1.5$, Equation 42 was rewritten as

$$\tau_{cr} = 0.524\alpha_t\tau_y \quad (45)$$

The inelastic transition zone is defined by the range $1.5 < \alpha < 9$ and the buckling stress is:

$$\tau_{cr} = \tau_y\left(0.813 + 0.068\sqrt{\alpha_t - 1.5}\right) \quad (46)$$

when $\alpha > 9$, the limit state is shear yielding.

Zhang and Han (2007)

Based on a theoretical analysis, Zhang and Han (2007) showed that the number of buckling waves and the post-buckling strength decreases with increasing values of Z (and increasing length, L). A sensitivity analysis, which used an initial imperfection shape that was identical to the buckled shape, showed that even small imperfections reduce the buckling load, and the imperfection direction (inward or outward) has no effect on the reduction. The buckling reduction factor, α, is plotted against the normalized imperfection ratio, δ_o/t, in Figure 4.

Devi and Singh (2021)

A parametric study by Devi and Singh (2021) was based on finite element models of steel HSS members with a yield stress of 56.1 ksi. For the nonslender members that failed by shear yielding, the maximum torsional moments from the finite element models were accurately predicted using AISC *Specification* Equation H3-1 with $F_{cr} = 0.6F_y$. However, the strengths were overpredicted by AISC *Specification* Equations H3-1 and H3-2 for the slender sections that failed by buckling. In this case, the mean model-to-calculated ratio was only 0.91.

DISCUSSION

General Comments

Low values of Batdorf's parameter, Z, which is defined according to Equation 23, are typical of short shell structures such as tanks and silos. Almost all HSS structural

members will be either long or intermediate length, with $Z > 2,000$.

Definition of Intermediate Length

According to Batdorf et al. (1947), Equation 22, which was developed for intermediate-length cylinders, is applicable in the approximate range, $100 \leq Z \leq 10(R/t)^2$. Gerard (1962) recommended a range of applicability of $50 \leq Z \leq 10(1 - v^2)(R/t)^2$, Schilling (1965) recommended a range of $50 \leq Z \leq 9(R/t)^2$, and Ziemian (2010) recommended $100 \leq Z \leq 19.2(1 - v^2)(D/t)^2$. The range defined by NASA (1965) was adjusted to include an imperfection factor, resulting in $50 \leq 0.59Z \leq 78(1 - v^2)(R/t)^2$. Gerard's range is equivalent to:

$$\frac{5.12}{\sqrt{\dfrac{D}{t}}} \leq \frac{L}{D} \leq 1.09\sqrt{\frac{D}{t}} \tag{47}$$

The range defined in Ziemian (2010) is equivalent to

$$\frac{7.24}{\sqrt{\dfrac{D}{t}}} \leq \frac{L}{D} \leq 3.03\sqrt{\frac{D}{t}} \tag{48}$$

The range defined by Eurocode 3, Part 1-6 (CEN, 2007), $10 \leq \omega \leq 8.7R/t$, is equivalent to

$$\frac{7.07}{\sqrt{\dfrac{D}{t}}} \leq \frac{L}{D} \leq 3.08\sqrt{\frac{D}{t}} \tag{49}$$

The range defined by NASA (1965) is equivalent to:

$$\frac{6.66}{\sqrt{\dfrac{D}{t}}} \leq \frac{L}{D} \leq 3.97\sqrt{\frac{D}{t}} \tag{50}$$

AISC *Specification*

AISC *Specification* Equation H3-2a is for intermediate-length members. Intermediate-length members are defined by

$$\frac{L}{D} \leq 4.20\sqrt{\frac{D}{t}} \tag{51}$$

AISC *Specification* Equation H3-2b was developed using Equation 28, which is for infinitely long cylinders. According to AISC *Specification* Section H3.1 Commentary, the theoretical value for the constant is 0.73; however, this is based on $v = \frac{1}{3}$. Equation 29 shows that the theoretical constant should be 0.716 for $v = 0.3$. Long members are defined by

$$\frac{L}{D} > 4.20\sqrt{\frac{D}{t}} \tag{52}$$

Because the critical shear stress is defined as the largest value from Equations H3-2a and H3-2b, with a maximum value of $0.6F_y$, the applicability range for each equation is defined by the crossover point where the two equations are equal. Therefore, Equations 51 and 52 are not required for design. In Figure 5, F_{cr} versus L/D is plotted using Equations H3-2a and H3-2b. The curves for $D/t = 50$, 75, and 100
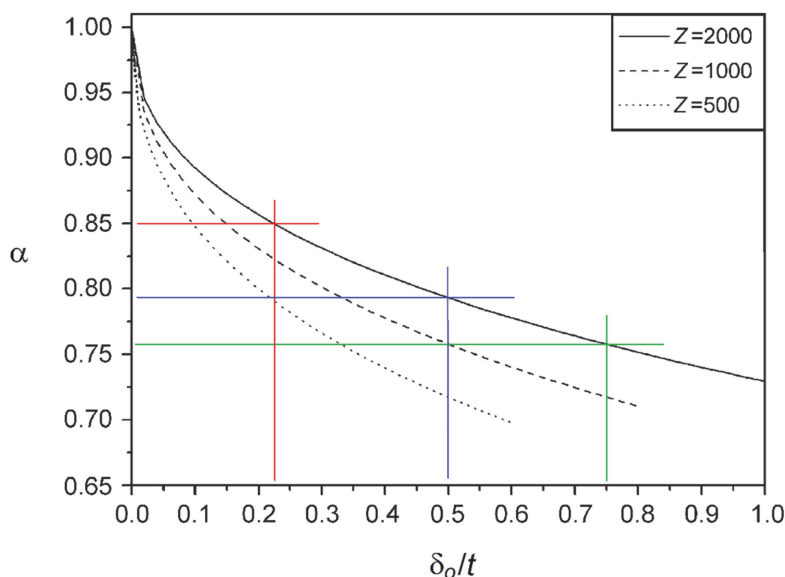
Fig. 4. Buckling reduction factor, α, versus the normalized imperfection ratio, δ_o/t (adapted from Zhang and Han, 2007).

are shown in green, blue, and red, respectively. The horizontal lines represent Equation H3-2b and the curved lines represent Equation H3-2a. The maximum of the two curves for each D/t ratio is shown with the solid lines. The graphs show that intermediate-length members can have significantly more strength than long members.

Cross-Sectional Tolerances

The initial out-of-roundness was defined by Chen and Sohal (1988) with Equation 53, which results in the ovalized shape shown in Figure 6.

$$\delta = \delta_o \cos 2\theta \qquad (53)$$

where
$\quad \theta \ $ = angle from the major axis of the ovalized shape
$\quad \delta_o$ = maximum initial radial deviation from the nominal shape

δ_o can be defined with Equation 54 using the maximum and minimum diameters of the ovalized shape.

$$\delta_o = \frac{D_{max} - D}{2} \qquad (54)$$
$$= \frac{D - D_{min}}{2}$$

where
$\quad D_{max}$ = major axis dimension of the ovalized shape
$\quad D_{min}$ = minor axis dimension of the ovalized shape

In their research, Chen and Sohal (1988) used an ovalization parameter, ρ, of 1%, where the ovalization parameter is:

$$\rho = \frac{D_{max} - D_{min}}{D} \qquad (55)$$
$$= \frac{4\delta_o}{D}$$
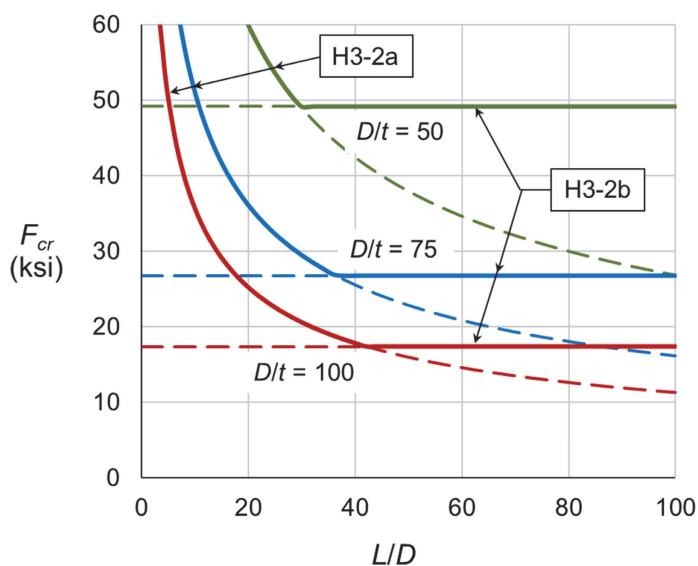
Fig. 5. Graph of AISC Specification Equations H3-2.
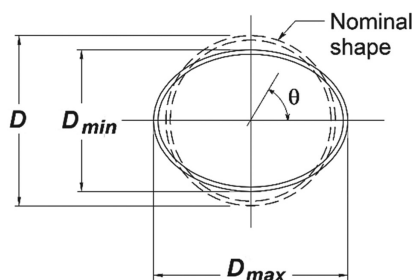
Fig. 6. Ovalization distortion.

This results in $\delta_o = D/400$. Based on the applicable ASTM tolerances, this value is significantly lower than the maximum deviations allowed for these members:

- For 2.00 in. diameter and larger ASTM A500/A500M (2021) and A1085/A1085M (2015a) HSS shapes, the outside diameter does not vary more than ±0.75%, rounded to the nearest 0.005 in., from the specified outside diameter. This results in a maximum δ_o for symmetrical ovalization of $D/267$.

- For 2.00 in. diameter and larger ASTM A53/A53M (2020), A501/A501M (2014), and A618/A618M (2015b) HSS shapes, the outside diameter does not vary more than ±1% from the specified outside diameter. This results in a maximum δ_o for symmetrical ovalization of $D/200$.

Table 1 lists the ovalization tolerances, ρ_{max}, specified in Eurocode 3, Part 1-6 (CEN, 2007), based on the fabrication quality class. Class C ovality tolerance is the most reasonable representation of the ASTM pipe and HSS diameter tolerances.

Effect of Imperfections

Nash (1957) showed that the buckling strength of intermediate-length cylinders subjected to torsion is reduced by geometric imperfections. For long cylinders, the buckling mode with $n = 2$ described by Sezawa and Kubo (1931), Batdorf et al. (1947), Sturm (1948), and Schmidt and Wintersetter (2004) is as a helical ovalization of the cross section as shown in Figure 1. For this case, the buckled cross-sectional shape is similar to the initial out-of-roundness imperfection in Figure 6. However, for the current manufacturing methods for HSS members that use linear weld seams, the initial imperfection is expected to be at a constant rotational location along the length instead of forming a helical curve. Although the use of spiral welding is increasing, it is primarily used for shapes with larger diameters.

Loo (1955) used large-deflection theory to determine the effect of initial geometric imperfections on the buckling of cylindrical shells subjected to torsion. For the condition with no geometric imperfection, the results were in close agreement with those of Donnell (1935), which were based on small-deflection theory. The pattern of the initial geometric imperfection was assumed to correspond to the buckled shape. The buckling reduction factor, α, defined by Equation 56, was developed using trial-and-error to best represent the theoretical reductions in buckling stress over a wide range of geometries. The dimensionless length parameter, ω, is defined according to Equation 12.

$$\alpha = 1 - \frac{3}{4}\left(\frac{2\delta_o/t}{\omega^{0.6}}\right)^{0.6} \tag{56}$$

Seide et al. (1960) noted that the experimental buckling loads can be as much as 40% lower than the theoretical small-deflection solutions. The average experimental-to-calculated ratio was 0.84, and the authors recommended a "design" reduction factor of 0.75 for intermediate-length cylinders.

Based on the work of Batdorf et al. (1947) and Timoshenko and Gere (1961), NASA (1965) published reduction factors "to approximate the lower limit of most data." It was determined that the appropriate reduction factors for Equations 26 and 29 are 0.67 and 0.59, respectively.

Imperfections were considered in AISC *Specification* Equation H3-2b by reducing the constant from 0.73 (or 0.716) to 0.60, resulting in a reduction factor of 0.82 (or 0.84). According to AISC *Specification* Section H3.1 Commentary, Equation H3-2a includes a 15% reduction to account for initial imperfections. However, it appears that the 0.85 constant in Equation 22 was erroneously assumed to be a reduction for imperfections. The 0.85 constant was calculated theoretically, and the resulting Equation 26 is different from Equation H3-2a only because $\nu = \frac{1}{3}$ was used in Equation H3-2a instead of $\nu = 0.30$. Batdorf et al. (1947) showed that Equations 26 and H3-2a provide a reasonable upper-bound solution compared to the experimental results that were available at the time. Accordingly, Schilling (1965) recommended that the theoretical critical stress should be reduced by 15%, resulting in a coefficient of $0.85 \times 1.25 = 1.06$, as provided in Equation 30.

For the shapes listed in the 16th Edition *Steel Construction Manual* (AISC, 2023), the highest D/t ratio is 74.5 for a pipe section with $D = 26.0$ in. and $t = 0.349$ in. For this shape the ASTM A53/A53M tolerance is $\delta_o = D/200$, resulting in a maximum permissible $\delta_o/t = 74.5/200 = 0.373$. With a reasonable lower-bound length of 97.5 in., $Z = 2,000$. From Figure 4 with $Z = 2,000$, the buckling reduction factor, $\alpha = 0.85$ at $\delta_o/t = 0.22$ and $\alpha = 0.82$ at $\delta_o/t = 0.373$. Equation 56 results in similar values, with $\alpha = 0.88$ at $\delta_o/t = 0.22$ and $\alpha = 0.84$ at $\delta_o/t = 0.373$.

Post-Buckling Strength

As noted previously by Lunquist (1932), although short cylinders had a significant post-buckling strength increase, long cylinders have negative post-buckling strength. This conclusion was verified by Budiansky (1969), Yamaki (1974), and Zhang and Han (2007).

EXPERIMENTAL COMPARISONS

A review of the available research on the torsional strength of round hollow steel cylinders revealed 125 experimental tests from seven previously published research projects. A total of 106 of the specimens had an ultimate failure mode of buckling. Many of these specimens buckled in the inelastic

range. The remaining 19 specimens failed by yielding with no post-yield buckling. Several of the researchers tested multiple materials; however, only the steel specimens were included in the database used in this paper. The details of all test specimens are listed in Table A1 of Appendix A, and the experimental results are listed in Table A2.

Popplewell and Coker (1895)

Popplewell and Coker (1895) tested five hollow mild steel shafts with a tensile yield stress of 34.8 ksi. The specimens had very large rotations at failure. Because the torsional strengths at the failure rotations were almost three times the first-yield moments, the strengths used in this paper are the first-yield values. Supplementary tension and double-shear tests were also conducted.

Seely and Putnam (1919)

Seely and Putnam (1919) tested six hollow cylinders that were machined from solid round bars to form the desired inner diameter. The bars had outer diameters of 1.88 and 3.75 in. Soft, mild, and medium steels were tested, with tensile yield points of 28.4 ksi, 33.0 ksi, and 46.8 ksi, respectively. All specimens failed by shear yielding.

Bridget, Jerome, and Vosseller (1934)

Bridget et al. (1934) tested nine round HSS specimens with diameters between 0.625 and 2.875 in. The steel specimens had tensile yield stresses between 36.0 and 57.7 ksi. All specimens failed by buckling.

Donnell (1935)

Donnell (1935) tested 30 steel round HSS members between 1.88 in. and 27.0 in. diameter that were proportioned for buckling well below the elastic shear yielding limit. The specimens were fabricated by rolling thin plates to the appropriate diameter and soldering at the longitudinal seam, which were lapped approximately 1/16 in. The research showed that small-diameter specimens can be used to accurately predict the behavior of much larger members.

Stang, Ramberg, and Back (1937)

Stang et al. (1937) tested 63 chromium-molybdenum steel round HSS members between 5/8 and 2.5 in. diameter. The tensile yield stresses varied from 67.7 to 110 ksi. The specimens failed by either elastic "two-lobe" buckling with $n = 2$ or inelastic buckling.

Schmidt and Winterstetter (2004)

Schmidt and Winterstetter (2004) tested four specimens of approximately 8 in. diameter and 24 ksi tensile yield stress. All of the specimens failed by buckling.

Wu, He, Ghafoori, and Zhao (2018)

Wu et al. (2018) tested eight round HSS sections that failed by shear yielding before buckling distortion occurred at large rotation angles. The diameters were 3.50, 4.00, and 4.50 in., and the tensile yield strengths were between 41.2 and 58.0 ksi. Additional tests were conducted on specimens that were reinforced with carbon-fiber reinforced polymer (CFRP) composites.

Discussion

For the 19 specimens that failed by yielding, the maximum experimental torsional moment, T_e, was greater than the calculated torsional yield moment, $T_y = 0.6\sigma_y C$, where σ_y is the measured uniaxial yield stress in tension. The specimens tested by Popplewell and Coker (1895) sustained moments of $2.5T_y$ at large rotations; however, experimental measurements indicated that the proportional limit averaged $0.927T_y$.

For designing according to the AISC *Specification*, the critical stress can be defined by either Equation H3-2a or H3-2b. Therefore, the experimental data is plotted in Figure 7 using the controlling slenderness parameter, λ, which corresponds to the equation resulting in the highest critical stress. For Equation H3-2a, the slenderness parameter is:

$$\lambda = \frac{0.6\sigma_y}{1.23E}\sqrt{\frac{L}{D}}\left(\frac{D}{t}\right)^{5/4} \tag{57}$$

For Equation H3-2b, the slenderness parameter is:

$$\lambda = \frac{0.6\sigma_y}{0.60E}\left(\frac{D}{t}\right)^{3/2} \tag{58}$$

Figure 7 shows the AISC *Specification* nominal strength (without ϕ) curve for T_e/T_y versus λ. The LRFD available strength (including ϕ) curve is shown with the dashed line. For the calculation of λ and T_y for the experimental data points, the measured dimensions and material properties were used in lieu of the nominal values. The AISC curve predicts the data trend accurately; however, for λ greater than about 1.5, most of the data points are below the nominal curve and several are well below the LRFD available strength curve.

RELIABILITY ANALYSIS

The resistance factor required to obtain a specific reliability level is (Galambos and Ravinda, 1978):

$$\phi = C_R \rho_R e^{-\beta \alpha_R V_R} \tag{59}$$

where
C_R = correction factor
V_R = coefficient of variation

α_R = separation factor

β = reliability index

ρ_R = bias coefficient

Galambos and Ravinda (1973) proposed a separation factor, α_R, of 0.55. For $L/D = 3.0$, Li et al. (2007) developed Equation 60 for calculating the correction factor.

$$C_R = 1.40 - 0.156\beta + 0.0078\beta^2 \qquad (60)$$

Based on AISC *Specification* Section B3.1 Commentary, the target reliability index, β_T, is 2.6, which results in $C_R = 1.05$. The coefficient of variation and bias coefficient are calculated using the statistical parameters of the specific joint. The bias coefficient is:

$$\rho_R = \rho_M \rho_G \rho_P \qquad (61)$$

where

ρ_G = bias coefficient for the geometric properties

ρ_M = bias coefficient for the material properties

ρ_P = bias coefficient for the test-to-predicted strength ratios; mean value of the professional factor calculated with the measured geometric and material properties

The coefficient of variation is:

$$V_R = \sqrt{V_M^2 + V_G^2 + V_P^2} \qquad (62)$$

where

V_G = coefficient of variation for the geometric properties

V_M = coefficient of variation for the material properties

V_P = coefficient of variation for the test-to-predicted strength ratios

The author was unable to locate statistical data regarding deviations from the nominal diameter. However, for members meeting the required ASTM tolerances, any diameter variation results in only a 1% worst-case strength reduction. Historically, the effect of initial imperfections has been addressed with a reduction factor. Therefore, the diameter is considered a deterministic quantity. Also, the effect of length variation was assumed to be negligible. For these conditions, ρ_G and V_G are dependent only on the wall thickness, t.

Osterhof and Driver (2011) used $\rho_t = 1.00$ and $V_t = 0.050$ for the wall thickness characteristics of HSS members. The slightly more conservative values from Dowswell (2021) were used for the calculations in this paper: $\rho_t = 0.994$ and $V_t = 0.050$.

The material characteristics for modulus of elasticity are $\rho_E = 1.04$ and $V_E = 0.026$ (Schmidt and Bartlett, 2002). Liu et al. (2007) determined the material characteristics for yield stress of round HSS members: for A500 Grade B, $\rho_F = 1.36$ and $V_F = 0.07$; for A53 Grade B, $\rho_M = 1.59$, $V_M = 0.11$.
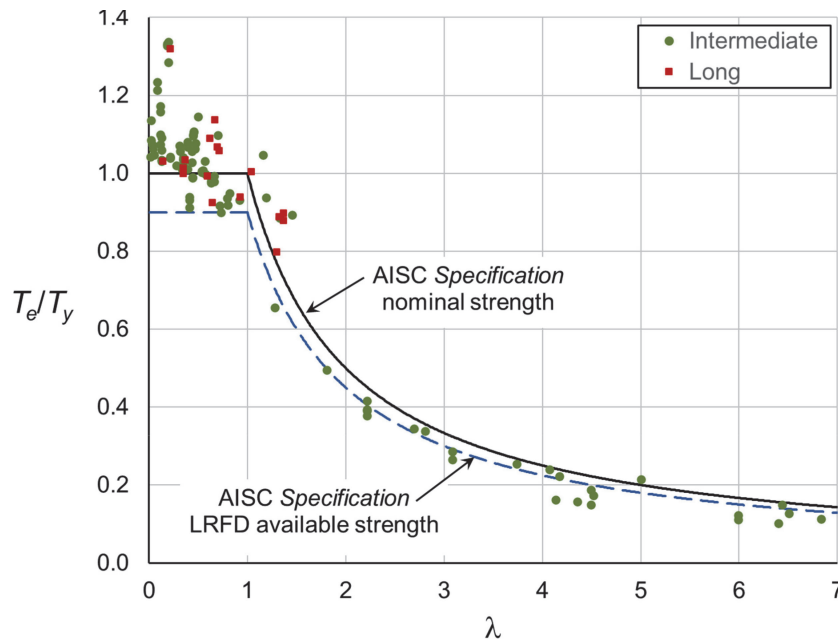

Fig. 7. Graph of AISC Specification *equations with experimental data.*

Table 2. Reliability Functions

		Yielding	Buckling	
			Intermediate	Long
Material	ρ_M	$\rho_F = 1.36$	$\rho_E = 1.04$	$\rho_E = 1.04$
	V_M	$V_F = 0.07$	$V_E = 0.026$	$V_E = 0.026$
Geometric	ρ_G	$\rho_t = 0.994$	$(\rho_t)^{9/4} = 0.987$	$(\rho_t)^{5/2} = 0.985$
	V_G	$V_t = 0.050$	$(9/4)(V_t) = 0.113$	$(5/2)(V_t) = 0.125$

For the 19 specimens with low wall slenderness parameters, where the maximum value for $(D/t)(F_y/E)$ is 0.0551, the ultimate experimental torsion resulted in large inelastic rotation angles. Therefore, for these specimens, the proportional limit on the torsion-rotation curve was used for the experimental yield torsion.

The reliability analysis must be based on the three equations for yielding, buckling of intermediate-length members, and buckling of long members. For a first-order multivariate analysis, the mean and variance of T_c can be approximated with Equations 63 and 64, respectively (Benjamin and Cornell, 1970).

$$T_{cm} \approx f\left(X_{1m}, X_{2m}, ..., X_{nm}\right) \tag{63}$$

$$\sigma_{T_c}^2 \approx \sum_{i=1}^{n}\left[\left(\frac{\partial T_c}{\partial X_i}\right)_m\right]^2 \sigma_{X_i}^2 \tag{64}$$

where

T_c = critical torsional strength

T_{cm} = mean value of the critical torsional strength

X_i = uncorrelated variables affecting T_c

Substituting Equation 2 into Equation H3-1 and setting F_{cr} equal to $0.6F_y$, the critical torsion for the limit state of yielding is:

$$T_c = 0.3\pi F_y D_m^2 t \tag{65}$$

Because Equation 65 is linear with respect to both F_y and t, the statistical parameters for the geometric and material properties are used without manipulation as listed in the third column of Table 2.

Substituting Equation H3-2a and Equation 2 into Equation H3-1, the buckling strength of intermediate-length members is:

$$T_c = \frac{0.615\pi E D_m^2 t}{\sqrt{\dfrac{L}{D}\left(\dfrac{D}{t}\right)^{5/4}}} \tag{66}$$

Equation 66 is linear with respect to E. The derivative of T_c with respect to t is:

$$\frac{\partial T_c}{\partial t} = \left(\frac{9}{4}\right)\frac{0.615\pi E D_m^2}{\sqrt{\dfrac{L}{D}\left(\dfrac{D}{t}\right)^{5/4}}} \tag{67}$$

The statistical parameters for the geometric and material properties for buckling of intermediate-length members are listed in the fourth column of Table 2. Substituting Equations H3-2b and 2 into Equation H3-1, the buckling strength of long members is:

$$T_c = \frac{0.30\pi E D_m^2 t}{\left(\dfrac{D}{t}\right)^{3/2}} \tag{68}$$

Equation 68 is linear with respect to E. The derivative of T_c with respect to t is:

$$\frac{\partial T_c}{\partial t} = \left(\frac{5}{2}\right)\frac{0.30\pi E D_m^2}{\left(\dfrac{D}{t}\right)^{3/2}} \tag{69}$$

The statistical parameters for the geometric and material properties for buckling of long members are listed in the fifth column of Table 2.

AISC *Specification* Equations

Because the reliability functions are separated into three groups (yielding, buckling of intermediate-length members, and buckling of long members), each group was analyzed separately. Statistical parameters for test-to-predicted strength ratios, ρ_P and V_P, as well as the number of specimens, N, within each group are listed in Table 3.

From Table 3, $\rho_P = 1.00$ when the AISC *Specification* equations are used with all specimens. However, an observation of the statistical parameters for buckling of intermediate-length members reveals the inaccuracy of Equation H3-2a. Using $\phi = 0.90$ resulted in $\beta = 4.06$ for the specimens with a predicted failure mode of yielding, and $\beta = 1.71$ for the intermediate-length specimens with a predicted failure mode of buckling. Because 1.71 is below the target reliability index, Equation 70 is proposed to replace Equation H3-2a.

Table 3. Statistical Parameters for Test-to-Predicted Strength Ratios						
				Buckling		
		All	Yielding	All	Intermediate	Long
AISC Specification	N	125	84	41	36	5
	ρ_P	1.00	1.02	0.967	0.944	1.14
	V_P	0.170	0.112	0.254	0.266	0.0717
Proposed equation	N	125	76	49	39	10
	ρ_P	1.12	1.02	1.27	1.28	1.23
	V_P	0.217	0.115	0.246	0.266	0.187
N = number of specimens						

$$F_{cr} = \frac{0.85E}{\sqrt{\frac{L}{D}\left(\frac{D}{t}\right)^{5/4}}} \qquad (70)$$

$$\frac{L}{D} \le 2.01\sqrt{\frac{D}{t}} \qquad (71)$$

The statistical parameters for test-to-predicted strength ratios using the proposed equation are listed in Table 3. With $\phi = 0.90$, Equation 70 results in $\beta = 2.64$ for the 39 intermediate-length specimens with a predicted failure mode of buckling. At the target reliability index ($\beta_T = 2.6$), $\phi = 0.910$. The revised range for intermediate-length members is defined by Equation 71.

For the remaining groups, β always exceeded β_T, with the 76 yielding specimens resulting in $\beta = 4.12$ and all 49 buckling specimens resulting in $\beta = 2.98$. Figure 8 shows the proposed nominal strength (without ϕ) curve for T_e/T_y versus λ. The LRFD available strength (including ϕ) curve is shown with the dashed line.
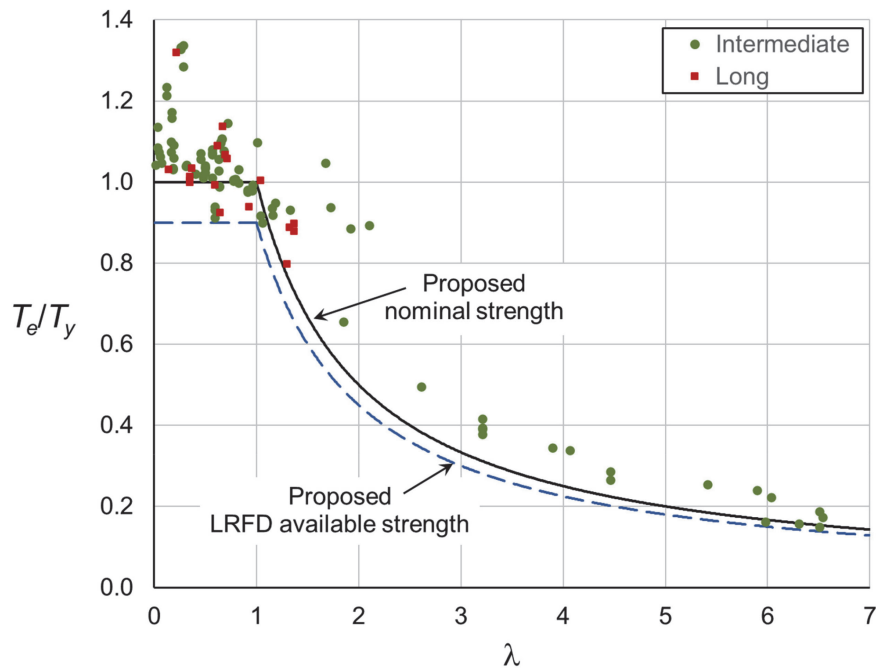

Fig. 8. Graph of proposed equations with experimental data.

CONCLUSIONS

A historical review of the available research on the torsional strength of round HSS members revealed 125 experimental tests from seven projects, leading to evolving design methods over the last century. Theoretical and experimental research indicated two failure modes—yielding and buckling. To consider the effect of length, members with a buckling failure mode were further divided into long and intermediate-length members.

The experimental research showed that members with low wall slenderness parameters, $(D/t)(F_y/E)$, have significant inelastic strength. However, the large inelastic rotation angles required to realize this additional strength make the upper limit, $F_{cr} = 0.6F_y$, for AISC *Specification* H3-1 appropriate based on typical serviceability considerations. Both the theoretical and experimental research indicated that imperfections can significantly reduce the buckling strength.

An evaluation of the AISC *Specification* provisions revealed inconsistent reliability indices that are dependent on the predicted failure mode and the member geometry. The reliability level for the yielding limit state is appropriate; however, the target reliability for buckling is met only for long specimens. For intermediate-length members, the target reliability index can be met if AISC *Specification* Equation H3-2a is replaced with Equation 70.

REFERENCES

AISC (2022), *Specification for Structural Steel Buildings*, ANSI/AISC 360-22, American Institute of Steel Construction, Chicago, Ill.

AISC (2023), *Steel Construction Manual*, 16th Ed., American Institute of Steel Construction, Chicago, Ill.

ASTM (2014), *Standard Specification for Hot-Formed Welded and Seamless Carbon Steel Structural Tubing,* ASTM 501/501M, ASTM International, West Conshohocken, Pa.

ASTM (2015a), *Standard Specification for Cold-Formed Welded Carbon Steel Hollow Structural Sections (HSS),* ASTM 1085/1085M, ASTM International, West Conshohocken, Pa.

ASTM (2015b), *Standard Specification for Hot-Formed Welded and Seamless High-Strength Low-Alloy Structural Tubing,* ASTM 618/618M, ASTM International, West Conshohocken, Pa.

ASTM (2020), *Standard Specification for Pipe, Steel, Black and Hot-Dipped, Zinc-Coated, Welded and Seamless,* ASTM 53/53M, ASTM International, West Conshohocken, Pa.

ASTM (2021), *Standard Specification for Cold-Formed Welded and Seamless Carbon Steel Structural Tubing in Rounds and Shapes,* ASTM 500/500M, ASTM International, West Conshohocken, Pa.

Batdorf, S.B., Schildcrout, M., and Stein, M. (1947), *Critical Stress of Thin-Walled Cylinders in Torsion*, NACA Technical Note No. 1344, July.

Benjamin, J.R. and Cornell, C.A. (1970), *Probability, Statistics and Decision for Civil Engineers*, McGraw-Hill.

Bridget, F.J., Jerome, C.C., and Vosseller, A.B. (1934), "Some New Experiments on Buckling of Thin-Wall Construction," *Transactions of the American Society of Mechanical Engineers*, Applied Mechanics Division, Vol. 56.

Budiansky, B. (1969), "Post-Buckling Behavior of Cylinders in Torsion," *Theory of Thin Shells*, F.I. Niordson, ed., Springer-Verlag.

CEN (2007), *Eurocode 3—Design of Steel Structures—Part 1-6: Strength and Stability of Shell Structures*, Comite Européen de Normalisation, Brussels, Belgium.

Chen, D.H. (2016), *Crush Mechanics of Thin-Walled Tubes*, CRC Press.

Chen, W.F. and Sohal, I.S. (1988), "Cylindrical Members in Offshore Structures," *Thin-Walled Structures*, Vol. 6, pp. 153–285.

Devi, S.V. and Singh, K.D. (2021), "The Continuous Strength Method for Circular Hollow Sections in Torsion," *Engineering Structures*, Vol. 242.

Donnell, L.H. (1935), "Stability of Thin-Walled Tubes under Torsion," *NACA Technical Report No. 479*, National Advisory Committee for Aeronautics.

Dowswell, B. (2021), "Analysis of the Shear Lag Factor for Slotted Rectangular HSS Members," *Engineering Journal*, AISC, Vol. 58, No. 3.

Ellinas, C.P., Supple, W.J., and Walker, A.C. (1984), *Buckling of Offshore Structures—A State-of-the-Art Review*, Gulf Publishing Company.

Felton, L.P. and Dobbs, M.W. (1967), "Optimum Design of Tubes for Bending and Torsion," *Journal of the Structural Division*, ASCE, No. ST 4, August.

Flugge, W. (1973), *Stresses in Shells*, 2nd Ed., Springer-Verlag.

Galambos, T.V. and Ravinda, M.K. (1973), *Tentative Load and Resistance Factor Design Criteria for Steel Buildings*, Research Report No. 18, September, Department of Civil and Environmental Engineering, Washington University, St. Louis, Mo.

Galambos, T.V. and Ravinda, M.K. (1978), "Properties of Steel for Use in LRFD," *Journal of the Structural Division*, ASCE, Vol. 104, No. ST9, September, pp. 1,459–1,468.

Gerard, G. (1962), *Introduction to Structural Stability Theory*, McGraw-Hill.

Holland, M. (1970), *Torsion of Prismatic Members*, Draughtsmen's & Allied Technicians' Association.

Li, C., Grondin, G.Y., and Driver, R.G. (2007), *Reliability Analysis of Concentrically Loaded Fillet Welded Joints*, Structural Engineering Report No. 271, University of Alberta, October.

Liu, J., Sabelli, R., Brockenbrough, R.L., and Fraser, T.P. (2007), "Expected Yield Stress and Tensile Strength Ratios for Determination of Expected Member Capacity in the AISC *Seismic Provisions*," *Engineering Journal*, AISC, Vol. 44, No. 1, pp. 15–25.

Loo, T.T. (1955), "Effects of Large Deflections and Imperfections on the Elastic Buckling of Cylinders under Torsion and Axial Compression," *Proceedings of the Second U.S. National Congress of Applied Mechanics*, American Society of Mechanical Engineers, pp. 345–357.

Lunquist, E.E. (1932), "Strength Tests on Thin-Walled Duralumin Cylinders in Torsion," *NACA Technical Note 427*, National Advisory Committee for Aeronautics.

NASA (1965), *Buckling of Thin-Walled Circular Cylinders*, SP-8007, September.

Nash, W.A. (1957), "Buckling of Initially Imperfect Shells Subject to Torsion," *Journal of Applied Mechanics*, Vol. 24, No. 1.

Osterhof, S.A. and Driver, R.G. (2011), "Performance of the Unified Block Shear Equation for Common Types of Welded Steel Connections," *Engineering Journal*, AISC, Vol. 48, No. 2, pp. 77–92.

Popplewell, W.C. and Coker, E.G. (1895), "Experiments on the Torsional Strength of Solid and Hollow Shafts," *Proceedings of the Institution of Civil Engineers*, Paper No. 2853, pp. 291–298.

Schilling, C.G. (1965), "Buckling Strength of Circular Tubes," *Journal of the Structural Division*, ASCE, Vol. 91, No. ST5.

Schmidt, B.J. and Bartlett, F.M. (2002), "Review of Resistance Factor for Steel: Data Collection," *Canadian Journal of Civil Engineering*, Vol. 29, pp. 98–108.

Schmidt, H. and Wintersetter, T.A. (2004), "Cylindrical Shells under Torsional and Transverse Shear," Chapter 8, *Buckling of Thin Metal Shells*, J.G. Teng and J.M. Rotters, eds., Spon Press.

Schwerin, E. (1924), "Torsional Stability of Thin-Walled Tubes," *Proceedings of the First International Congress for Applied Mechanics*.

Seaburg, P.A. and Carter, C.J. (1997), *Torsional Analysis of Structural Steel Members*, Design Guide 9, AISC, Chicago, Ill.

Seely, F.B. and Putnam, W.J. (1919), "The Relation between the Elastic Strengths of Steel in Tension, Compression and Shear," *Bulletin No. 115*, Engineering Experiment Station, University of Illinois, Urbana-Champaign, Ill.

Seide, P., Weingarten, V.I., and Morgan, E.J. (1960), *The Development of Design Criteria for Elastic Stability of Thin Shell Structures*, Space Technology Laboratories, Inc., December 31.

Sezawa, K. and Kubo, K. (1931), *The Buckling of a Cylindrical Shell under Torsion*, Report No. 76, Vol. VI, No. 10, Aeronautical Research Institute, Tokyo Imperial University, December.

Sherman, D.R. (1975), "Structural Behavior of Tubular Sections," *Proceedings of the International Specialty Conference on Cold-Formed Steel Structures*.

Stang, A.H., Ramberg, W., and Back, G. (1937), "Torsion Tests of Tubes," NACA Technical Report No. 601, National Advisory Committee for Aeronautics.

Sturm, R.G. (1948), "Stability of Thin Cylindrical Shells in Torsion," *Transactions of the American Society of Civil Engineers*, Vol. 113, Paper No. 2345, pp. 681–717.

Timoshenko, S.P. and Gere, J.M. (1961), *Theory of Elastic Stability*, McGraw-Hill.

Wu, C., He, L., Ghafoori, E., and Zhao, X.L. (2018), "Torsional Strengthening of Steel Circular Hollow Sections (CHS) Using CFRP Composites," *Engineering Structures*, Vol. 171.

Yamaki, N. (1974), "Experiments on the Postbuckling Behavior of Circular Cylindrical Shells under Torsion," *Buckling of Structures, Symposium Proceedings*, June 17–21, Springer-Verlag.

Zhang, X. and Han, Q. (2007), "Buckling and Postbuckling Behaviors of Imperfect Cylindrical Shells Subjected to Torsion," *Thin-Walled Structures*, Vol. 45, pp. 1,035–1,043.

Ziemian, R.D. (2010), *Guide to Stability Design Criteria for Metal Structures*, 6th Ed., John Wiley & Sons.

Table A-1. Specimen Details										
Specimen	D in.	L in.	t in.	E ksi	σ$_y$ ksi	Specimen	D in.	L in.	t in.	E ksi	σ$_y$ ksi
Popplewell and Coker (1895)						**Donnell (1935) continued**					
36	0.500	5.00	0.0935	27,744	34.8	18	5.67	12.0	0.00205	31,300	—[b]
37	0.500	5.00	0.0935	27,744	34.8	19	3.75	12.0	0.00201	31,300	—[b]
38	0.500	5.00	0.0935	27,744	34.8	20	1.88	12.0	0.00201	31,300	—[b]
39	0.501	5.00	0.0920	27,744	34.8	21	1.88	24.0	0.00284	31,300	—[b]
40	0.501	5.00	0.0925	27,744	34.8	22	1.88	30.0	0.00201	31,300	—[b]
Seely and Putnam (1919)						23	0.319	4.53	.00192	31,300	—[b]
L1	2.88	8.25	0.125	29,000[a]	28.4	24	0.319	7.81	.00192	31,300	—[b]
L2	2.63	8.25	0.188	29,000[a]	28.4	25	0.319	12.4	.00192	31,300	—[b]
M1	0.750	3.25	0.125	29,000[a]	33.6	26	0.319	13.1	.00192	31,300	—[b]
M2	0.625	3.25	0.0625	29,000[a]	33.6	27	0.319	15.8	.00190	31,300	—[b]
M3	0.563	3.25	0.0313	29,000[a]	33.6	28	0.319	21.4	.00199	31,300	—[b]
H1	0.625	3.25	0.0625	29,000[a]	45.8	29	0.319	29.5	.00192	31,300	—[b]
Bridget et al. (1934)						30	0.319	53.5	.00192	31,300	—[b]
A	1.88	5.32	.00204	31,400	37.7	**Stang et al. (1937)**					
C	3.75	5.32	0.00295	30,600	48.6	A1	0.750	19.0	0.0304	29900	84.0
D	1.88	11.32	0.00204	27,060	53.3	A2	0.750	19.0	0.0303	29900	84.0
E	1.88	5.32	0.00295	30,600	48.6	A3	0.751	60.0	0.0302	29900	84.0
F	3.75	1.32	0.00204	31,400	57.7	B1	1.001	19.0	0.0381	28800	89.0
G1	1.88	5.32	0.00395	29,600	36.0	B2	1.001	19.0	0.0380	28800	89.0
G2	1.88	5.32	0.00395	29,600	36.0	B3	1.001	19.0	0.0380	28800	89.0
G3	1.88	5.32	0.00395	29,600	36.0	C1	1.128	19.0	0.0479	29000	93.0
G4	1.88	5.32	0.00395	29,600	36.0	C2	1.127	19.0	0.0480	29000	93.0
Donnell (1935)						C3	1.127	60.0	0.0480	29000	93.0
1	27.0	85.8	0.0115	31,300	—[b]	D1	1.503	19.0	0.0580	29100	99.0
2	5.88	.469	.00193	31,300	—[b]	D2	1.503	19.0	0.0580	29100	99.0
3	5.88	.375	.00193	31,300	—[b]	D3	1.503	19.0	0.0581	29100	99.0
4	5.88	.290	.00193	31,300	—[b]	D4	1.503	19.0	0.0581	29100	99.0
5	5.67	6.00	0.00292	31,300	—[b]	D5	1.503	48.0	0.0581	29100	99.0
6	5.67	6.00	0.00280	31,300	—[b]	E1	2.004	19.0	0.0652	28700	108
7	3.75	6.00	0.00288	31,300	—[b]	E2	2.004	19.0	0.0652	28700	108
8	3.75	6.00	0.00288	31,300	—[b]	E3	2.004	19.0	0.0653	28700	108
9	1.88	6.00	0.00292	31,300	—[b]	E4	2.005	48.0	0.0652	28700	108
10	5.67	6.00	0.00217	31,300	—[b]	F1	1.377	19.0	0.0382	28800	81.0
11	5.67	6.00	0.00217	31,300	—[b]	F2	1.377	19.0	0.0382	28800	81.0
12	3.75	6.00	0.00213	31,300	—[b]	F3	1.385	45.0	0.0381	28800	81.0
13	3.75	6.00	0.00213	31,300	—[b]	G1	1.498	19.0	0.0349	29000	69.2
14	1.88	6.00	0.00205	31,300	—[b]	G2	1.499	19.0	0.0349	29000	69.2
15	5.67	12.0	0.00268	31,300	—[b]	G3	1.498	45.0	0.0349	29000	69.2
16	3.75	12.0	0.00280	31,300	—[b]	H1	1.510	19.0	0.0528	28800	78.6
17	1.88	12.0	0.00280	31,300	—[b]	(Table A-1 continues on the next page)					

	D	**L**	**t**	**E**	**σ_y**	**Specimen**	**D**	**L**	**t**	**E**	**σ_y**
Specimen	**in.**	**in.**	**in.**	**ksi**	**ksi**		**in.**	**in.**	**in.**	**ksi**	**ksi**
Stang et al. (1937) continued						**Stang et al. (1937) continued**					
I1	1.510	19.0	0.0685	28600	67.7	H2	1.511	19.0	0.0527	28800	78.6
I2	1.510	19.0	0.0687	28600	67.7	S1	1.250	19.0	0.0338	28400	87.8
J1	1.503	19.0	0.0845	28800	82.2	S2	1.251	19.0	0.0338	28400	87.8
J2	1.503	19.0	0.0845	28800	82.2	T1	1.503	19.0	0.0352	28200	93.8
J3	1.503	47.0	0.0845	28800	82.2	T2	1.503	19.0	0.0352	28200	93.8
K1	1.502	19.0	0.0928	28800	110	T3	1.503	60.0	0.0352	28200	93.8
K2	1.503	19.0	0.0925	28800	110	U1	1.505	19.0	0.0501	28800	103.8
L1	1.500	19.0	0.1259	28500	96.0	U2	1.506	19.0	0.0501	28800	103.8
L2	1.499	19.0	0.1258	28500	96.0	U3	1.508	60.0	0.0501	28800	103.8
L3	1.500	45.0	0.1258	28500	96.0	V1	2.500	19.0	0.0341	30200	75.0
M1	1.630	19.0	0.0495	27300	90.5	V2	2.506	19.0	0.0336	30200	75.0
M2	1.631	19.0	0.0495	27300	90.5	V3	2.501	60.0	0.0340	30200	75.0
N1	1.753	19.0	0.0509	27600	96.8	**Schmidt and Winterstetter (2004)**					
N2	1.752	19.0	0.0509	27600	96.8	1	7.87	7.86	0.0418	29,153	23.9
N3	1.752	45.0	0.0507	27600	96.8	2	7.89	7.85	0.0266	29,443	24.4
O1	1.626	19.0	0.0359	27500	93.0	3	7.89	15.7	0.0420	29,153	23.9
O2	1.625	19.0	0.0358	27500	93.0	4	7.87	15.7	0.0267	29,443	24.4
O3	1.628	60.0	0.0357	27500	93.0	**Wu et al. (2018)**					
P1	1.751	19.0	0.0356	27600	105	1-1	3.50	14.2	0.120	30,755	58.0
P2	1.752	19.0	0.0354	27600	105	1-2	3.50	14.2	0.120	30,755	58.0
P3	1.751	60.0	0.0354	27600	105	2-1	4.00	16.1	0.119	30,143	44.4
Q1	2.005	19.0	0.0361	27600	99.1	2-2	4.00	16.1	0.119	30,143	44.4
Q2	1.998	60.0	0.0360	27600	99.1	3-1	4.50	18.1	0.143	29,566	45.9
R1	1.124	19.0	0.0316	29000	95.2	3-2	4.50	18.1	0.143	29,566	45.9
R2	1.124	19.0	0.0317	29000	95.2	4-1	4.50	18.1	0.166	29,853	41.2
R3	1.124	60.0	0.0317	29000	95.2	5-1	4.50	18.1	0.201	30,266	53.9

Table A-1. Specimen Details (continued)

[a] The modulus of elasticity was not measured for these specimens. 29,000 ksi is the nominal value.
[b] The yield stress was not measured for these specimens.

	Experimental		AISC *Specification*			Proposed		
Specimen	T_e kip-in.	**FM**	T_c kip-in.	**FM**	T_e/T_c	T_c kip-in.	**FM**	T_e/T_c
Table A-2. Experimental Results								
Popplewell and Coker (1895)								
36	0.475[a]	Y	0.507	Y	0.937	0.507	Y	0.937
37	0.425[a]	Y	0.507	Y	0.838	0.507	Y	0.838
38	0.425[a]	Y	0.507	Y	0.838	0.507	Y	0.838
39	0.425[a]	Y	0.505	Y	0.842	0.505	Y	0.842
40	0.425[a]	Y	0.507	Y	0.839	0.507	Y	0.839
Seely and Putnam (1919)								
L1	21.2[a]	Y	25.3	Y	0.839	25.3	Y	0.839
L2	28.9[a]	Y	29.8	Y	0.968	29.8	Y	0.968
M1	1.61[a]	Y	1.55	Y	1.042	1.55	Y	1.042
M2	0.662[a]	Y	0.626	Y	1.057	0.626	Y	1.057
M3	0.273[a]	Y	0.279	Y	0.977	0.279	Y	0.977
H1	0.836[a]	Y	0.854	Y	0.979	0.854	Y	0.979
Bridget et al. (1934)								
A	0.0550	B	0.0511	I	1.08	0.0353	I	1.56
C	0.217	B	0.271	I	0.801	0.187	I	1.16
D	0.0360	B	0.0302	I	1.19	0.0209	I	1.73
E	0.106	B	0.114	I	0.929	0.0789	I	1.34
F	0.160	B	0.243	I	0.657	0.168	I	0.951
G1	0.178	B	0.213	I	0.837	0.147	I	1.21
G2	0.196	B	0.213	I	0.921	0.147	I	1.33
G3	0.186	B	0.213	I	0.874	0.147	I	1.27
G4	0.184	B	0.213	I	0.865	0.147	I	1.25
Donnell (1935)								
1	12.8	B	16.1	I	0.797	11.1	I	1.15
2	0.960	B	0.631	I	1.52	0.436	I	2.20
3	1.02	B	0.705	I	1.45	0.488	I	2.09
4	1.40	B	0.802	I	1.75	0.554	I	2.53
5	0.286	B	0.428	I	0.669	0.296	I	0.968
6	0.268	B	0.389	I	0.689	0.269	I	1.00
7	0.202	B	0.247	I	0.817	0.171	I	1.18
8	0.218	B	0.247	I	0.882	0.171	I	1.28
9	0.096	B	0.107	I	0.894	0.0742	I	1.29
10	0.162	B	0.219	I	0.738	0.152	I	1.07
11	0.146	B	0.219	I	0.666	0.152	I	0.963
12	0.0840	B	0.125	I	0.670	0.0867	I	0.969
13	0.106	B	0.125	I	0.845	0.0867	I	1.22
14	0.0460	B	0.0485	I	0.949	0.0335	I	1.37
15	0.206	B	0.249	I	0.826	0.172	I	1.20

(Table A-2 continues on the next page)

Table A-2. Experimental Results (continued)								
	Experimental		AISC *Specification*			Proposed		
Specimen	T_e kip-in.	FM	T_c kip-in.	FM	T_e/T_c	T_c kip-in.	FM	T_e/T_c
Donnell (1935) continued								
16	0.128	B	0.164	I	0.780	0.113	I	1.13
17	0.0640	B	0.069	I	0.926	0.0478	I	1.34
18	0.0900	B	0.136	I	0.659	0.0943	I	0.954
19	0.0600	B	0.0778	I	0.771	0.0538	I	1.12
20	0.032	B	0.0328	I	0.975	0.0227	I	1.41
21	0.048	B	0.0504	I	0.952	0.0349	I	1.38
22	0.0200	B	0.0207	I	0.964	0.0143	I	1.39
23	0.00520	B	0.00364	I	1.43	0.00359	I	1.45
24	0.00339	B	0.00364	I	0.932	0.00273	I	1.24
25	0.00381	B	0.00314	I	1.21	0.00266	L	1.43
26	0.00341	B	0.00305	I	1.12	0.00266	L	1.28
27	0.00319	B	0.00272	I	1.17	0.00259	L	1.23
28	0.00301	B	0.00291	L	1.04	0.00291	L	1.04
29	0.00327	B	0.00266	L	1.23	0.00266	L	1.23
30	0.00320	B	0.00266	L	1.20	0.00266	L	1.20
Stang et al. (1937)								
A1	1.25	B	1.25	Y	1.00	1.25	Y	1.00
A2	1.24	B	1.24	Y	1.00	1.24	Y	1.00
A3	1.26	B	1.24	Y	1.01	1.24	Y	1.01
B1	3.16	B	2.96	Y	1.07	2.96	Y	1.07
B2	3.17	B	2.96	Y	1.07	2.96	Y	1.07
B3	3.19	B	2.96	Y	1.08	2.96	Y	1.08
C1	4.95	B	4.90	Y	1.01	4.90	Y	1.01
C2	4.98	B	4.90	Y	1.02	4.90	Y	1.02
C3	5.07	B	4.90	Y	1.03	4.90	Y	1.03
D1	11.7	B	11.3	Y	1.04	11.3	Y	1.04
D2	11.8	B	11.3	Y	1.04	11.3	Y	1.04
D3	11.7	B	11.3	Y	1.03	11.3	Y	1.03
D4	11.6	B	11.3	Y	1.02	11.3	Y	1.02
D5	11.4	B	11.3	Y	1.01	11.3	Y	1.01
E1	23.4	B	24.9	Y	0.940	24.9	Y	0.940
E2	22.8	B	24.9	Y	0.912	24.9	Y	0.912
E3	23.2	B	25.0	Y	0.931	25.0	Y	0.931
E4	23.1	B	25.0	Y	0.924	25.0	Y	0.924
F1	5.74	B	5.23	Y	1.10	5.23	Y	1.10
F2	5.73	B	5.23	Y	1.10	5.23	Y	1.10
F3	5.75	B	5.28	Y	1.09	5.28	Y	1.09
G1	5.40	B	4.87	Y	1.11	4.87	Y	1.11
							Table A-2 continues on the next page	

	Experimental		AISC *Specification*			Proposed		
Specimen	T_e kip-in.	FM	T_c kip-in.	FM	T_e/T_c	T_c kip-in.	FM	T_e/T_c
Table A-2. Experimental Results (continued)								
Stang et al. (1937) continued								
G2	5.39	B	4.88	Y	1.11	4.88	Y	1.11
G3	5.54	B	4.87	Y	1.14	4.87	Y	1.14
H1	8.89	B	8.31	Y	1.07	8.31	Y	1.07
H2	8.77	B	8.30	Y	1.06	8.30	Y	1.06
I1	12.1	B	9.08	Y	1.34	9.08	Y	1.34
I2	11.7	B	9.11	Y	1.29	9.11	Y	1.29
J1	17.5	B	13.2	Y	1.33	13.2	Y	1.33
J2	17.5	B	13.2	Y	1.33	13.2	Y	1.33
J3	17.4	B	13.2	Y	1.32	13.2	Y	1.32
K1	19.9	B	19.1	Y	1.04	19.1	Y	1.04
K2	19.9	B	19.1	Y	1.04	19.1	Y	1.04
L1	23.5	B	21.5	Y	1.09	21.5	Y	1.09
L2	22.7	B	21.5	Y	1.06	21.5	Y	1.06
L3	22.2	B	21.5	Y	1.03	21.5	Y	1.03
M1	10.8	B	10.5	Y	1.03	10.5	Y	1.03
M2	11.2	B	10.6	Y	1.06	10.6	Y	1.06
N1	14.5	B	13.5	Y	1.08	13.5	Y	1.08
N2	14.3	B	13.4	Y	1.06	13.4	Y	1.06
N3	14.2	B	13.4	Y	1.06	13.4	Y	1.06
O1	7.78	B	7.96	Y	0.978	7.96	Y	0.978
O2	7.87	B	7.92	Y	0.993	7.92	Y	0.993
O3	7.96	B	7.62	L	1.05	7.62	L	1.05
P1	9.71	B	10.4	Y	0.937	9.00	I	1.08
P2	9.49	B	10.3	Y	0.919	8.89	I	1.07
P3	9.17	B	7.79	L	1.18	7.79	L	1.18
Q1	12.4	B	13.1	Y	0.949	11.0	I	1.12
Q2	11.6	B	8.90	I	1.30	8.72	L	1.33
R1	3.38	B	3.38	Y	1.00	3.38	Y	1.00
R2	3.50	B	3.39	Y	1.03	3.39	Y	1.03
R3	3.62	B	3.39	Y	1.07	3.39	Y	1.07
S1	4.16	B	4.14	Y	1.01	4.14	Y	1.01
S2	4.15	B	4.14	Y	1.00	4.14	Y	1.00
T1	6.58	B	6.70	Y	0.981	6.70	Y	0.981
T2	6.54	B	6.70	Y	0.975	6.70	Y	0.975
T3	6.30	B	6.70	Y	0.940	6.70	Y	0.940
U1	10.3	B	10.4	Y	0.991	10.4	Y	0.991
U2	10.3	B	10.4	Y	0.989	10.4	Y	0.989
U3	10.4	B	10.4	Y	0.994	10.4	Y	0.994
(Table A-2 continues on the next page)								

	Experimental		AISC *Specification*			Proposed		

Table A-2. Experimental Results (continued)

Specimen	T_e kip-in.	FM	T_c kip-in.	FM	T_e/T_c	T_c kip-in.	FM	T_e/T_c
Stang et al. (1937) continued								
V1	13.5	B	14.7	Y	0.918	14.1	I	0.952
V2	13.1	B	14.5	Y	0.900	13.7	I	0.952
V3	9.59	B	11.4	I	0.838	9.34	L	1.03
Schmidt and Winterstetter (2004)								
1	59.0	B	57.8	Y	1.02	57.8	Y	1.02
2	43.3	B	37.8	Y	1.15	37.8	Y	1.15
3	59.0	B	58.4	Y	1.01	58.4	Y	1.01
4	41.5	B	37.7	Y	1.10	37.4	I	1.11
Wu et al. (2018)								
1-1	66.4[a]	Y	74.7	Y	0.888	74.7	Y	0.888
1-2	66.4[a]	Y	74.7	Y	0.888	74.7	Y	0.888
2-1	66.4[a]	Y	74.9	Y	0.886	74.9	Y	0.886
2-2	66.4[a]	Y	74.9	Y	0.886	74.9	Y	0.886
3-1	106[a]	Y	117	Y	0.904	117	Y	0.904
3-2	106[a]	Y	117	Y	0.904	117	Y	0.904
4-1	124[a]	Y	121	Y	1.02	121	Y	1.02
5-1	204[a]	Y	189	Y	1.08	189	Y	1.08

[a] For these specimens, the ultimate experimental torsion resulted in large inelastic rotation angles. The proportional limit on the torsion-rotation curve was used for the experimental torsion.

T_c = calculated torsional moment, kip-in.

T_e = experimental torsional moment, kip-in.

FM: Failure mode

B: Buckling

I: Buckling of an intermediate-length member

L: Buckling of a long member

Y: Yield

Lateral-Torsional Buckling Modification Factors in Steel I-Shaped Members: Recommendations Using Energy-Based Formulations

NAMITA NAYAK, P.M. ANILKUMAR, and LAKSHMI SUBRAMANIAN

ABSTRACT

Lateral torsional buckling (LTB) is of concern in long-span flexural members, particularly in the negative flexure regions of continuous-span, steel I-shaped members and during construction. While the elastic critical LTB capacity of a simply supported I-shaped member subjected to uniform moment has a closed-form solution, most LTB modification factors for beams subjected to moment gradients in the literature are empirical and work well only for specific loading and boundary conditions. This paper investigates the suitability of the different LTB modification factors in literature and design specifications for various loading and boundary conditions, accomplished via comparisons with analytical solutions using the Rayleigh-Ritz method and numerical solutions from finite element analyses. The analytical LTB modification factors are derived for doubly symmetric I-shaped members with different combinations of ideal flexural and torsional boundary conditions (simply supported and fixed) and subjected to different loading scenarios. The validity of the LTB modification factors determined using the Rayleigh-Ritz method and other formulae in the literature are also assessed for realistic intermediate restraint conditions, which are neither fully pinned nor fixed, by examining laterally continuous beams. Demonstrating that current design specifications for elastic critical LTB modifications are overly conservative for beams with complete or partial warping fixity, the authors recommend practical and simple alternatives to design such beams.

Keywords: lateral torsional buckling, LTB modification factor, Rayleigh-Ritz method, warping restraints, continuous beams.

INTRODUCTION

This paper investigates the elastic critical lateral torsional buckling (LTB) capacities of doubly symmetric, steel I-shaped members loaded at their centroidal axes, considering a spectrum of loading and boundary conditions. The classical solution for the elastic critical lateral torsional buckling capacity was first proposed by Timoshenko (1936) for simply supported, doubly symmetric, I-shaped members subjected to uniform moment, which is used worldwide as the elastic critical lateral torsional buckling capacity. Several empirical formulae for LTB modification factors have since been developed to account for the enhancement in the flexural capacities of beams with nonuniform moments within the unbraced spans (such as Salvadori, 1956; Nethercot and Rockey, 1972; Kirby and Nethercot, 1979; Serna et

al., 2006; Wong and Driver, 2010). Design codes and specifications (BS 5950-1, 2000; AASHTO, 2020; AISC, 2022) employ these modification factors with or without elastic lateral effective length factors. The British standard recommends using an effective length based on the restraint conditions at the ends of the unbraced segments. While AISC *Specification* (2022) Equation F2-4 stipulates the use of a full unbraced length instead of an effective unbraced length by defining the unbraced length as the distance between lateral braces, its Commentary discusses using an effective length factor based on the end restraints as per Ziemian (2010). Similarly, the AASHTO *Specification* Commentary (2020) explores using an effective length factor in rehabilitation design or extraordinary circumstances, which may be calculated based on Nethercot and Trahair (1976) and Ziemian (2010). The recommendation of $K = 1.0$ in the American specifications (AASHTO, 2020; AISC, 2022) can lead to significantly conservative estimates of elastic critical LTB capacities of I-shaped members, whose ends are torsionally fixed (both twist and warping are fixed). This is true irrespective of the in-plane flexural boundary conditions. Such beams are practically found in cases such as rigid beam-column joints or in typical moment connection details. However, using an elastic effective length factor, K (as suggested in the AISC and AASHTO *Specification* Commentaries), along with the current equations for the LTB modification factors (C_b) may lead to inaccurate estimates of the flexural capacities of I-shaped members.

Namita Nayak, Research scholar, Department of Civil Engineering, Indian Institute of Technology Madras, Tamil Nadu, India. Email: ce20d041@smail.iitm.ac.in

P.M. Anilkumar, Institute of Structural Analysis, Gottfried Wilhelm Leibniz University Hannover, Hannover, Germany. Email: a.nair@isd.uni-hannover.de

Lakshmi Subramanian, Assistant Professor, Department of Civil Engineering, Indian Institute of Technology Madras, Tamil Nadu, India. Email: lakshmipriya@iitm.ac.in (corresponding)

An inaccurate estimation of C_b, and thereby, the elastic critical buckling capacities, affects the entire beam design curve. For example, the AISC *Specification* beam design curve consists of three parts: the plateau for short unbraced lengths ($L_b < L_p$) with the maximum cross-section capacity, an elastic LTB curve for long unbraced lengths ($L_b > L_r$), and an inelastic LTB equation that is a linear interpolation between the maximum cross-section capacity and the elastic LTB curves. The inelastic and elastic LTB design capacities in the AISC and AASHTO *Specifications* are scaled by C_b for nonuniform moment loading conditions, limited by the maximum cross-section capacity. Such scaling often leads to an extended plateau length several times larger than L_p, and a greatly enhanced inelastic LTB capacity. Hence, an inaccurate estimation of C_b may result in either overly conservative or unconservative estimates of the beam capacities in a significant portion of the beam design space. Subramanian and White (2017a) also noted that the extended plateau resulting from scaling the flexural capacity by C_b in the inelastic LTB region tends to overestimate the true strengths even for beams which are free to warp at their ends ($K = 1.0$). Although the available literature provides numerous formulations for estimating C_b, the existing equations are generally fit to the results of numerical parametric studies for specific loading and boundary conditions.

The objective of this study is to evaluate the appropriateness of the existing C_b factors in design specifications and literature for ideal boundary conditions, including fork boundary conditions (flexurally and torsionally simply supported), fully fixed (flexurally and torsionally) conditions, and flexurally simply supported and torsionally fixed boundary conditions. More practical conditions, including laterally continuous beams, are also subsequently examined. The loading conditions include linear moment gradients, a concentrated load at mid-span, and uniformly distributed loads. The available empirical equations are compared with analytical solutions using the Rayleigh-Ritz method and finite element (FE) simulations. The Rayleigh-Ritz method is an energy-based approach, wherein the LTB capacity is obtained by minimizing the total potential energy of the system. Although the energy method has been previously used by others (Timoshenko, 1936; Galambos and Surovek, 2008; Yoo and Lee, 2011) to calculate the elastic critical buckling moments, those studies were limited to simply supported I-shaped members and cantilever beams subjected to concentrated loads. This work seeks to establish accurate formulations for predicting the elastic critical moment of steel I-shaped members for standard loading and end-restraint conditions, while also defining the specific conditions for which the available commonly used equations are most suitable. The results from the Rayleigh-Ritz method are also compared with FE test simulations. The

comparisons with the literature and FE simulations also help identify practical design scenarios where one must exercise caution when using the existing equations in the design specifications and the recommendations in the commentaries for LTB resistances.

Following the studies on beams with ideal boundary conditions, this paper looks at practical design conditions with laterally continuous beams. In beams with intermediate lateral braces, the critical lateral spans are restrained by their adjoining segments. A correct estimate of the flexural capacity of such beams depends on the effective length of the critical unbraced span and the appropriate C_b factor. While the effective lateral length factor, K, for the ideal boundary conditions, may be taken as 1.0 for torsionally simply supported conditions, and 0.5 for torsionally fixed conditions, the appropriate K for laterally continuous beams is determined using other methods.

White (2008) and White and Jung (2008) briefly described the evolution of the AISC *Specification* beam design equations, which are largely a fit to a vast body of experimental data. They explained that the current coefficient in the equation for L_p (AISC *Specification* Equation F4-7) may be taken as devoid of any implicit effective length factors. They further cautioned that employing $K = 1.0$, as outlined in the AISC *Specification*, is conservative for several design conditions and recommended using the effective length proposed by Nethercot and Trahair (1976) and Galambos (1998). Nethercot and Trahair first proposed a method to estimate the elastic effective length factor for laterally continuous beams, akin to the method for braced columns. They stipulated that the restraints to the critical span from the immediately adjoining segments are functions of the loading in both the critical and restraining segments, and the far-end boundary conditions. Later, Subramanian et al. (2018) discussed the effect of inelasticity in the critical segments, leading to a consideration of $K_{inelastic}$ in interpreting experimental test data. They demonstrated an improved reliability when the plateau length, L_p, was reduced to a coefficient of 0.63 instead of 1.1, and the anchor point for the elastic stresses, F_L, was decreased to $0.5F_{yc}$, as recommended in Kim (2010) and Subramanian and White (2017b).

More recently, John and Subramanian (2019) proposed modifications to the original method by Nethercot and Trahair (1976), noting that the restraint also depends on whether the adjoining segment braces the critical span at the location of the maximum or the minimum moment within the critical span. Additionally, John and Subramanian discussed situations where the farther segments further influence the restraints from the spans immediately adjoining the critical span. They also observed conditions where the critical lateral span may be identified incorrectly. This paper examines the various C_b formulations for

laterally continuous beams by applying the effective length factors from both the Nethercot and Trahair (1976) method and the modified methods suggested by John and Subramanian (2019).

These exhaustive comparisons of the LTB modification factors for ideal boundary conditions and laterally continuous beams with partial restraint conditions lead the authors to recommend design methods better suited for a broader range of beam design conditions.

EVALUATION OF M_{cr} USING EXISTING DESIGN CODES AND EMPIRICAL FORMULAE

Timoshenko (1936) derived the elastic critical LTB capacity for flexurally and torsionally simply supported, doubly symmetric, I-shaped members subjected to a uniform moment. The AISC *Specification* Commentary discusses using an elastic effective length instead of the full unbraced length to enhance the elastic critical buckling moment by using the method prescribed in Ziemian (2010), which considers the lateral and torsional boundary conditions in the beams. This modified elastic critical LTB capacity, M_{ocr}, may be written as given in Equation 1 by considering the effective length KL for the different flexural and torsional boundary conditions. This basic critical moment equation is typically modified for different loading and boundary conditions by multiplying the expression for M_{ocr} with the LTB modification factor, C_b. Some of the commonly used expressions for C_b are listed in Table 1.

$$M_{ocr} = \sqrt{\frac{\pi^2 E I_y}{(KL)^2}\left(\frac{\pi^2 E I_w}{(KL)^2} + GJ\right)} \qquad (1)$$

where
- E = Young's modulus of elasticity, ksi
- G = elastic shear modulus, ksi
- I_y = minor axis moment of inertia, in.[4]
- I_w = warping constant, in.[4]
- J = St.-Venant torsional constant, in.[4]
- L = lateral unbraced length, in.

The American specifications use Equation 2 (AISC *Specification* Equation F2-4 and AASHTO *Specification* Equation A6.3.3) to estimate the elastic critical LTB stress of an I-shaped member. This equation is similar to Timoshenko's solution for a flexurally and torsionally simply supported, doubly symmetric, I-shaped member (with $K = 1.0$) subjected to uniform moment.

$$F_{cr} = \frac{C_b \pi^2 E}{\left(\frac{L_b}{r_{ts}}\right)^2}\sqrt{1 + 0.078\frac{Jc}{S_x h_o}\left(\frac{L_b}{r_{ts}}\right)^2} \qquad (2)$$

$$r_{ts}^2 = \frac{\sqrt{I_y C_w}}{S_x}$$

where
- C_b = LTB modification factor for nonuniform moment diagrams
- L_b = lateral unbraced length, in.
- S_x = elastic section modulus taken about the major axis of the cross section, in.[3]
- c = 1.0 for doubly symmetric I-sections
- h_o = distance between the flange centroids, in.

Table 1 provides expressions for LTB modification factors from the literature, commonly derived from a fit to the data from finite element or finite difference methods for moment gradients. These equations are derived for specific loading conditions but are, however, usually applied to all loading and boundary conditions. For example, the equation proposed by Salvadori (1956), incorporated in the AASHTO *Specification*, applies to members with linear bending moment diagrams between the two braced points. While this equation is simple to use and yields good results for bending in single curvature, it is significantly conservative when applied to beams with double curvature. Similarly, Nethercot and Rockey (1972) provided the LTB modification factors for beams with warping-fixed boundary conditions subjected to a concentrated load at mid-span and a uniformly distributed load (Ziemian, 2010); however, the in-plane boundary conditions in the warping-fixed cases were not specified.

Serna et al. (2006) found that the equations provided in the AISC *Specification* and the British standard (BS 5950-1, 2000) are unconservative for warping-fixed conditions. They proposed an alternate equation, where the LTB modification factor is a function of the torsional boundary conditions. Wong and Driver (2010) opined that the equation proposed by Serna et al. (2006) overestimates the elastic critical LTB capacity, and they proposed the C_b factor presented in Table 1. The equation developed by Wong and Driver (2010) fits the numerical data considering the effect of moment gradients in beams whose ends are free to warp.

The British standard BS 5950-1 (2000) employs a LTB modification coefficient similar to the AISC *Specification* with different coefficients for the bending moments at quarter-, mid-, and three-quarter span locations. The British standard further recommends using an effective length factor, K, of 1.0 and 0.7 for warping-free and fixed boundary conditions, respectively. While the AISC *Specification* recommends using the C_b factor (Equation F1-1) proposed by Kirby and Nethercot (1979), several other C_b factors are presented in the Commentary. These equations include Wong and Driver's (2010) equation (AISC *Specification* Commentary Equation C-F1-2b) for nonlinear moment diagrams, and the C_b factor proposed by Yura and Helwig

	Table 1. Review of LTB Modification Factors, C_b, from the Literature	
Source	**Equation**	**Remarks**
Salvadori (1956) AISC *Specification* (2022) Equation C-F1-1 AASHTO *Specification* (2020)* Equation A6.3.3.7	$C_b = 1.75 + 1.05\left(\dfrac{M_1}{M_2}\right) + 0.30\left(\dfrac{M_1}{M_2}\right)^2 \leq 2.30$	M_1—smaller moment at the end of the unbraced length M_2—larger moment at the end of the unbraced length The ratio of M_1 to M_2 is positive for double curvature and negative for single curvature bending
Nethercot and Rockey (1972) Ziemian (2010)	1.35^a 1.13^b $C_b = 1.92 - 0.42\left(\dfrac{\pi}{L}\sqrt{\dfrac{EI_w}{GJ}}\right)^2 + 1.85\left(\dfrac{\pi}{L}\sqrt{\dfrac{EI_w}{GJ}}\right)^c$ $C_b = 1.64 - 0.41\left(\dfrac{\pi}{L}\sqrt{\dfrac{EI_w}{GJ}}\right)^2 + 1.77\left(\dfrac{\pi}{L}\sqrt{\dfrac{EI_w}{GJ}}\right)^d$	[a] Flexurally and torsionally simply supported with a concentrated load at mid-span [b] Flexurally and torsionally simply supported with a uniformly distributed load [c] Flexurally and torsionally fixed with a concentrated load at mid-span [d] Flexurally and torsionally fixed with a uniformly distributed load
Kirby and Nethercot (1979) (AISC *Specification* Equation F1-1)	$C_b = \dfrac{12.5M_{max}}{2.5M_{max} + 3.0M_A + 4.0M_B + 3.0M_C}$	M_{max}—absolute value of the maximum moment in the unbraced segment M_A, M_B, M_C—absolute values of the moments at the quarter-, mid-, and three-quarter points of the unbraced segment
British standard (BS 5950-1, 2000)	$C_b = \dfrac{M_{max}}{0.20M_{max} + 0.15M_2 + 0.50M_3 + 0.15M_4} \leq 2.27$	M_{max}—absolute value of the maximum moment in the unbraced segment M_2, M_3, M_4—absolute values of the moments at the quarter-, mid-, and three-quarter points of the unbraced segment
Serna et al. (2006)	$C_b = \dfrac{\sqrt{\sqrt{k}A_1 + \left[\dfrac{(1-\sqrt{k})}{2}A_2\right]^2} + \dfrac{(1-\sqrt{k})}{2}A_2}{A_1}$	$A_1 = \dfrac{M_{max}^2 + 9kM_2^2 + 16M_3^2 + 9kM_4^2}{(17 + 18k)M_{max}^2}$ $A_2 = \left\|\dfrac{M_{max} + 4M_1 + 8M_2 + 12M_3 + 8M_4 + 4M_5}{37M_{max}}\right\|$ $k = 1$ (lateral bending and warping are free) $= 0.5$ (lateral bending and warping are prevented) M_{max}—maximum bending moment M_1, M_5 are the bending moment at brace locations M_2, M_3, M_4—moments at the quarter-, mid-, and three-quarter points of the unbraced segment
Wong and Driver (2010) (AISC *Specification* Commentary Equation C-F1-2b)	$C_b = \dfrac{4M_{max}}{\sqrt{M_{max}^2 + 4M_A^2 + 7M_B^2 + 4M_C^2}} \leq 2.50$	M_{max}—absolute value of the maximum moment in the unbraced segment M_A, M_B, M_C—absolute values of the moments at the quarter-, mid-, and three-quarter points of the unbraced segment
* The moment modification factor in AASHTO *Specification* (2020) is expressed in the form of compression flange stresses at the brace locations.		

(AISC *Specification* Commentary Equation C-F1-5) (Yura, 1995; Yura and Helwig, 2010) for beams with reverse curvature continuously braced at their top flanges.

While the AISC *Specification* offers several equations that consider the moment gradient and the effect of bracing, there needs to be more discussion on the range of support and loading conditions for which the equations are applicable. Given the differences in the existing C_b formulae, particularly for end conditions with warping restraints, a general theoretical model based on the Rayleigh-Ritz formulation is presented in this paper to assess the accurate C_b for each loading and boundary condition. The frequent assertion in literature that using the C_b expressions derived for warping-free conditions is conservative when used in beams with warping restraint is also examined in this paper.

ELASTIC CRITICAL LTB CAPACITY USING THE RAYLEIGH-RITZ FORMULATION

This section provides the elastic critical LTB solutions obtained using the Rayleigh-Ritz method for beams with ideal boundary conditions subjected to different loading conditions. The standard case of a doubly symmetric I-beam with fork boundary conditions (flexurally and torsionally simply supported) subjected to uniform moments is shown in Figure 1. The traditional assumptions while deriving the LTB equation (Timoshenko, 1936) for I-shaped members are not stated here for brevity.

According to the principle of virtual work, the total potential, $\prod$, of a system may be determined by summing the elastic energy of the system, U, and the potential of the external forces, V. The total potential of the system is constant.

$$\prod = U + V \tag{3}$$

The total elastic strain energy of the beam is given by:

$$U = \frac{1}{2} \int_0^L \left[EI_y (u'')^2 + EI_w (\phi'')^2 + GJ (\phi')^2 \right] dz \tag{4}$$

And the potential of external force is equal to:

$$V = \frac{1}{2} \int_0^L M_x \left[2\phi (u'') \right] dz \tag{5}$$

The total potential of the system can hence be written as:

$$\prod = \frac{1}{2} \int_0^L \left[EI_y (u'')^2 + EI_w (\phi'')^2 + GJ (\phi')^2 \right] dz \tag{6}$$
$$+ \frac{1}{2} \int_0^L M_x \left[2\phi (u'') \right] dz$$

where
  M_x = bending moment about the major principal axis
  u'' = second derivative of the lateral deflection of the centroidal axis u
  ϕ' = first derivative of the twist ϕ
  ϕ'' = second derivative of ϕ

The potential energy is a function of the loading conditions (the bending moment M) and the unknown coefficients of the displacement functions (u and ϕ). These unknowns are calculated by applying the Rayleigh-Ritz technique to Equation 6 by minimizing the system's potential energy ($\delta\prod = 0$).

Derivation of the elastic critical LTB capacity of a simply supported beam with fork boundary conditions subjected to uniform moment

The elastic critical LTB capacity for the doubly symmetric I-shaped member in Equation 1 is derived using the Rayleigh-Ritz approach described here.

The boundary conditions for a simply supported beam are given by

$$u = u'' = \phi = \phi'' = 0 \qquad \text{at } z = 0 \text{ and } z = L \tag{7}$$

The assumed displacement functions satisfying the above boundary conditions are:

$$u = A \sin \frac{\pi z}{L}, \ \phi = B \sin \frac{\pi z}{L} \tag{8}$$

(a) In-plane displacement   *(b) Out-of-plane displacement*   *(c) Twist of cross section*
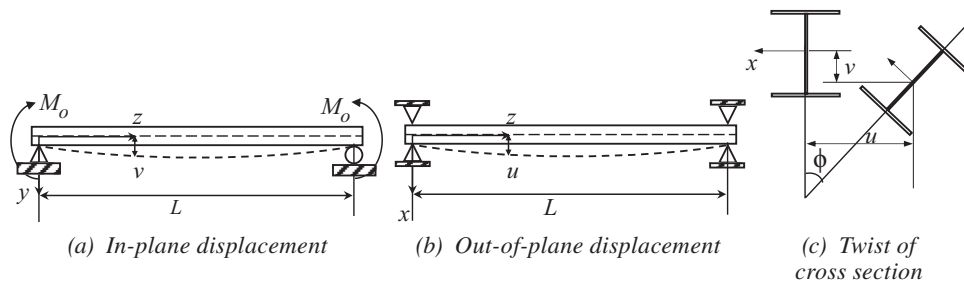
Fig. 1. Displacement of a simply supported doubly symmetric I-shaped member subjected to uniform moment.

The bending moment at any section along the length of the beam is $M_x = M$.

The total potential energy calculated using Equation 6 is given by

$$\Pi = U + V = \frac{\pi^4 EI_y A^2}{4L^3} + \frac{\pi^4 EI_w B^2}{4L^3} + \frac{\pi^2 GJB^2}{4L} - \frac{\pi^2 MAB}{2L} \tag{9}$$

Differentiating the total energy with respect to the unknowns A and B, the following equations are obtained.

$$\frac{\partial \Pi}{\partial A} = \frac{\pi^4 EI_y A}{2L^3} - \frac{\pi^2 MB}{2L} \tag{10}$$

$$\frac{\partial \Pi}{\partial B} = \frac{\pi^4 EI_w B}{2L^3} + \frac{\pi^2 GJB}{2L} - \frac{\pi^2 MA}{2L} \tag{11}$$

The total potential being constant, Equations 10 and 11 are equated to zero.

$$\begin{bmatrix} \dfrac{\pi^2 EI_y}{L^2} & -M \\ -M & \dfrac{\pi^2 EI_w}{L^2} + GJ \end{bmatrix} \begin{Bmatrix} A \\ B \end{Bmatrix} = 0$$

The solution for the elastic critical lateral torsional moment, M_{cr}, can be obtained by evaluating the determinant of this matrix. Equation 12 is the same as the classical buckling solution derived by Timoshenko (1936), with an effective length factor, K, of 1.0.

$$M_{cr} = \sqrt{\frac{\pi^2 EI_y}{L^2}\left(\frac{\pi^2 EI_w}{L^2} + GJ\right)} \tag{12}$$

The different loading and boundary conditions studied in this paper are listed in Table 2. The in-plane boundary conditions and loading are illustrated through the images, and the warping restraint is described in the text. The transverse loads are applied at the centroidal axes, precluding instability from load-height effects.

Table 3 lists the elastic critical LTB capacities for the nine different loading and ideal boundary conditions listed in Table 2. These expressions are derived using the energy method. The cross-sectional twist is restrained at both beam ends in all cases in this paper. The assumed displacement functions listed in the last column of Table 2 satisfy the corresponding boundary conditions. The number of terms shown in the displacement functions is based on convergence studies for each case. The critical buckling load or moment is thus obtained by minimizing the potential energy given by Equation 6, using the same procedure outlined for a beam subjected to uniform moment (loading type 1).

All critical moments are observed to be multiples of the basic critical moment, M_{ocr}, in Equation 1 with the corresponding K listed in Table 3 (1.0 for torsionally simply supported conditions and 0.5 for torsionally fixed conditions). The LTB modification factor, C_b, presented in Table 3, is the ratio of M_{cr} to M_{ocr}. The derivations for several cases listed in Table 3 are presented in Nayak et al. (2023). The derivations for loading types 6 and 9 are also presented in the appendix of this paper. The derivations for other cases are mathematically repetitive and can be obtained using the shape functions and boundary conditions listed in Table 2. They are not shown in this paper.
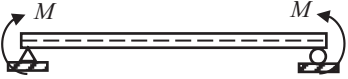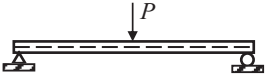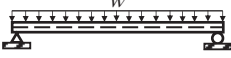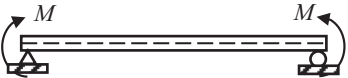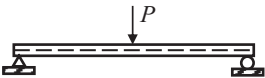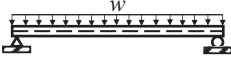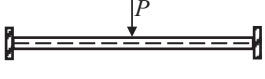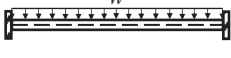
COMPARATIVE STUDIES WITH NUMERICAL RESULTS AND THE LITERATURE

The elastic critical LTB capacities calculated using the LTB modification factors derived in Table 3 are compared with the results from the elastic buckling analyses using FE simulations in SABRE2 (White et al., 2021). SABRE2 is a structural analysis and design software that employs beam elements with 7 degrees of freedom at each node, including the warping degree of freedom. The solutions from SABRE2 are also verified with several studies using elastic buckling analyses in ABAQUS (2022). Following a mesh convergence study, each beam unbraced segment is modeled with eight elements. The boundary conditions used are presented in Figure 2.

The results for two wide-flange sections (W16×40 and W30×90) of 6.0 m (19 ft 8 in) length are presented in this paper for the validation studies. Table 4 compares the critical elastic critical LTB capacities calculated using the LTB modification factors, C_b, established using the Rayleigh-Ritz method, $M_{cr,energy}$, and the elastic critical LTB capacities from the finite element analyses (FEA), $M_{cr,FEA}$, for the two sections for the 16 different cases that make use of results from the nine loading types chosen in Table 2. The results for a broader range of wide-flange sections are similar and do not add value to this paper. Cases 1–11 in Table 4 are flexurally and torsionally simply supported (twist restrained, warping free), while Cases 12–14 are flexurally simply supported in-plane, but torsionally fixed (twist and warping restrained). Cases 15 and 16 are modeled with both flexurally and torsionally fixed boundary conditions.

Figure 3 compares the elastic critical LTB capacities estimated using the empirical C_b equations given in the AISC *Specification* and in BS 5950-1 and those obtained from the energy method, with the elastic critical LTB capacities obtained from the FE simulations for the W16×40 and W30×90 sections, respectively. The values reported for the energy method employ $K = 0.5$ for conditions with warping fixity (Cases 12–16). In reporting the values for the AISC

Table 2. Assumed Displacement Functions for the Ideal Loading and Boundary Conditions Studied in This Paper				
Loading Type	**Loading Condition**	**Boundary Condition**		**Displacement Functions**
		In-Plane Flexural	**Warping**	
1		Simply supported	Free	$u = A\sin\dfrac{\pi z}{L}$ $\phi = B\sin\dfrac{\pi z}{L}$
2[a]		Simply supported	Free	$u = A\sin\dfrac{\pi z}{L} + B\sin\dfrac{2\pi z}{L}$ $\phi = C\sin\dfrac{\pi z}{L}$
3[b]		Simply supported	Free	$u = A\sin\dfrac{\pi z}{L} + B\sin\dfrac{2\pi z}{L}$ $\phi = C\sin\dfrac{\pi z}{L}$
4[b]		Simply supported	Free	$u = A\sin\dfrac{\pi z}{L} + B\sin\dfrac{2\pi z}{L}$ $\phi = C\sin\dfrac{\pi z}{L}$
5		Simply supported	Fixed	$u = A\left(1-\cos\dfrac{2\pi z}{L}\right)$ $\phi = B\left(1-\cos\dfrac{2\pi z}{L}\right)$
6[b]		Simply supported	Fixed	$u = A\left(1-\cos\dfrac{2\pi z}{L}\right) + B\left(1-\cos\dfrac{4\pi z}{L}\right)$ $\phi = C\left(1-\cos\dfrac{2\pi z}{L}\right)$
7[b]		Simply supported	Fixed	$u = A\left(1-\cos\dfrac{2\pi z}{L}\right) + B\left(1-\cos\dfrac{4\pi z}{L}\right)$ $\phi = C\left(1-\cos\dfrac{2\pi z}{L}\right)$
8[b]		Fixed	Fixed	$u = A\left(1-\cos\dfrac{2\pi z}{L}\right) + B\left(1-\cos\dfrac{4\pi z}{L}\right)$ $\phi = C\left(1-\cos\dfrac{2\pi z}{L}\right)$
9[b]		Fixed	Fixed	$u = A\left(1-\cos\dfrac{2\pi z}{L}\right) + B\left(1-\cos\dfrac{4\pi z}{L}\right)$ $\phi = C\left(1-\cos\dfrac{2\pi z}{L}\right)$

[a] β is positive for single curvature and negative for reverse curvature.
[b] The transverse loads are applied at the centroidal axes.

Loading Type	K	Elastic Critical LTB Capacity	$C_b = M_{cr}/M_{ocr}$
		Table 3. Elastic Critical LTB Capacities and LTB Modification Factor Obtained for the Different Cases Considered in Table 2 Using the Energy Method	
1	1.0	$M_{cr} = \sqrt{\dfrac{\pi^2 EI_y}{L^2}\left(\dfrac{\pi^2 EI_w}{L^2} + GJ\right)}$	1.00
2	1.0	$M_{cr} = \dfrac{1}{\sqrt{\left[0.50(1+\beta)\right]^2 + \left[0.18(1-\beta)\right]^2}}\sqrt{\dfrac{\pi^2 EI_y}{L^2}\left(\dfrac{\pi^2 EI_w}{L^2} + GJ\right)}$	$\dfrac{1}{\sqrt{\left[0.50(1+\beta)\right]^2 + \left[0.18(1-\beta)\right]^2}}$
3	1.0	$M_{cr} = 1.42\sqrt{\dfrac{\pi^2 EI_y}{L^2}\left(\dfrac{\pi^2 EI_w}{L^2} + GJ\right)}$	1.42
4	1.0	$M_{cr} = 1.15\sqrt{\dfrac{\pi^2 EI_y}{L^2}\left(\dfrac{\pi^2 EI_w}{L^2} + GJ\right)}$	1.15
5	0.5	$M_{cr} = \sqrt{\dfrac{\pi^2 EI_y}{(0.5L)^2}\left[\dfrac{\pi^2 EI_w}{(0.5L)^2} + GJ\right]}$	1.00
6	0.5	$M_{cr} = 1.07\sqrt{\dfrac{\pi^2 EI_y}{(0.5L)^2}\left[\dfrac{\pi^2 EI_w}{(0.5L)^2} + GJ\right]}$	1.07
7	0.5	$M_{cr} = 0.97\sqrt{\dfrac{\pi^2 EI_y}{(0.5L)^2}\left[\dfrac{\pi^2 EI_w}{(0.5L)^2} + GJ\right]}$	0.97
8	0.5	$M_{cr} = 1.08\sqrt{\dfrac{\pi^2 EI_y}{(0.5L)^2}\left[\dfrac{\pi^2 EI_w}{(0.5L)^2} + GJ\right]}$	1.08
9	0.5	$M_{cr} = 1.77\sqrt{\dfrac{\pi^2 EI_y}{(0.5L)^2}\left[\dfrac{\pi^2 EI_w}{(0.5L)^2} + GJ\right]}$	1.77

Loading type 1-4
at shear center, a
$u_x = u_y = u_z = 0$ (pin end)
$\theta_z = 0$ (pin end)
$u_x = u_y = 0$ (roller end)
$\theta_z = 0$ (roller end)
warping free

Loading type 5-7
at shear center, a, at the ends
$u_x = u_y = u_z = 0$
$\theta_y = \theta_z = 0$
warping fix

Loading type 8-9
at shear center, a, at the ends
$u_x = u_y = u_z = 0$
$\theta_x = \theta_y = \theta_z = 0$
warping fix
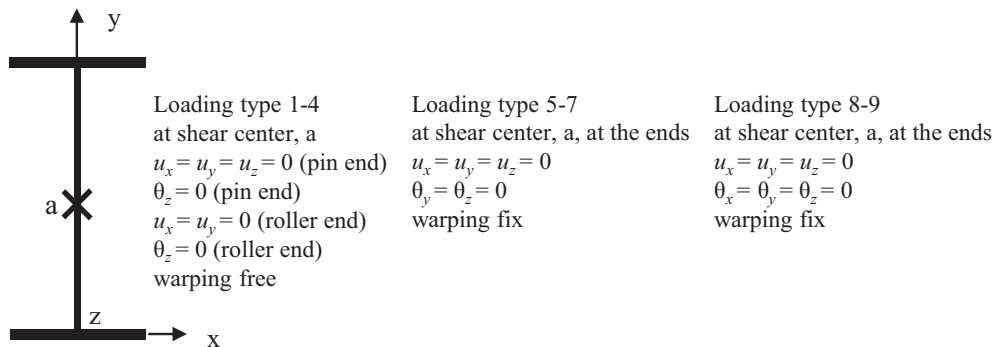
Fig. 2. Boundary conditions used in FE simulations.

Specification, a value of $K = 1.0$ is used in all cases, as per the current definition of L_b. Additionally, the AISC *Specification* C_b is also used with the correct effective length factor $K = 0.5$, for Cases 12–16, as proffered in the AISC *Specification* Commentary. Similarly, an effective length factor of 0.7 is employed in estimating the elastic critical LTB capacity while using BS 5950-1 for warping-fixed conditions.

Figure 4 compares the elastic critical LTB capacities estimated using the empirical equations in the literature and the energy-based solutions, with the elastic critical LTB capacities obtained from the FE simulations for the two sections. Nethercot and Rockey's (1972) equations were derived for

warping-fixed support conditions. However, their direction on the appropriate effective length to use in their equations is ambiguous. Hence, an effective length factor of 1.0 is used here, even for cases with warping-fixed end conditions in their expressions for C_b. Using the full lateral unbraced length ($K = 1.0$) rather than an effective lateral length ($K = 0.5$) in their equations yields more realistic results, preventing grossly unconservative calculations. However, in other comparative studies, the critical moment is estimated using $K = 1.0$ for flexurally and torsionally simply supported boundary conditions and $K = 0.5$ for torsionally fixed end conditions irrespective of the in-plane flexural boundary conditions.
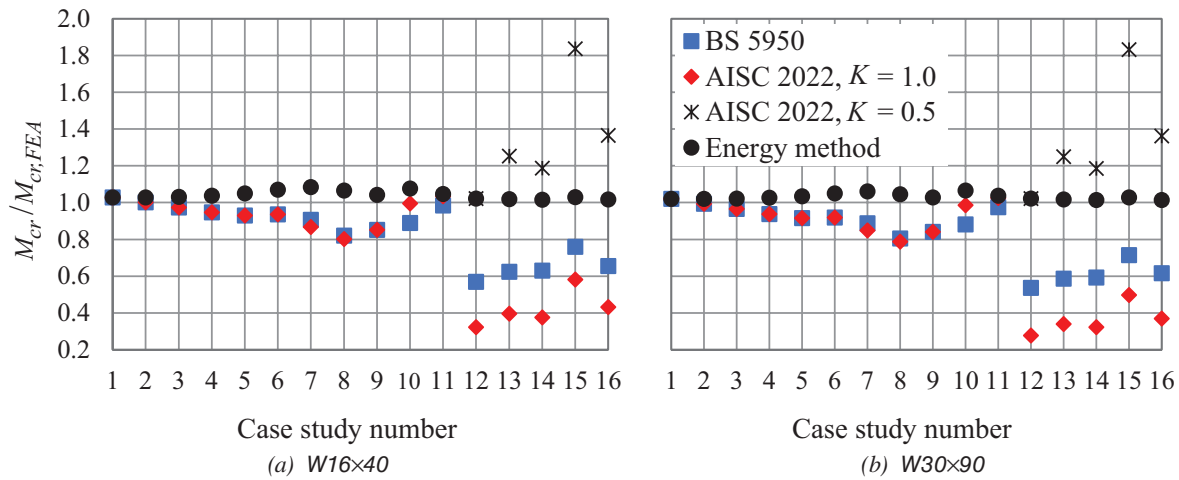
Fig. 3. Comparison of $\mathrm{M_{cr}}$ obtained from FEA with the Rayleigh-Ritz method and equations given in the design standards for 6 m (19 ft 8 in) long I-shaped members.
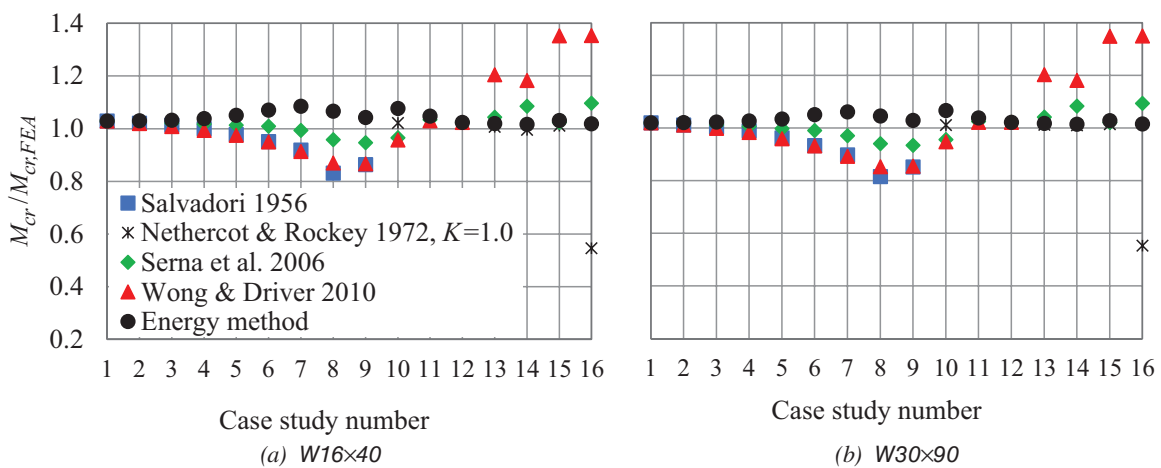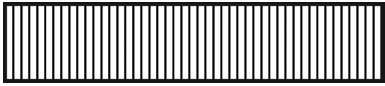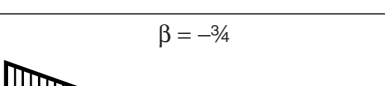

Fig. 4. Comparison of $\mathrm{M_{cr}}$ obtained from FEA with the Rayleigh-Ritz method and empirical equations in literature for 6 m (19 ft 8 in) long I-shaped members

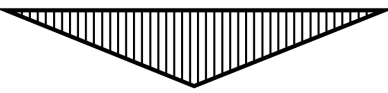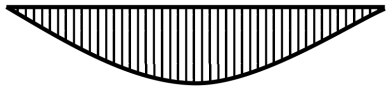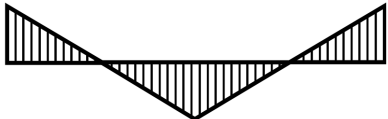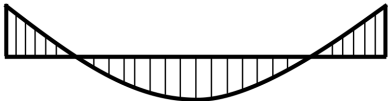| Table 4. Comparison of the LTB Capacities Obtained from the Energy Method with FE Solutions				W16×40	W30×90
Case Study No.	**Boundary Condition**		**Bending Moment Diagram**	$M_{cr,FEA}/M_{cr,energy}$	$M_{cr,FEA}/M_{cr,energy}$
	Flexure	**Warping**			
1	Simply supported	Free	$\beta = +1$	0.97	0.98
2	Simply supported	Free	$\beta = +\frac{3}{4}$	0.97	0.98
3	Simply supported	Free	$\beta = +\frac{1}{2}$	0.97	0.98
4	Simply supported	Free	$\beta = +\frac{1}{4}$	0.96	0.97
5	Simply supported	Free	$\beta = 0$	0.95	0.97
6	Simply supported	Free	$\beta = -\frac{1}{4}$	0.93	0.95
7	Simply supported	Free	$\beta = -\frac{1}{2}$	0.92	0.94
8	Simply supported	Free	$\beta = -\frac{3}{4}$	0.94	0.96
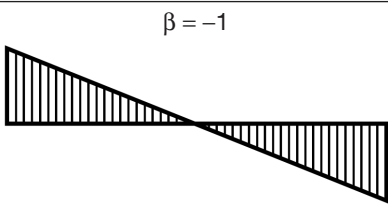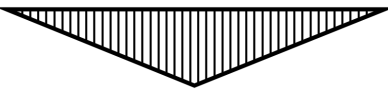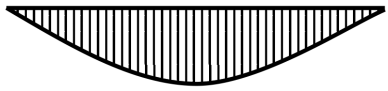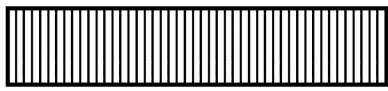
(Table 4 continues on the next page)

The following conclusions are drawn from Figures 3 and 4:

1. The calculated elastic critical LTB capacities for beams in the design code and specifications are typically conservative for torsionally simply supported end conditions, and the conservatism increases with an increase in the gradation of the moment. This is particularly true for the beams subjected to reverse curvature (Cases 6–9 in Figure 3). The elastic critical LTB capacity of a simply supported beam, calculated using the British standard (BS 5950-1, 2000) and the AISC *Specification* (2022) equations are nearly equal, and the maximum conservative strength estimations are 0.81 and 0.80 times $M_{cr,FEA}$, respectively, for Case 8 with an end moment ratio (β) of −0.75.

Case Study No.	Boundary Condition		Bending Moment Diagram	W16×40	W30×90
	Flexure	Warping		$M_{cr,FEA}/M_{cr,energy}$	$M_{cr,FEA}/M_{cr,energy}$
9	Simply supported	Free	$\beta = -1$	0.96	0.97
10	Simply supported	Free		0.93	0.94
11	Simply supported	Free		0.95	0.96
12	Simply supported	Fixed		0.98	0.98
13	Simply supported	Fixed		0.98	0.98
14	Simply supported	Fixed		0.99	0.99
15	Fixed	Fixed		0.97	0.97
16	Fixed	Fixed		0.98	0.98

Table 4. Comparison of the LTB Capacities Obtained from the Energy Method with FE Solutions (continued)

2. The equations in the design code and specifications are overly conservative for beams with warping fixed at both beam ends (by 40–70%), when the comparisons use a *K* of 0.7 in the British standard and 1.0 in the AISC *Specification* equations. The British standard predicts elastic critical LTB capacities as low as 0.6 times those of the FE solutions for flexurally and torsionally fixed beams subjected to a uniformly distributed load (Case 16 in Figure 3). Similarly, the AISC *Specification* elastic critical LTB capacity is significantly conservative for beams with warping-fixed conditions (such as Case 15 in Figure 3), with a strength underestimation of up to 0.4−0.5 times the true solutions.

On the other hand, if the comparison is made by including the true *K* of 0.5 for warping fixed conditions in the AISC *Specification*, such as in conditions with rigid beam-column joints, the strengths may be unconservatively estimated by up to 1.8 times the true strengths.

3. Figures 4(a) and (b) show that Salvadori's equation, although derived for linear moment gradients, conservatively estimates the elastic critical LTB capacity with a ratio of $M_{cr}/M_{cr,FEA}$ equal to 0.82 for Case 8 (with β equal to −0.75). Wong and Driver's equation underestimates the strength, with the smallest value of $M_{cr}/M_{cr,FEA}$ equal to 0.85 for simply supported beams with reverse curvature bending (Cases 8 and 9). Conversely, Wong and Driver's equation overestimates the strength in beams with warping-fixed end conditions,

with the largest $M_{cr}/M_{cr,FEA}$ ratio being 1.35 (in Cases 15 and 16), using $K = 0.5$. On the other hand, using $K = 1.0$ in Wong and Driver's equation for warping-fixed conditions will result in 50–70% conservative estimates of the true capacities. The excessively unconservative or conservative estimates of C_b shows the limitation of Wong and Driver's equation in warping-fixed end conditions.

4. The Nethercot and Rockey solutions estimate values of C_b greater than 3 for beams with warping fixity at their ends. Using $K = 0.5$ will make the equations unconservative, with the maximum value of the $M_{cr}/M_{cr,FEA}$ ratio equaling 3.19. Hence, these C_b factors are used along with an M_{cr} for an effective length factor of 1.0 rather than 0.5 to make the comparisons presented here more realistic. Figures 4(a) and (b) show that the solutions by Nethercot and Rockey (1972), derived for beams subjected to concentrated loads at their mid-spans and uniformly distributed loads, provide a reasonable estimate of M_{cr} for Cases 10 and 11 and Cases 13 and 14. All four of these cases are simply supported in-plane. Cases 10 and 11 are torsionally simply supported, while Cases 13 and 14 are torsionally fixed.

The elastic critical LTB capacities for warping-fixed beams subjected to concentrated loads at their mid-spans are the same despite the difference in their in-plane flexural boundary conditions (i.e., in Cases 13 and 15). Consequently, ascribing the same LTB modification factor to Case 15 as Case 13 appears acceptable. However, the moment capacity of a flexurally and torsionally fixed beam subjected to a uniformly distributed load (Case 16) significantly differs from that of a flexurally simply supported and warping-fixed beam with the same loading scenario (Case 14). Therefore, using the same C_b for Cases 14 and 16 results in significantly conservative estimates of flexural strengths, with a ratio of $M_{cr}/M_{cr,FEA}$ of 0.55, suggesting that Nethercot and Rockey's equations for LTB modification factors for warping-fixed cases are better suited for in-plane simply supported boundary conditions, and are significantly conservative for Case 16, where the I-beam is flexurally fixed in-plane (resulting in reverse curvature, and torsional bracing at the location of the maximum moment within the unbraced span).

5. The equations by Serna et al. (2006) predict strengths that are typically smaller than the FEA results (up to 0.93 times $M_{cr,FEA}$ for simply supported beams with reverse curvature bending with $\beta = -1$, Case 9) and are unconservative (by approximately 10% of the FE solution) for a fully fixed beam subjected to a uniformly distributed load (Case 16). These equations, however, appear to provide the best estimates of C_b for the wide range of ideal loading and boundary conditions, even

while exploiting the enhanced strengths from smaller effective lengths, and will be examined subsequently in this paper for laterally continuous beams.

6. Table 4 indicates that the LTB capacities estimated using the Rayleigh-Ritz method (denoted as the energy method) compare well with the FE results, with a maximum overestimation of 9% of $M_{cr,FEA}$ for a simply supported beam with moment gradient factor β equal to -0.5 (Case 7). These studies show that the energy formulations are most beneficial when applied to simply supported beams subjected to reverse curvature and for beams with warping fixed at their ends.

Impact of C_b on the limiting plateau length and the inelastic flexural strength

Having shown that the AISC *Specification* elastic critical LTB capacity is either overly conservative or unconservative for warping-fixed conditions depending on the assumed K, the import of applying the AISC *Specification* equations using $K = 1$ and 0.5, and C_b as per Equation F1-1 on the inelastic flexural strength and the plateau length is now examined. Figures 5(a) and (b) plot the normalized design strengths (M_n/M_p) for the flexurally and torsionally fixed beams with a concentrated load at the mid-span (Case 15, Table 4), and a uniformly distributed load (Case 16, Table 4) for the W16×40 section. The cross-section L_p is 1.7 m (5 ft 7 in), and $L_r = 7.0$ m (23 ft). These figures show the AISC *Specification* design strengths modified with the C_b as per Equation F1-1 and $K = 1.0$ and 0.5, and the design strengths estimated using the C_b factor derived using the energy method with a $K = 0.5$. On the other hand, the equations for C_b in the AASHTO *Specification* (Equations 6.10.8.2.3-7 and A6.3.3.7) recommend using an LTB modification factor of unity for cases where the compression flange stresses or the bending moments at the braced locations are zero. The AASHTO *Specification* commentary discusses that this would be conservative only in rare cases (in bridge girders) where the span is simply supported with no intermediate cross-frames. Figure 5 shows that using the AISC *Specification* C_b and $K = 1.0$ for warping fixed conditions is already on the safe side. Hence, the comparative study only includes the AISC *Specification* with the understanding that the use of the AASHTO *Specification* (with $K = 1.0$ and $C_b = 1.0$) will lead to still more conservative estimates of the beam capacity.

These plots further show that using a C_b factor as per the AISC *Specification* equation with an effective length factor of 1.0 results in a smaller plateau length and conservative estimates of design strengths when compared with the beam strengths estimated using the C_b factors derived from the energy method. It is important to note that the results presented in the paper are not specific to the two

cross-sections shown, and any doubly symmetric hot-rolled section will produce similar results.

Using an inaccurate C_b along with $K = 0.5$ modifies the design strength curves such that the plateau lengths are 3.0 and 1.25 times those of the design curves obtained using the energy-based C_b factors for Cases 15 and 16, respectively. Furthermore, using an elastic K also inappropriately amplifies the inelastic LTB capacity.

Although the current AISC *Specification* equations sometimes lead to excessively conservative estimates of the flexural strengths when K is taken as 1.0 for warping fixed conditions, the degree of conservatism is such that such a simplification may not be suitable for design purposes. Conversely, using an effective length factor of $K = 0.5$ and the C_b factor from the current AISC *Specification* will result in highly unconservative estimates of flexural strengths. Therefore, any recommendation to use an effective length factor with the current C_b equations must be treated with caution.

APPLICABILITY OF THE LTB MODIFICATION FACTORS TO CONTINUOUS BEAMS

LTB modification factors are hitherto derived for ideal boundary conditions, which are simply supported and fixed flexurally and torsionally. However, even a single-span simply supported girder may have multiple lateral braces. The critical lateral span in such conditions receives partial restraint from its adjacent segments, and hence, the boundary conditions for the critical lateral span lie between the ideal simply supported and fixed conditions. In investigating the appropriate C_b, one must also use an appropriate effective lateral length factor, K. The K calculations in laterally continuous beams are more complex than those discussed with ideal boundary conditions.

Nethercot and Trahair (1976) were the first to suggest a method to estimate the effective length factor for beams, analogous to the buckling of braced columns, by accounting for the restraints from the adjacent spans. John and Subramanian found that the Nethercot and Trahair (N&T) method sometimes predicts significantly conservative or unconservative effective length factors. John and Subramanian contended that (1) the critical lateral span may receive restraint from segments further away from the immediate adjoining segments (the extended restraint effect); (2) the restraint received from the adjoining segment also depends on whether the brace is at the location of the maximum or the minimum moment within the critical span [resolved by the load and boundary condition effect (LBC)]; and (3) there are situations where the N&T method may incorrectly identify the critical lateral span and, thereby, the critical buckling load (resolved by an iteration of the N&T method). Three practical cases with laterally continuous spans are shown in Figure 6, for which the use of the appropriate C_b is discussed in this paper. The LBC interaction method proposed by John and Subramanian (2019) (referred to as J&S in this paper) is used in Cases I and II, while their iteration method is used in Case III.

In calculating M_{cr}, the different C_b formulations are combined with different K estimates. The C_b values from the proposed solutions and Serna et al. (2006) (previously shown to be the best estimates of C_b for a wide range of ideal boundary conditions) are used along with the elastic effective length factors derived using the classical N&T method and the modified method from J&S.

Figure 6 shows the loading and bending moment diagrams for the three cases discussed here. The beam is simply supported in-plane, and the lateral spans are marked as I, II, and III. The example discussed here considers a W30×90 beam section with a critical span length, L, of 6 m

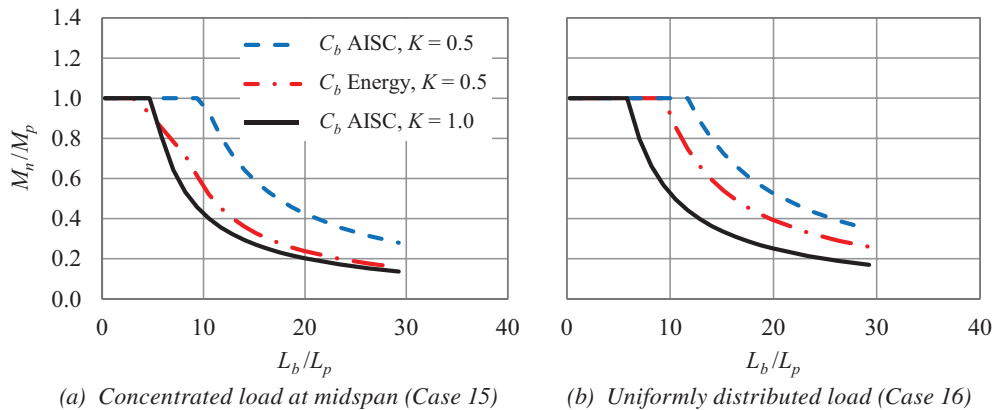(a) *Concentrated load at midspan (Case 15)*   (b) *Uniformly distributed load (Case 16)*

Fig. 5. *Comparison of the design flexural strengths predicted using the* C_b *factors in AISC* Specification *Equation F1-1 and the energy method for warping-fixed conditions for* W16×40 *section.*

(19 ft 8 in). The critical lateral span for this beam geometry in Case I is span I, and in Case II is span II. The critical lateral spans are marked by the hatched bending moment diagrams. The N&T method suggests that span II is critical in Case III, while span III is identified as the critical span using the iteration method (J&S) and FE test simulations. The difference in the critical spans identified by the two methods in Case III may be attributed to the restraint span II would receive at one end from span I, thereby enhancing its buckling strength. The increased elastic critical LTB capacity of span II will also result in greater restraint to the critical segment, span III.

Figure 7 shows the design flexural capacities for the example case by combining each of the two C_b formulations (from Serna et al., 2006, and the C_b evaluated using the energy method) with three different elastic effective length factors ($K = 1$, K from the N&T method, and K from the J&S method). The strengths are normalized by the true strengths from the FE test simulations. These calculations use the appropriate K in the C_b equations by Serna et al. instead of the binary values of 0.5 and 1.0 provided by the authors.

The following conclusions are drawn from Figure 7:

1. The flexural strengths calculated using C_b from the energy method and Serna et al., are conservative by 17–32% if K is taken as 1.0. The more conservative predictions are for Cases II and III, where the critical spans are braced by their adjoining segments at the locations of their maximum bending moments.

2. In Case I, where the adjacent span braces the smaller end moment location of the critical span, the N&T method, when used with the C_b from the energy method and Serna et al., estimates the elastic critical LTB capacities reasonably well. However, in Case II, with the larger end moment at the brace location, the estimated M_{cr} using the N&T method is conservative, with a ratio of $M_{cr}/M_{cr,FEA}$ equal to 0.87 for C_b from the energy method and 0.90 for C_b from Serna et al. In Case III, the estimated strengths exceed the FE solutions by 17% and 26% due to the incorrect identification of the critical span, as noted by John and Subramanian (2019).

3. The modified effective lengths proposed by John and Subramanian, along with the C_b from the energy method, predict the elastic critical LTB capacities with an error of less than 6% of the FE solutions across all cases.
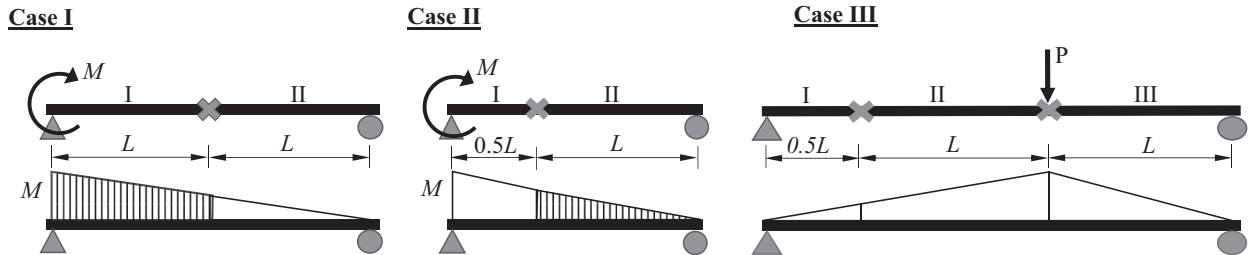

Fig. 6. *Laterally continuous beams, where the critical lateral spans are indicated with a hatched bending moment diagram.*
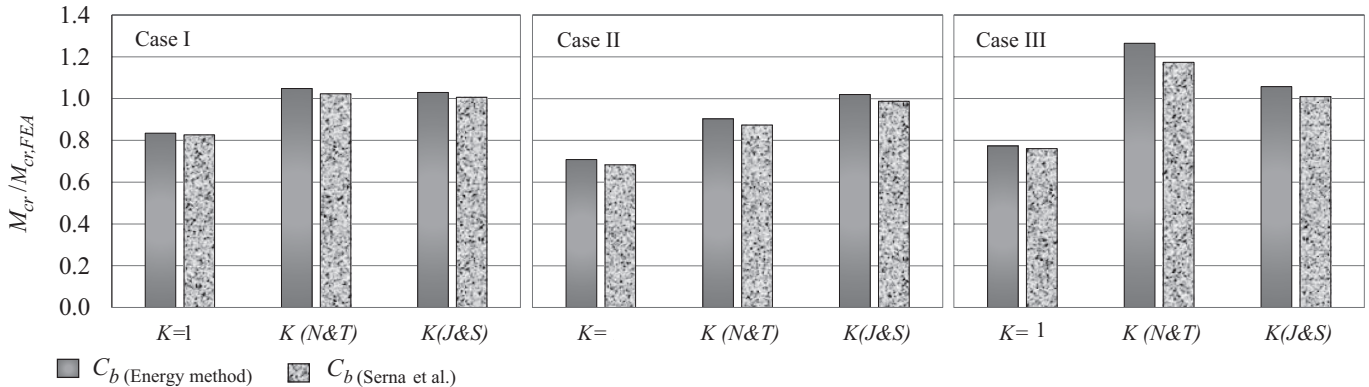

Fig. 7. *Comparison of flexural strengths of the laterally continuous beams in Figure 6 using various* C_b *factors for W30×90, with L = 6 m (19 ft 8 in.)*

4. In lieu of a rigorous formulation from the Rayleigh-Ritz method, the authors suggest using the C_b from Serna et al. (2006) in conjunction with the K from the J&S method, which best predicts the strengths of laterally continuous beams, with an error of less than 2%.

DISCUSSIONS ON PRACTICAL LOADING AND BOUNDARY CONDITIONS

The paper presents the behavior of I-shaped members subjected to transverse loads through the shear center. Many practical loading scenarios on I-section members in steel construction involve top flange loading, whereas gantry girders are typically loaded at their bottom flanges. A transverse load on an unbraced top flange reduces the elastic critical moment, while the load on an unbraced bottom flange increases the buckling moment. In such cases where the top flange is not braced, the load height effect must be considered in addition to the LTB modification factor, as also discussed in the AISC *Specification* Commentary. However, the presence of a concrete slab or deck precludes the tipping effect due to top flange loading. Members with ideal boundary conditions, such as simply supported and fixed flexurally and torsionally, are studied in this paper. The detailing of the beam-to-beam or beam-to-column connections dictates the warping fixity at the beam ends. For example, a simple shear connection is often torsionally simply supported at its ends. However, when a steel beam is encased into a concrete column, the column offers complete fixity against twisting and warping. Similarly, a moment connection offers significant restraint to warping and partially restrains in-plane and out-of-plane bending. Likewise, the secondary beams in a building often provide full or partial restraints to the primary beams at discrete locations, leading to the conditions of laterally continuous spans discussed in this paper. It is clearly important to be cognizant of the various in-plane and out-of-plane restraints that steel detailing provides and apply design equations accordingly.

CONCLUSIONS

This paper reviews the expressions for the LTB modification factor C_b for elastic lateral torsional buckling (LTB) of doubly symmetric I-shaped members in design codes and literature for different loading conditions, and different flexural and torsional boundary conditions. The paper includes combinations of ideal simply supported and fixed boundary conditions for flexure and torsion, as well as intermediate restraint conditions modeled using laterally continuous beams. The empirical equations for C_b are compared with analytical solutions derived by the authors using the Rayleigh-Ritz approach and finite element (FE) solutions. The key findings are summarized here:

1. The current equations in the AISC *Specification* (2022) and the British standard for C_b work well for flexurally and torsionally simply supported beams bending in single curvature, and are mildly conservative for such beams bending in reverse curvature. They are conservative by less than 10% when the beams are subjected to single curvature, and by less than 20% when they are subjected to reverse curvature bending.

2. AISC *Specification* Equation F1-1 is conservative by up to 268% for beams that are torsionally fixed and flexurally either simply supported or fixed, and loaded by a mid-span concentrated load and a uniformly distributed load (i.e., Cases 13–16). The equation is conservative for a beam with warping fixed at its ends and subjected to uniform moment at the ends (Case 12) by up to 72%. This is true if the full unbraced length ($K = 1.0$) is used. Further, the equations are excessively unconservative by up to 84% if an effective length factor of 0.5 is used as suggested in AISC *Specification* Section F1 Commentary. This would not be an ideal design solution for beams with laterally unbraced beams with moment connections at their ends, such as in rigid beam-column joints.

3. An inaccurate C_b results in falsely exaggerated plateau lengths and inelastic LTB capacities, especially when used together with an effective length factor, as discussed in the commentary of the AISC and AASHTO specifications.

4. The efficiency of the C_b factor is further examined using different K factors for laterally continuous beams. The energy method best predicts the moment modification factor, C_b, for ideal boundary conditions, although the C_b formulation from Serna et al. (2006) produces comparable results. However, when used in laterally continuous beams, one also must rely on empirical formulations to calculate the elastic effective length factor, K. For such beams, where the calculations combine an empirical K with a C_b, the authors find that the C_b from the energy method and Serna et al. when used along with the K from John and Subramanian (2019) produce similar results. The comparable predictions may be attributed to the approximate nature of the calculation methods for K. Recognizing the impracticality of the rigorous calculations involved in using the Rayleigh-Ritz approach for design, the authors recommend using the equations by Serna et al. for C_b along with effective length factors calculated using the methods by John and Subramanian.

Although the paper only presents the energy-based solutions for a few select cases, similar displacement shape functions may be used for other loading conditions to obtain the corresponding expressions for the LTB capacities. This offers a more rigorous approach to formulating the LTB

modification factor than empirical fits to numerical data, especially for beams with warping fixity and reverse curvature. The procedure is outlined for a few typical loading and boundary conditions in the Appendix.

Despite the excessively conservative predictions when using the full unbraced lengths, the authors counsel against using an effective length factor for beams with warping restraints with the current C_b equations. The current AISC design equations work well for flexurally and torsionally simply supported laterally unbraced beams subjected to single curvature bending.

SYMBOLS

C_b	Lateral torsional buckling modification factor for nonuniform bending moment diagrams
E	Young's modulus of elasticity of steel, ksi
F_L	Nominal compression flange stress above which the inelastic buckling limit states apply, ksi
F_{yc}	Yield stress of compression flange, ksi
G	Shear modulus of elasticity, ksi
I_w	Warping constant, in.^{4}
I_y	Moment of inertia of the cross section about the minor principal axis, in.^{4}
J	St.-Venant torsional constant, in.^{4}
L, L_b	Lateral unbraced length of the I-beam, in.
K	Elastic effective length factor for lateral torsional buckling
$K_{inelastic}$	Inelastic effective length factor for lateral torsional buckling
L_p	Limiting laterally unbraced length for the limit state of yielding, in.
L_r	Limiting laterally unbraced length for the limit state of inelastic lateral-torsional buckling, in.
M	Bending moment, kip-in.
M_{cr}	Elastic critical lateral torsional buckling moment, kip-in.
$M_{cr,energy}$	Elastic critical lateral torsional buckling moment using the energy method, kip-in.
$M_{cr,FEA}$	Elastic critical lateral torsional buckling moment obtained from finite element simulations, kip-in.
M_n	Nominal flexural strength as per the design specifications, kip-in.
M_{ocr}	Elastic critical lateral torsional moment of beam subjected to uniform moment, kip-in.
M_p	Plastic moment, kip-in.
P	Magnitude of the transverse concentrated load, kips
P_{cr}	Elastic critical buckling load, kips
U	Elastic strain energy of the system
V	Potential of the external forces
u	Lateral/out-of-plane deflection, in.
w	Magnitude of the uniformly distributed load, kip/in.
w_{cr}	Elastic critical buckling load, kip/in.
Π	Total potential of the system
ϕ	Twist of the cross section
β	Ratio of end moments, negative for reverse curvature bending

ACKNOWLEDGMENT

REFERENCES

AASHTO (2020), *LRFD Bridge Design Specifications*, 7th Ed., Washington, D.C.

ABAQUS (2022), *Dassault Systémes*, Waltham, Mass.

AISC (2022), *Specification for Structural Steel Buildings,* ANSI/AISC 360-22, American Institute of Steel Construction, Chicago, Ill.

BS (2000), *Structural Use of Steelwork in Building. Part 1: Code of Practice for Design-Rolled and Welded Sections*, BS 5950-1, British Standards Institute, London, UK.

Galambos, T.V. (1998), *Guide to Stability Design Criteria for Metal Structures*, 5th Ed., John Wiley & Sons, New York, N.Y.

Galambos, T.V. and Surovek, A.E. (2008), *Structural Stability of Steel: Concepts and Applications for Structural Engineers,* Wiley & Sons, New York, N.Y.

John, J.B. and Subramanian, L.P. (2019), "A Modified Approach Towards Estimating the Lateral Torsional Buckling Effective Length," *Proceedings of the Annual Stability Conference*, SSRC, St. Louis, Mo., pp. 623–642.

Kim, Y.D. (2010), "Behavior and Design of Metal Building Frames Using General Prismatic and Web-Tapered Steel I-Section Members," Doctoral Dissertation, Georgia Institute of Technology, Atlanta, Ga.

Kirby, P.A. and Nethercot, D.A. (1979), *Design for Structural Stability*, John Wiley & Sons, New York, N.Y.

Nayak, N., Anilkumar, P.M., and Subramanian, L. (2023), "Rayleigh-Ritz Formulation for Moment Modification Factors on Lateral-Torsional Buckling of I-Beams," *Proceedings of the Annual Stability Conference*, SSRC, Charlotte, N.C., pp. 1–20.

Nethercot, D.A. and Rockey, K.C. (1972), "A Unified Approach to the Elastic Lateral Buckling of Beams," *Engineering Journal,* AISC, Vol. 9, No. 3, pp. 96–107.

Nethercot, D.A. and Trahair, N.S. (1976), "Lateral Buckling Approximations for Elastic Beams," *Structural Engineer*, Vol. 54, No. 6, pp. 197–204.

Salvadori, M.G. (1956), "Lateral Buckling of I-Beams," *Transactions of the American Society of Civil Engineers*, ASCE, Vol. 120, No. 1, pp. 1,165–1,177.

Serna, M.A., López, A., Puente, I., and Yong, D.J. (2006), "Equivalent Uniform Moment Factors for Lateral-Torsional Buckling of Steel Members," *Journal of Constructional Steel Research*, Vol. 62, No. 6, pp. 566–580.

Subramanian, L., Jeong, W.Y., Yellepeddi, R., and White, D.W. (2018), "Assessment of I-Section Member LTB Resistances Considering Experimental Test Data and Practical Inelastic Buckling Design Calculations," *Engineering Journal*, AISC, Vol. 55, No. 1, pp. 15–44.

Subramanian, L. and White, D.W. (2017a), "Reassessment of the Lateral Torsional Buckling Resistance of Rolled I-Section Members: Moment Gradient Tests," *Journal of Structural Engineering*, Vol. 143, No. 4, pp. 04016203.

Subramanian, L. and White, D.W. (2017b), "Reassessment of the Lateral Torsional Buckling Resistance of I-Section Members: Uniform-Moment Studies," *Journal of Structural Engineering*, Vol. 143, No. 3, pp. 04016194.

Timoshenko, S.P. (1936), *Theory of Elastic Stability*, 1st Ed., McGraw-Hill, New York, N.Y.

White, D.W. (2008), "Unified Flexural Resistance Equations for Stability Design of Steel I-Section Members: Overview," *Journal of Structural Engineering*, Vol. 134, No. 9, pp. 1,405–1,424.

White, D.W. and Jung, S. (2008), "Unified Flexural Resistance Equations for Stability Design of Steel I-Section Members: Uniform Bending Tests," *Journal of Structural Engineering*, Vol. 134, No. 9, pp. 1,450–1,470.

White, D.W., Tougay, O., Slein, R., and Jeong, W.Y. (2021), SABRE2, http://www.white.ce.gatech.edu/sabre.

Wong, E. and Driver, R.G. (2010), "Critical Evaluation of Equivalent Moment Factor Procedures for Laterally Unsupported Beams," *Engineering Journal*, AISC, Vol. 47, No. 1, pp. 1–20.

Yoo, C.H. and Lee, S.C. (2011), *Stability of Structures: Principles and Applications*, Elsevier, Oxford.

Yura, J.A. (1995), "Bracing for Stability—State-of-the-Art," *Proceedings of the ASCE Structures Congress XIII*, Boston, Mass., pp. 88–103.

Yura, J.A. and Helwig, T.A. (2010), "Buckling of Beams with Inflection Points," *SSRC Annual Stability Conference,* Orlando, Fla., pp. 761–780.

Ziemian, R.D. (2010), *Guide to Stability Design Criteria for Metal Structures*, 6th Ed., John Wiley & Sons, Hoboken, N.J.

APPENDIX: DERIVATION OF THE C_b FACTOR USING THE RAYLEIGH-RITZ METHOD

Loading type 6: simply supported beam with fork boundary conditions subjected to a concentrated load at the mid-span centroidal axis

The boundary conditions for a simply supported beam are given by

$$u = u'' = \phi = \phi'' = 0 \qquad \text{at } z = 0 \text{ and } z = L \qquad (13)$$

The assumed displacement functions satisfying the above boundary conditions are

$$u = A\sin\frac{\pi z}{L} + B\sin\frac{2\pi z}{L}, \ \phi = C\sin\frac{\pi z}{L} \qquad (14)$$

The bending moment at any section along the length of the beam for a concentrated load P,

$$M_x = \begin{cases} \dfrac{Pz}{2} & 0 \le z \le \dfrac{L}{2} \\[2ex] \dfrac{P(L-z)}{2} & \dfrac{L}{2} \le z \le L \end{cases} \qquad (15)$$

The total potential energy calculated using Equation 6 is given by

$$\Pi = \frac{\pi^4 EI_y(A^2 + 16B^2)}{4L^3} + \frac{\pi^4 EI_w C^2}{4L^3} + \frac{\pi^2 GJC^2}{4L}$$

$$- \frac{(4+\pi^2)PAC}{16} \qquad (16)$$

Differentiating the total energy with respect to the unknowns A, B, and C, the following equations are obtained.

$$\frac{\partial \Pi}{\partial A} = \frac{\pi^4 EI_y A}{2L^3} - \frac{(4+\pi^2)PC}{16} \qquad (17)$$

$$\frac{\partial \Pi}{\partial B} = \frac{8\pi^4 EI_y B}{L^3} \qquad (18)$$

$$\frac{\partial \Pi}{\partial C} = \frac{\pi^4 EI_w C}{2L^3} + \frac{\pi^2 GJC}{2L} - \frac{(4+\pi^2)PA}{16} \tag{19}$$

The total potential being constant, Equations 17–19 are equated to zero.

$$\begin{bmatrix} \dfrac{\pi^4 EI_y}{2L^2} & 0 & -\dfrac{4+\pi^2}{16}P \\[3mm] 0 & \dfrac{8\pi^4 EI_y}{L^3} & 0 \\[3mm] -\dfrac{4+\pi^2}{16}P & 0 & \dfrac{\pi^4 EI_w + \pi^2 GJL^2}{2L^3} \end{bmatrix} \begin{Bmatrix} A \\ B \\ C \end{Bmatrix} = 0$$

The solution for the elastic critical buckling load, P_{cr}, can be obtained by evaluating the determinant of the above matrix.

$$P_{cr} = \frac{8\pi^2}{L(\pi^2+4)} \sqrt{\frac{\pi^2 EI_y}{L^2}\left(\frac{\pi^2 EI_w}{L^2}+GJ\right)} \tag{20}$$

Now from the elastic critical lateral torsional buckling moment can be estimated using the expression $M_{cr} = \dfrac{P_{cr}L}{4}$

$$M_{cr} = 1.42 \sqrt{\frac{\pi^2 EI_y}{L^2}\left(\frac{\pi^2 EI_w}{L^2}+GJ\right)} \tag{21}$$

The LTB modification factor, C_b, is estimated as the ratio of M_{cr} given in Equation 21 and M_{ocr} (Equation 1) resulting in a value of 1.42.

Loading type 9: flexurally and torsionally fixed beam subjected to uniformly distributed load along the centroidal axis

The boundary conditions for a flexurally and torsionally fixed beam are given by

$$u = u' = \phi = \phi' = 0 \qquad \text{at } z = 0 \text{ and } z = L \tag{22}$$

The assumed displacement functions satisfying the above boundary conditions are

$$u = A\left(1-\cos\frac{2\pi z}{L}\right) + B\left(1-\cos\frac{4\pi z}{L}\right), \ \phi = C\left(1-\cos\frac{2\pi z}{L}\right) \tag{23}$$

The bending moment at any section along the length of the beam for a uniformly distributed load w per unit length,

$$M_x = \frac{w}{12}\left(6Lz - L^2 - 6z^2\right) \tag{24}$$

The total potential energy calculated using Equation 6 is given by

$$\Pi = \frac{4\pi^4 EI_y(A^2 + 16B^2)}{L^3} + \frac{4\pi^4 EI_w C^2}{L^3} + \frac{\pi^2 GJC^2}{L} \\ - \frac{7LACw}{8} + \frac{11LBCw}{9} \tag{25}$$

Differentiating the total energy with respect to the unknowns A, B and C, the following equations are obtained.

$$\frac{\partial \Pi}{\partial A} = \frac{8\pi^4 EI_y A}{L^3} - \frac{7LCw}{8} \tag{26}$$

$$\frac{\partial \Pi}{\partial B} = \frac{128\pi^4 EI_y B}{L^3} + \frac{11LCw}{9} \tag{27}$$

$$\frac{\partial \Pi}{\partial C} = \frac{8\pi^4 EI_w C}{L^3} + \frac{2\pi^2 GJC}{L} - \frac{7LAw}{8} + \frac{11LBw}{9} \tag{28}$$

The total potential being constant, Equations 26–28 are equated to zero.

$$\begin{bmatrix} \dfrac{8\pi^4 EI_y}{L^3} & 0 & -\dfrac{7Lw}{8} \\[3mm] 0 & \dfrac{128\pi^4 EI_y}{L^3} & \dfrac{11Lw}{9} \\[3mm] -\dfrac{7Lw}{8} & \dfrac{11Lw}{9} & \dfrac{8\pi^4 EI_w + 2\pi^2 GJL^2}{L^3} \end{bmatrix} \begin{Bmatrix} A \\ B \\ C \end{Bmatrix} = 0$$

The solution for the elastic critical buckling load, w_{cr}, can be obtained by evaluating the determinant of the above matrix.

$$w_{cr} = \frac{144\pi^2}{\sqrt{4453}L^2} \sqrt{\frac{\pi^2 EI_y}{(0.5L)^2}\left[\frac{\pi^2 EI_w}{(0.5L)^2}+GJ\right]} \tag{29}$$

Now, the elastic critical lateral torsional buckling capacity can be estimated using the expression $M_{cr} = \dfrac{w_{cr}L^2}{12}$

$$M_{cr} = 1.77 \sqrt{\frac{\pi^2 EI_y}{(0.5L)^2}\left[\frac{\pi^2 EI_w}{(0.5L)^2}+GJ\right]} \tag{30}$$

The LTB modification factor, C_b, is estimated by taking the ratio of M_{cr} given in Equation 28 and M_{ocr} for warping-fixed condition (Equation 1) with effective unbraced length $0.5L$, resulting in a value of 1.77.

Tensile Coupon Testing and Residual Stress Measurements of High-Strength Steel Built-Up I-Shaped Sections

KARA STALL, ANDREA CULHANE, LIKUN SUN, RACHEL CHICCHI CROSS, and MATTHEW STEINER

ABSTRACT

High strength structural steels (with yield stresses greater than 65 ksi) may have notably different material characteristics when compared to structural steels conventionally used in building construction [i.e., ASTM A992/A992M (2022) or A572/A572M Gr. 50 (2021)]. This paper presents findings from an experimental program that investigated the material characterization of ASTM A656/A656M Gr. 80 (2024) plate steel. The results obtained were compared to conventional ASTM A572/A572M Gr. 50 steel. Two types of testing were performed for this work: tensile coupon testing and residual stress testing. The tensile coupon testing was carried out for both the A656/A656M Gr. 80 and A572/A572M Gr. 50 plate material. The A656/A656M Gr. 80 plate material showed more variation between the two different plate thicknesses in both mechanical behavior and microstructure due to differences in steel production. The 0.375 in. thick plate exhibited a clear yield plateau with an ultimate/yield stress ratio similar to the Gr. 50 material. In contrast, the 0.5 in. plate did not have a yield plateau and reached lower ultimate strain. The residual stress testing was performed using a sectioning technique for one A572/A572M Gr. 50 and five A656/A656M Gr. 80 built-up sections that were fabricated from 0.5 in. and 0.375 in. plate material. Residual stresses obtained from measurements were compared to previously published predictive models. The ECCS model (ECCS, 1984) and BSK99 (Boverket, 2003) models were found to be reasonable predictors of residual stresses for all specimens except the one section fabricated from 0.5 in. thick Gr. 80 plate. When comparing the Gr. 50 and Gr. 80 specimens of the same cross-sectional geometry, the residual stresses were similar, implying that cross-sectional geometry is more prevalent than the nominal yield stress in determining residual stresses in built-up I-sections.

Keywords: high strength structural steel, mechanical properties, residual stress, built-up sections.

INTRODUCTION

High-strength structural steel (HS3) is being classified as any structural grade of steel with a yield stress, F_y, greater than or equal to 65 ksi (450 MPa). These higher strengths can be achieved through alloying, quenching and tempering, or thermo-mechanically controlled processing. Implementation of these high-strength steels has become increasingly popular in international markets, such as Europe and Asia; however, the United States has been slower to adopt their use. In 2019, the AISC Ad Hoc Task Group on High-Strength Steel published a final report (AISC, 2019) that discussed the benefits of HS3, paths forward for implementation into the AISC *Specification for Structural Steel Buildings* (AISC, 2022), hereafter referred to as the AISC *Specification*, and possible barriers that could block adoption of HS3 in the U.S. market.

Currently, select rolled shapes can be produced up to a yield stress of 80 ksi [ASTM A913/913M, Gr 80 (2019)] and plate material can be produced up to approximately 130 ksi. Although U.S.-based steel producers are capable of producing these HS3 products, a lack of guidance and standards has seemingly kept designers from implementing HS3 into their building designs, which has in turn limited the production of the material. This work is the beginning of a U.S.-based effort to study and promote the use of high-strength steel in buildings through better understanding of its behavior and realizing the potential of these materials.

One of the primary advantages of using HS3 in building applications is a potential reduction in steel tonnage when compared to the more conventional steel grades being used today. A higher yield strength may allow section sizes to be reduced and lead to material cost savings, faster

Kara Stall, PE, Graduate Research Assistant, Department of Civil and Architectural Engineering and Construction Management, University of Cincinnati, Cincinnati, Ohio. Email: pradzika@mail.uc.edu

Andrea Culhane, Graduate Research Assistant, Department of Civil and Architectural Engineering and Construction Management, University of Cincinnati, Cincinnati, Ohio. Email: clark3an@mail.uc.edu

Likun Sun, Graduate Research Assistant, Department of Mechanical and Materials Engineering, University of Cincinnati, Ohio. Email: sunlk@mail.uc.edu

Rachel Chicchi Cross, PhD, SE, Assistant Professor, Department of Civil and Architectural Engineering and Construction Management, University of Cincinnati, Cincinnati, Ohio. Email: rachel.cross@uc.edu (Corresponding)

Matthew Steiner, PhD, Assistant Professor, Department of Mechanical and Materials Engineering, University of Cincinnati, Ohio. Email: matt.steiner@ucmail.uc.edu

erection times, reductions in foundation size, and reduced carbon emissions. ArcelorMittal has reported weight savings of 30% for columns that use Gr. 80 high-strength steel relative to conventional Gr. 50 steel. It also demonstrated potential fabrication cost savings of up to 46% when rolled high-strength steel shapes can be used in lieu of Gr. 50 built-up members that may be needed for very large loads (ArcelorMittal, 2019).

The mechanical properties of conventional (low carbon and/or high strength-low alloy) structural steel vary from HS3. A previous study completed by Ban et al. (2011) found that as the yield strength of the steel increased, the length of its yield plateau decreased until it completely disappeared in ultra-high-strength steels. This study also concluded that the value of ultimate strain decreased, and the yield/tensile ratio approached a value of 1.0 as the strength of the material increased. This can be seen in Figure 1, where an increase in material strength is generally accompanied by shorter strain-hardening regions, rupture at lower strain values, and a reduction in ductility. For some materials, an increase in material strength may also be accompanied by an elimination of the yield plateau within the stress-strain curve. However, the modulus of elasticity is unchanged; thus, to be utilized most effectively, HS3 should be used for force-controlled members instead of deflection-controlled members. It is important to note that while higher yield materials tend to see a reduction in ductility, this is due to specific processing choices and, if desired, higher yield materials can be produced with similar ductility properties to more conventional strength steels.

Residual stresses are formed in built-up sections due to uneven cooling during rolling of the individual plates and uneven heating during the welding process. Because residual stresses can greatly influence the behavior of a member, researchers have studied the stress distribution within steel sections, but work is needed to further evaluate built-up high-strength steel sections.

Several studies have been completed to investigate residual stresses in high-strength steel built-up members, and a summary of their results can be found in Table 1. Early research work by Rasmussen and Hancock (1995) found the average compressive stresses in the flanges and webs of S690 built-up sections to be $0.2F_y$ and $0.05F_y$, respectively. A study by Beg and Hladnik (1996) found that compressive residual stresses in the flanges of 700 MPa (100 ksi) built-up members ranged from 0.09–$0.14F_y$. Studies by Ban et al. (2013) and Wang et al. (2012) conducted on 460 MPa (65 ksi) built-up I-sections found that average compressive residual stresses in the flanges increased as the sections became more compact. Testing completed by Liu (2017) found that residual stresses in S690 (100 ksi) built-up sections were "proportionally less" when compared to the residual stresses in S355 (50 ksi) members. This finding was also observed by Schaper et al. (2022), who studied residual stresses in cross sections fabricated from S355 (50 ksi) and S690 (100 ksi) steel material. They found that the cross-sectional geometry has a much larger influence on the residual stresses than the material strength. Specifically, they found that narrower flanges led to higher compressive residual stresses, and thinner flanges caused larger tensile stresses at the mid-point of the flanges.

Another study was completed by Simoes da Silva et al. (2021), and results were published in a report by STROnger steels in the Built Environment (STROBE.) This study measured residual stresses in the flanges and webs of built-up I-shaped sections consisting of S690 (100 ksi) and S460 (65 ksi) steel material. Results from this study found that maximum tensile stresses in the flanges were comparable to European Convention for Constructional Steelwork (ECCS, 1984) recommended values, but the measured
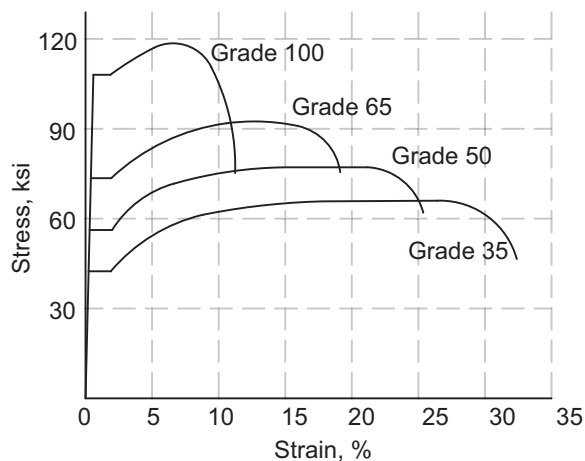

Fig. 1. Comparison of stress-strain relationships for different steel grades (NSC, 2015).

Table 1. Residual Stress Values from Literature							
Reference	Specimen	Steel Strength MPa	Specimen Thickness (nominal)		Average Compression Stress		Peak Tension Stress
			Web mm	Flange mm	Web MPa	Flange MPa	Flange MPa
Rasmussen and Hancock (1995)	N/A	690	8	8	32	135	NR
Beg and Hladnik (1996)	B	700	10	12	NR	73	NR
	D		10	12		123	
Ban et al. (2013)	RI1-460	460	10	10	233.9	276.6	277.5
	RI2-460		10	10	208.4	206.5	317.1
	RI3-460		14	14	123.7	93.0	254.9
	RI4-460		10	10	213.8	163.8	337.0
	R15-460		12	12	65.2	50.9	153.6
	RI6-460		10	12	74.9	80.4	135.8
	RI7-460		10	12	91.4	78.0	189.9
	RI8-460		10	10	142.2	190.6	301.2
Wang et al. (2012)	R-H-3	460	11	21	69.9	187.7	477.9
	R-H-5		11	21	108.1	124.7	414.0
	R-H-7		11	21	60.3	89.7	336.3
Liu (2017)	C1R-A	690	6	10	98.1	206.1	357
	C2R-A		6	10	75.9	214.1	452
	C3R-A		10	16	138.0	138.0	368
	C4R-A		10	16	133.4	120.3	354
Wang (2018)	B2	690	6	10	116	157	400
	B4		6	16	68	67	111
	B6		6	10	126	138	453
Schaper et al. (2022)	1fy	460	8	20	45.9	59.8	329
	3-1fy	460	8	20	46.1	104.2	329
Simoes de Silva (2021)	C1	690	8	8	170	42	336
	C2	690	8	8	235	156	336
	C3	690	8	16	150	116	484
	C4	690	8	16	112	85	237
	B1	460	8	16	101	75	228
	B2	690	8	16	80	63	277
	B3	460	10	16	20	83	118
	B4	460	8	16	107	57	310
	B5	690	8	16	69	53	357
	B6	460	9	15.5	160	32	113
	B7	690	8	16	72	83	339
	BC-1	690	8	16	87	72	145
NR = Not reported							

Table 2. Tensile Coupon Test Matrix	
Plate Material and Thickness	**Number of Tests**
A572-50_0.375 in.	12 (6L and 6T)
A572-50_0.5 in.	12 (6L and 6T)
A656-80_0.375 in.	12 (6L and 6T)
A656-80_0.5 in.	12 (6L and 6T)
L = Longitudinal direction, T = Transverse direction	

average compressive stresses were higher than the ECCS values. The higher compressive stresses were attributed to the measured tensile residual stresses at the flange tips due to the plates being flame cut during the fabrication process.

This paper focuses on the stress-strain behavior and residual stresses of built-up I-shape sections using ASTM A656/A656M Gr. 80 (2024) material, hereafter referred to as A656-80, relative to conventional ASTM A572/A572M Gr. 50 (2021) material, hereafter referred to as A572-50. A656 steel is commonly used for applications such as construction equipment, crane booms, heavy vehicle frames, and rail cars; while it may be useful in building applications, it is not currently included as a listed material in the AISC *Specification* (AISC, 2022). A656-80 material was used due to material availability at the time of the study and even though it is not typically used for building applications, it does have a comparable yield/tensile ratio and elongation value when compared to A913/A913M Gr. 80 steel, hereafter referred to as A913-80. Both A656 and A913 materials are high-strength low-alloy products, but A913 is specifically produced by quenching and self-tempering. A656 also has a thickness limit of 1 in. for its Gr. 80 material.

TENSILE COUPON TESTING

A total of 48 coupon tests were performed in this experimental program. The test matrix is shown in Table 2, which shows a combination of A572-50 and A656-80 plate in thicknesses of 0.375 in. and 0.5 in. The coupon specimens and testing protocols conformed to the ASTM A370-20 specification (ASTM, 2020) for subsize specimens. Each of the coupons were cut with a waterjet cutting machine in both the longitudinal and transverse directions relative to the rolled direction of the plate. The coupons were unfortunately returned unmarked, so the differentiation of rolling direction could not be determined. However, the data collected was very similar, so it is presumed that there was little to no difference between the longitudinal and transverse coupons.

A hydraulic-controlled Material Testing Systems (MTS) machine with wedge grips and an axial load capacity of 22 kips was used to perform the tensile coupon tests. An extensometer with a gage length of 1 in. was attached to the coupon specimens during testing to collect strain data. To avoid any possible damage to the extensometer at rupture, the testing program was set to be force controlled during the elastic region and then shifted to displacement controlled during the inelastic region. The testing program for the A656-80 coupons started as force controlled at 1 kip/min up to a maximum of 5 kips, and then switched to displacement controlled at a rate of 0.1 in/min to a maximum of 0.5 in. The testing program for the A572-50 coupons used the same force and displacement loading rates as the A656-80 tests with maximums of 3.5 kips and 0.65 in., respectively. Figure 2 shows the tensile coupon test setup with the extensometer attached at the center of the tensile specimen.

Tensile Coupon Testing Results

Table 3 reports the average modulus of elasticity, E, yield stress, F_y, yield strain, ε_y, tensile stress, F_u, tensile strain, ε_u, and strain at fracture, ε_f, measured for each of the plate material types and thicknesses. The 2% offset method was used to calculate the yield stress of each coupon. The standard deviation among the 12 tests for each category is provided in parentheses. As expected, the modulus of elasticity was comparable among the four-test series. The ratio F_y/F_u provides an indication of the material overstrength; the 80 ksi material exhibited ratios closer to 1.0. The strain hardening region, as demonstrated by the ratio $\varepsilon_u/\varepsilon_y$, was shorter for the 80 ksi material. The Gr. 80 material also exhibits lower ductility overall, as evidenced by the ratio $\varepsilon_f/\varepsilon_y$.

Figure 3 shows full stress-strain curves for each series of the material types and thicknesses that were tested. The graph presents the stress-strain curves for each of the 12 tests per material and thickness type. In order to avoid damaging the extensometer during testing, it was removed from

Table 3. Measured Material Properties from Tensile Coupon Tests[a]								
Plate Material	E ksi	F_y ksi	F_u ksi	ε_y %	ε_u %	ε_f %	F_y/F_u	$\varepsilon_u/\varepsilon_y$	$\varepsilon_f/\varepsilon_y$
50 ksi 0.375 in.	28695 (460)	63.2 (1.00)	72.6 (0.84)	0.42 (6.8E-3)	15.5 (1.09)	28.4 (1.17)	0.87	36.9	67.6
50 ksi 0.5 in.	28282 (579)	58.1 (0.73)	71.8 (0.60)	0.41 (6.8E-3)	17.8 (0.57)	30.6 (0.89)	0.81	43.4	74.6
80 ksi 0.375 in.	29058 (959)	98.9 (0.89)	110.4 (0.51)	0.55 (7.8E-3)	12.2 (0.33)	22.9 (0.58)	0.90	22.2	41.6
80 ksi 0.5 in.	27846 (443)	83.9 (0.59)	92.1 (1.33)	0.50 (6.7E-3)	8.36 (0.35)	19.4 (1.03)	0.91	16.7	38.8
[a] Standard deviation among coupon test results is listed in parentheses								

Fig. 2. Tensile coupon test setup.

the specimen at approximately 10–15% elongation of the coupon. Strains beyond approximately 10–15% were calculated based on the recorded displacement of the test frame.

It can be seen from Figure 3 that there was not a significant deviation in recorded stress among each test within the series. The strain at rupture was more variable within each test series. The A572-50 plate material produced very similar behavior for both the 0.5 in. and 0.375 in. plate material, while the A656-80 curves have a much more significant variation between the two thicknesses. The A656-80 0.5 in. plate exhibited almost no yield plateau, and its yield stress was much lower than the 0.375 in. plate. In contrast, despite its high strength, the A656-80 plate with 0.375 in. thickness behaved like more conventional steels with an established yield plateau and with comparable ductility and ultimate/yield stress ratios.

The differences between the Gr. 80 stress-strain curves for the 0.375 in. and 0.5 in. materials can be attributed largely to microstructural differences between the two plates, as these materials were produced by different steel producers. Table 4 shows the mill-certified chemical compositions for each of the plate materials that were tested. Comparing the A656-80 0.5 in. plate to the A656-80 0.375 in. plate, there are differences, but no major outliers, in the minor alloying elements added to provide higher strength and greater toughness. The microstructures of the two Gr. 80 plates, however, are significantly different from each other and explain the variation in mechanical behavior.

Analyses of Steel Microstructures

Samples from each plate along each of the three primary directions (rolling, transverse, plate normal) were sectioned and prepared to a mirror finish using standard metallographic techniques, then etched (2% nitric acid in methanol) to reveal both the ferritic grain boundaries and carbides under optical microscopy. The 0.375 in. Gr. 80 plate exhibits a nearly homogenous microstructure of both equiaxed
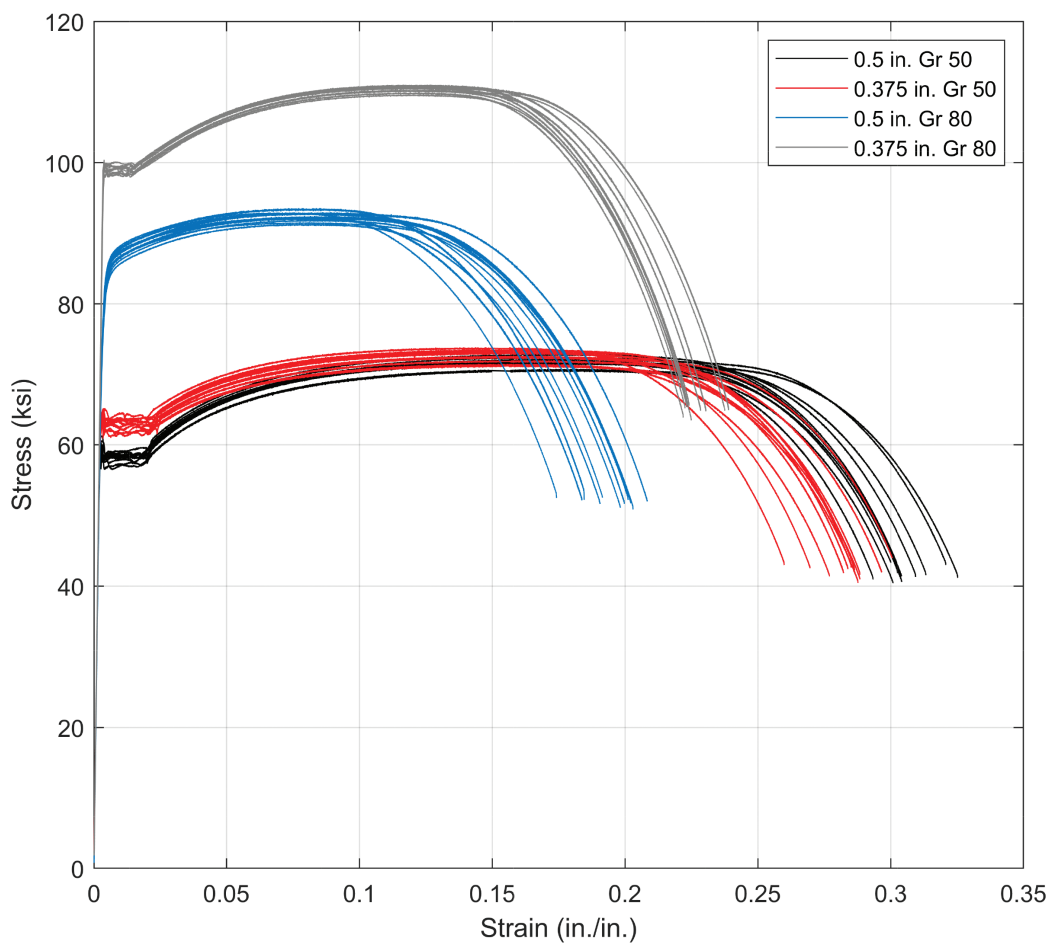

Fig. 3. Measured engineering stress-strain curves for each plate type.

Table 4. Plate Chemical Compositions					
	A572-50 0.375 in. PL %	A572-50 0.5 in. PL (1)[a] %	A572-50 0.5 in. PL (2)[a] %	A656-80 0.375 in. PL %	A656-80 0.5 in. PL %
C	0.04	0.06	0.06	0.06	0.07
Mn	0.8	0.82	0.83	1.45	1.48
P	0.01	0.012	0.014	0.014	0.013
S	0.002	0.007	0.006	0.004	0.003
Si	0.05	0.02	0.02	0.02	0.1
Al	0.023	0.038	0.039	0.028	0.043
Cu	0.08	0.13	0.13	0.1	0.02
Ni	0.03	0.05	0.05	0.05	0.01
Cr	0.08	0.07	0.09	0.06	0.04
Mo	0.02	0.02	0.02	0.09	—
Sn	0.005	0.03	0.03	0.006	0.001
Ti	0.001	0.002	0.002	0.106	0.07
V	0.002	0.002	0.003	0.007	0.003
Nb	0.047	0.024	0.026	0.034	0.032
N	0.008	0.007	0.008	0.0109	0.0048
B	0.0003	0.0001	0.0001	0.0007	0.0002
Ca	0.002	0.0026	0.0023	0.0007	0.0014
Zr	0.0003	—	—	—	—
Sb	—	0.001	0.001	—	0.001

[a] A572-50 0.5 in. plate material came from two different heats and, thus, the two different chemistries shown in the table for this plate type. All other plate types were from a single heat.

and acicular ferrite with a fine grain size and a uniform distribution of carbides (Figure 4). In contrast the 0.5 in. Gr. 80 plate presents a more conventional rolled microstructure with larger ferrite grains found in bands and elongated along the rolling direction (RD), interspersed with lamellar pearlite colonies (dark regions) in addition to the smaller carbides. Based upon these microstructures, it is clear that the two plates, sourced from different suppliers, were likely produced via different methods. The refined polygonal ferrite grains, acicular ferrite, and fine dispersed precipitates of the 0.375 in. Gr. 80 plate are consistent with what would be expected to be produced via a thermo-mechanically controlled process (TMCP) or similar processing route (Sampath, 2005). The 0.5 in. Gr. 80 plate with the banded structure of elongated grains and pearlitic colonies appears to have been controlled rolled and differs from the 0.5 in. Gr. 50 plate primarily in having a smaller grain size and a narrower grain size distribution (Figure 5). Consistent with the mechanical behavior in Figure 3, the microstructure of the 0.375 in. Gr. 80 would be expected to exhibit both a

higher yield strength and improved toughness compared to the microstructure of the 0.5 in. Gr. 80 plate.

Results from the microstructure analysis leads to the important conclusion that just knowing the yield strength of the material and its chemical composition may not be enough to accurately predict the material behavior. It will become increasingly important to understand how different rolling processes will affect the microstructure of the steel and ultimately material behavior, especially if different processes will result in such a large difference in material properties.

RESIDUAL STRESS TESTING

Experimental Test Specimens

Six built-up I-shaped specimens were fabricated from 0.375 in. and 0.5 in. thick Gr. 50 and Gr. 80 plate material in order to measure residual stresses. The plates were cut to size using waterjet cutting and then fillet-welded using automated welding collaborative robots. Five different

cross sections were fabricated using Gr. 80 steel and one section was fabricated with Gr. 50 steel in order to provide a comparison between the two materials. These sections and others are to be subjected to stub column testing in the future. The cross sections used in this study were admittedly small due to plate availability and limitations with the testing equipment available to apply adequate compressive load during column testing. Yet, they provide a valuable comparison between the conventional Gr. 50 material and the higher strength material.

Table 5 and Figure 6 display the section properties and dimensions of each built-up section using the naming convention "I nominal yield strength–b/t ratio–h/t ratio." The ratios, b/t and h/t, reflect the slenderness of the flange and web elements, respectively, by calculating the width, b or h, divided by the thickness, t. The cross-sectional slenderness
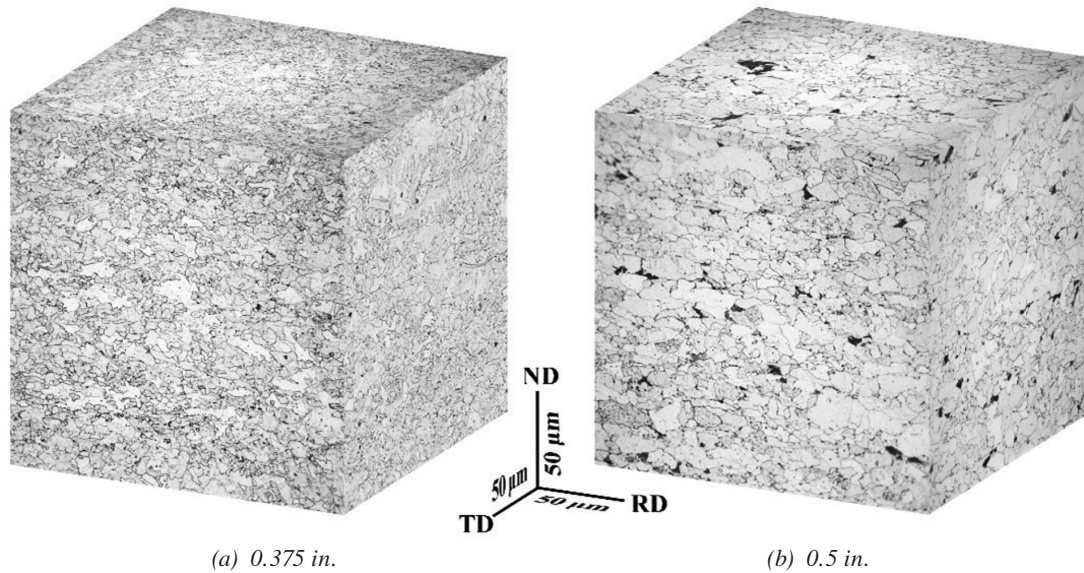
(a) 0.375 in.   *(b) 0.5 in.*

Fig. 4. Psuedo-3D microstructural reconstructions of the. Gr. 80 plates (RD = rolling direction, TD = transverse direction, ND = normal direction).
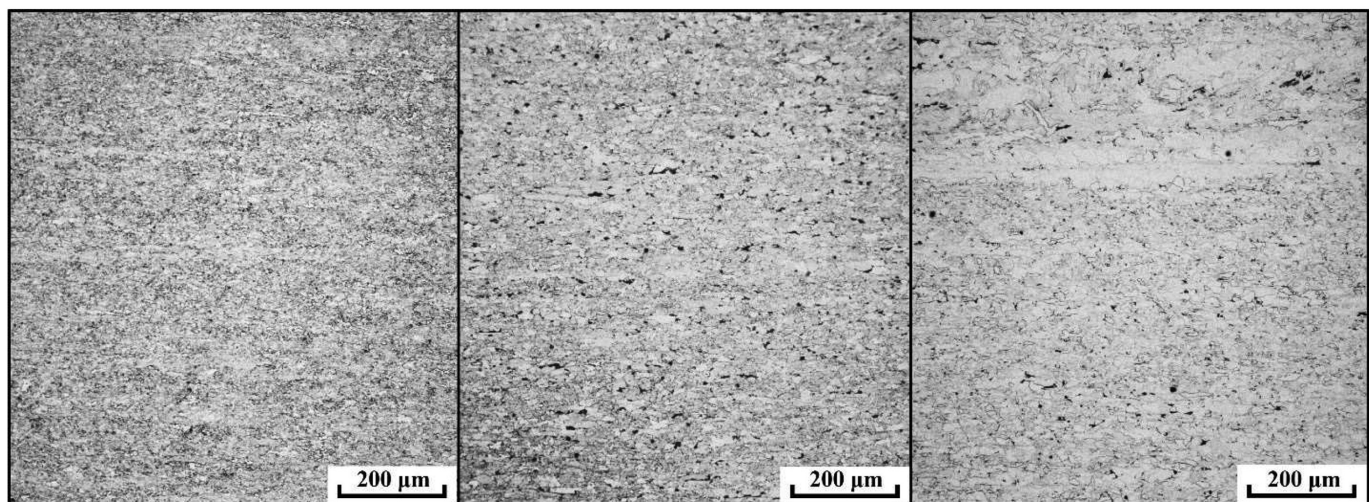
(a) 0.375 in. Gr. 80   *(b) 0.5 in. Gr. 80*   *(c) 0.375 in. Gr. 50*

Fig 5. Microstructural cross sections of the plates (RD = rolling direction, TD = transverse direction, ND = normal direction).

Table 5. Specimen Section Properties									
Specimen Name[a]	F_y ksi	Length in.	b in.	h in.	t in.	b/t	h/t	λ_{rf}[b]	λ_{rw}[c]
I 80-5.3-32	80	48	2	12	0.375	5.3	32.0	10.2	28.4
I 80-9.3-28	80	43.5	3.5	10.5	0.375	9.3	28.0	10.6	28.4
I 80-10.7-21.3	80	36	4	8	0.375	10.7	21.3	10.6	28.4
I 80-10.7-32	80	48	4	12	0.375	10.7	32.0	10.2	28.4
I 80-4-24	80	48	2	12	0.5	4.0	24.0	10.6	28.4
I 50-10.7-32	50	48	4	12	0.375	10.7	32.0	13.0	35.9

a Specimen naming convention: I "steel grade" – "b/t ratio" – "h/t ratio"
b λ_{rf} limiting ratios were calculated from AISC *Specification* Table B4.1a for Case 2 (flanges of I-shaped built-up sections).
c λ_{rw} limiting ratios were calculated from AISC *Specification* Table B4.1a for Case 5 (webs of I-shaped built-up sections).

limiting ratios, λ_{rf} and λ_{rw}, shown in Table 5 were calculated from AISC *Specification* Table B4.1a. It is important to note that the applicability of these equations have not yet been evaluated for Gr. 80 steel but will be explored in the future stub column testing of these specimens. Efforts were made to select cross-sections of various slenderness ratios relative to the slenderness limiting ratios. The Gr. 50 specimen had the same cross section as one of the Gr. 80 specimens.

Residual Stress Measurement Procedure

Residual stress testing was performed on six specimens and was completed using the sectioning technique outlined in Technical Memorandum No. 6 of the Structural Stability Research Council (SSRC) *Guide to Stability Design* (Ziemian, 2010). This common sectioning approach assumes for simplicity that transverse stresses in the specimen are negligible. The residual stress specimens were fabricated to

the lengths shown in Table 5, which conform to the SSRC *Guide*. A 12 in. test piece was then marked at the center of each specimen as shown in Figure 7. The test piece was then marked into 0.5-in.-wide strips along the top and bottom flanges and the web. Using a mill, holes were drilled into each test strip, 1 in. from each end, which provided a gauge length of 10 in.

Initial measurements between the holes were taken using a gauge similar to a Wittemore strain gauge, shown in Figure 8. This gauge has a tolerance of 0.0001 in. and a nominal gauge length of 10 in. When taking measurements, the gauge is used to measure the reference bar before and after each set of measurements. If the reference bar measurements vary by more than 0.001 in, then the temperature has changed, and the measurement set would need to be repeated.

After the collection of all initial measurements, the specimens were cut down using a waterjet. The waterjet was
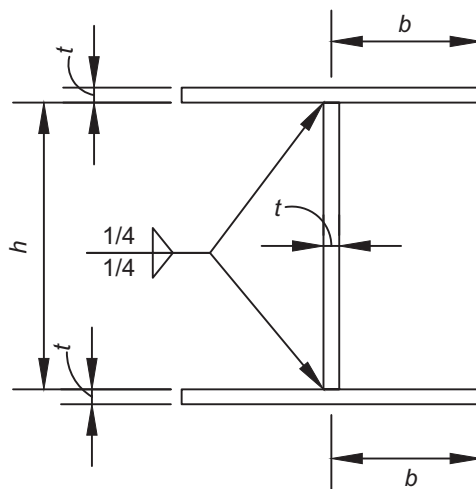

Fig. 6. Geometric dimensions.

used to minimize the amount of heat and stress that would be added to the specimen. The test piece was first cut from the full-length specimen, and then the test piece was cut down into its three main components (top flange, bottom flange, and web). Each component was then cut into its marked 0.5 in. strips. Figure 9 shows a fully sectioned test piece. Once the test piece had been fully sectioned into the 0.5 in. strips, all pieces were dried off and left overnight to come to room temperature. The final gauge length measurements were taken and followed the same procedure that was used for the initial measurements. The change in deformation recorded from the measurements was then converted into stresses using Hooke's law.

Due to limitations with the waterjet nozzle, the test strips at the flange-web interface were L-shaped, as shown in Figure 10, with an approximate thickness of 1 in. The final gauge length measurements were first taken when the strips were in this configuration. The excess material (weld and web) was then removed using a vertical band saw and mill, and measurements were taken again. Both sets of results are presented.

Residual Stress Results

The residual stress results that are presented in this section have been compared with previously published predictive models. The comparison models chosen for this work are
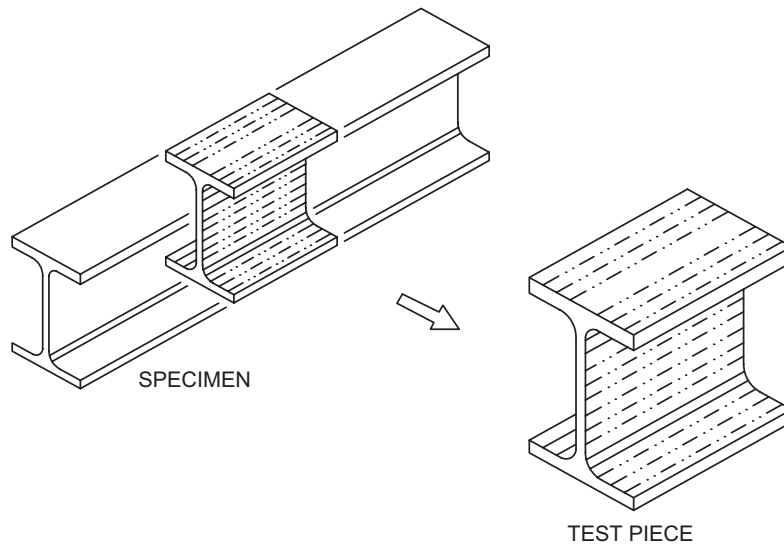

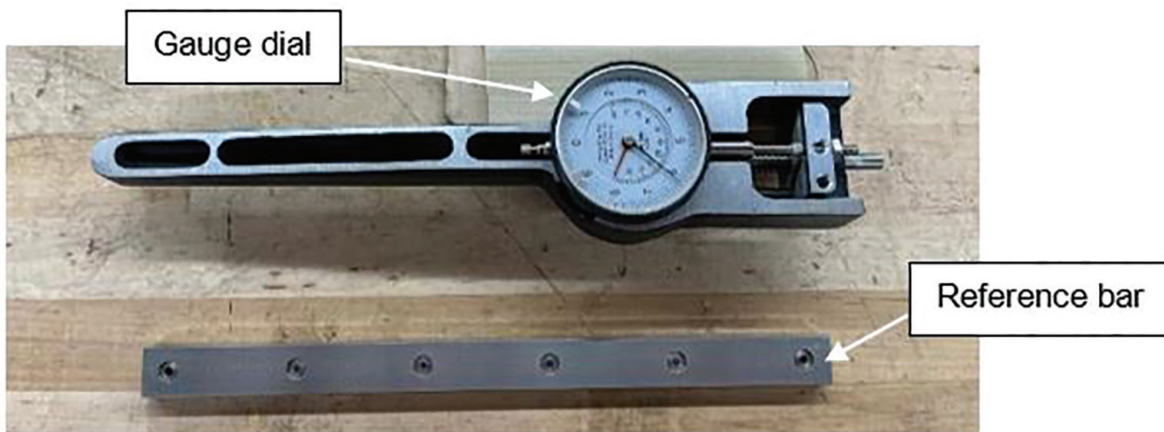*Fig. 7. Residual stress sectioning method schematic (Ziemian, 2010).*
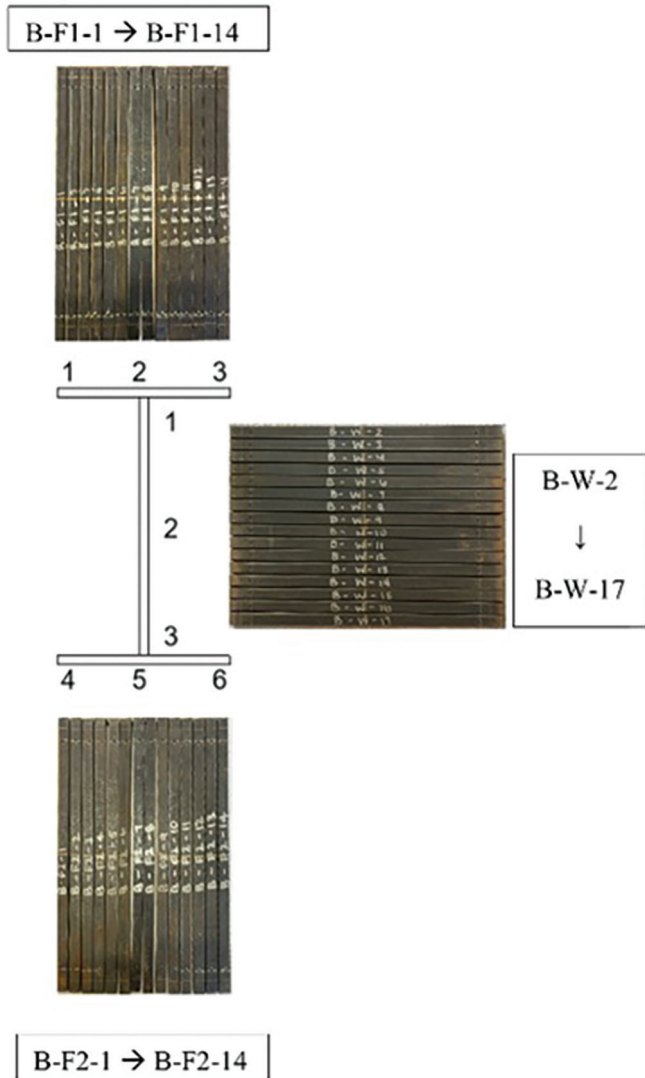

Fig. 8 Gauge to measure strain.

Fig. 9. Fully sectioned specimen I 80 9.3-28R.

Fig. 10. L-shaped sections at flange-web interface.

Table 6. Residual Stress Predictive Models for Welded I-Sections						
Predictive Model	**Peak Tensile Residual Stresses**	**Peak Compressive Residual Stresses**	***a***	***b***	***c***	***d***
ECCS (ECCS, 1984)	$1.0F_y$	$0.25F_y$	$0.05b_f$	$0.15b_f$	$0.075h$	$0.05h$
BSK 99 (Boverket, 2003)	$1.0F_y$	From equilibrium	$0.75t_f$	$1.5t_f$	$1.5t_w$	$1.5t_w$
Y. SUN (Sun, 2019)	$0.8F_y$	From equilibrium	$0.225b_f$	$0.15b_f$	$0.075h$	$0.225h$
Note: b_f = flange width, h = clear distance between flanges, t_w = web thickness, t_f = flange thickness						

Table 7. Peak and Average Residual Stress Values vs. Predictive Models									
	Web Compression Stress (ksi)			**Flange Compression Stress (ksi)**			**Flange Tensile Stress (ksi)**		
		Predicted Value			**Predicted Value**			**Predicted Value**	
Specimen	**Measured**	**ECCS**	**BSK 99**	**Measured**	**ECCS**	**BSK 99**	**Measured**	**ECCS**	**BSK 99**
I 80-5.3-32	21.2	20	21.8	11.9	20	21.7	61.9	80	80
I 80-9.3-28	16.6	20	11.9	11.1	20	11.3	51.9	80	80
I 80-10.7-21.3	9.2	20	9.5	18.3	20	9.5	74.7	80	80
I 80-10.7-32	8.9	20	9.9	19.4	20	9.5	71.2	80	80
I 80-4-24	12.3	20	31.0	9.6	20	31.2	14.5	80	80
I 50-10.7-32	13.0	12.5	6.0	11.9	12.5	6.2	54.2	50	50

predictive models by the ECCS (1984); the Swedish regulations BSK 99 (Boverket, 2003); and a proposed numerical model completed by Sun et al. (2019), called the Y.SUN model in this study. A summary of these three models can be found in Table 6. Each of these predictive models follow a residual stress distribution pattern that is presented in Figure 11.

Measured residual stress values for each of the six specimens are shown in Figure 12. Values in gray are the measured residual stress values prior to the excess web material
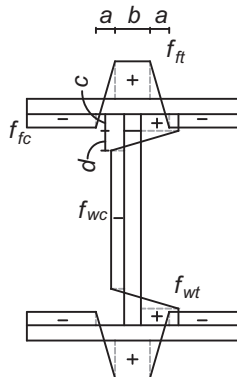
being removed from the flange test strips. The values in black are the measured values after removal. Table 7 presents key residual stress values for each specimen with a comparison to the corresponding values from the predictive models in Table 6. The tensile stress in the flanges is provided as a peak value, while the compressive stress values are taken as an average of all values recorded over the width of the flange or web.

Figure 13 presents the predictive model comparison results for specimen I80-10.7-21.3R. Overall, the compressive stresses in the flanges were most accurately predicted by the ECCS (1984) model, while the peak tensile stress in the flange was closest to the Y.SUN (Sun, 2019) model for the top flange, *F1*, and the ECCS and BSK 99 (Boverket, 2003) models for the bottom flange, *F2*. The transition zone slopes fall somewhere between the ECCS and BSK 99 models.

Figure 13(c) presents the results for the compressive residual stresses in the web of specimen I80-10.7-21.3. The stresses measured were fairly uniform along the full depth of the web, at a measured value of approximately 10 ksi (12.5% of nominal F_y). These stresses are most accurately predicted by the BSK 99 (Boverket, 2003) model. Due to the size of the strain gauge, measurements were unable to be taken close enough to the flange-web interface to measure results in the tensile stress region of the web, so no comparison can be made to the predictive models in that region. The results for specimens I80-10.7-32R and I50-10.7-32R closely
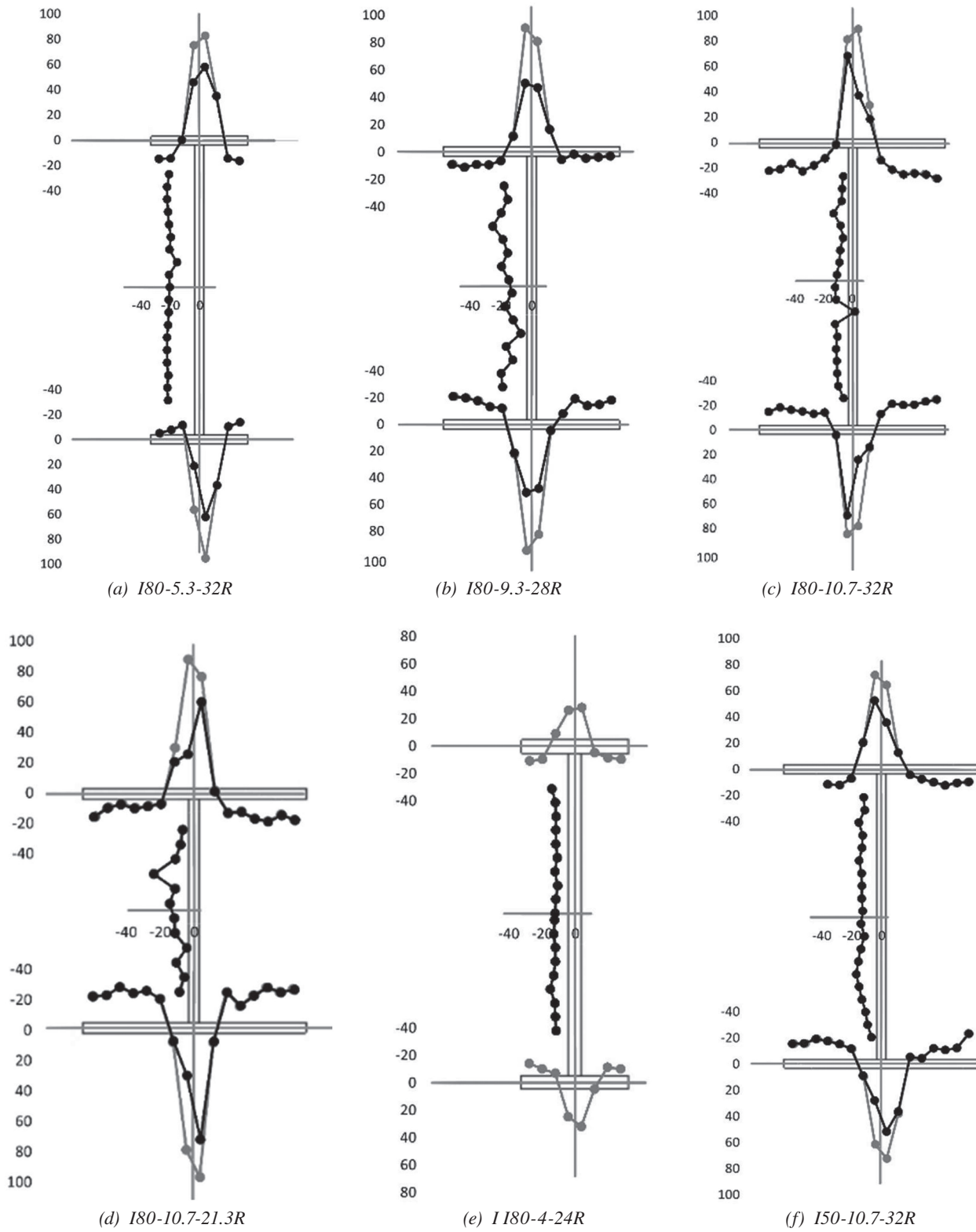
Fig. 11. General residual stress pattern for welded I-shaped sections (ECCS, 1984).

(a) I80-5.3-32R

(b) I80-9.3-28R

(c) I80-10.7-32R

(d) I80-10.7-21.3R

(e) I I80-4-24R

(f) I50-10.7-32R

Fig. 12. Residual stress measurements (all stress values are ksi).

match these presented results and are excluded for brevity. All other residual stress results not presented in this paper can be found in Clark (2022).

Figure 14 depicts the results and predictive model comparison for specimen I80-4-24R. This specimen is the only one that was fabricated with 0.5 in. thick flanges and web, and its results differ from the trends observed in the other specimens. Figures 14(a) and (b) show the results for the top (*F1*) and bottom (*F2*) flanges, respectively. The compressive stresses in the flanges are much lower than all three of the predictive models. The peak tensile stresses are significantly different from the models as well, with very little tensile stress recorded.

The web compressive stresses are shown in Figure 14(c). The compressive stresses in the web were uniform and were measured to be approximately 12 ksi, which is lower than all three of the predictive models. The closest match for the stresses in the web is the ECCS (1984) model; however, the measured values are about 50% lower than what this model predicts. These differences between the recorded values and predictive models for this specimen may be attributed to the very compact flange ($b/t = 4.0$). Differences may also be attributed to the production process for this plate, as the 0.5 in. plate was produced by a different manufacturer than the 0.375 in. plate. More testing is needed to understand this specimen's anomaly in results relative to the other test results.

Figure 15 shows the comparison of residual stresses between the I80-10.7-32R and I50-10.7-32R specimens. These two specimens are of equal dimensions and section properties, and the only difference between the two is the steel grade. Comparing these two specimens allows for a comparison between the 50 ksi and 80 ksi materials and their influence on residual stresses.

Figures 15(a) and (b) present the residual stresses in the top (*F1*) and bottom (*F2*) flanges, respectively. The maximum tensile stress in the flange for the 80 ksi section is approximately 70 ksi, or $0.875F_y$, while the maximum tensile stress in the 50 ksi section is 54 ksi, which is approximately equal to F_y. The average compressive stresses in the flanges are 20 ksi and 12 ksi for the 80 ksi and 50 ksi sections, respectively. These stresses equate to $0.25F_y$ for both materials. Figure 15(c) depicts the residual stresses in the web for the two sections. The average web compressive stress in the 80 ksi section is approximately 10 ksi ($0.125F_y$), and the average in the 50 ksi section is 13 ksi ($0.26F_y$).

A comparison of the residual stress values in each section shows that the flange compressive stresses increased proportionally to the increase in yield strength of the material. However, the maximum tensile stress in the flange and compressive stress in the web did not increase proportional to the increase in yield strength for the 80 ksi material. This comparison shows that the residual stresses among different material grades are generally not proportional to yield
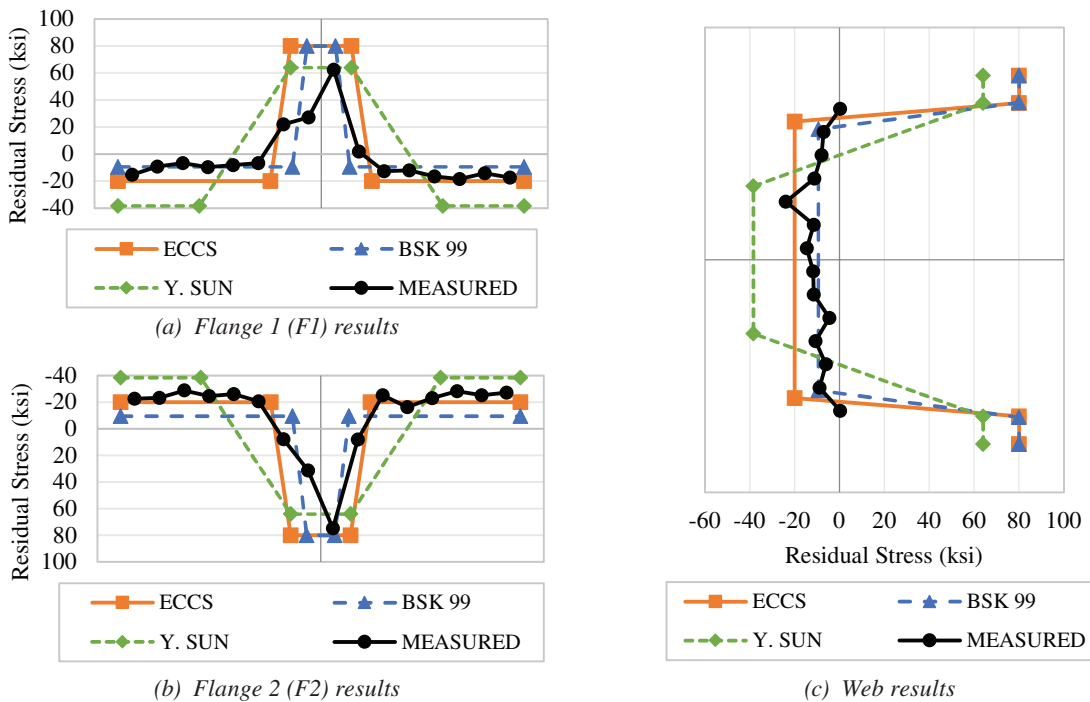

(a) Flange 1 (F1) results

(b) Flange 2 (F2) results

(c) Web results

Fig. 13. Specimen I80-10.7-21.3R residual stress predictive model comparison.

(a) Flange 1 (F1) results

(b) Flange 2 (F2) results

(c) Web results
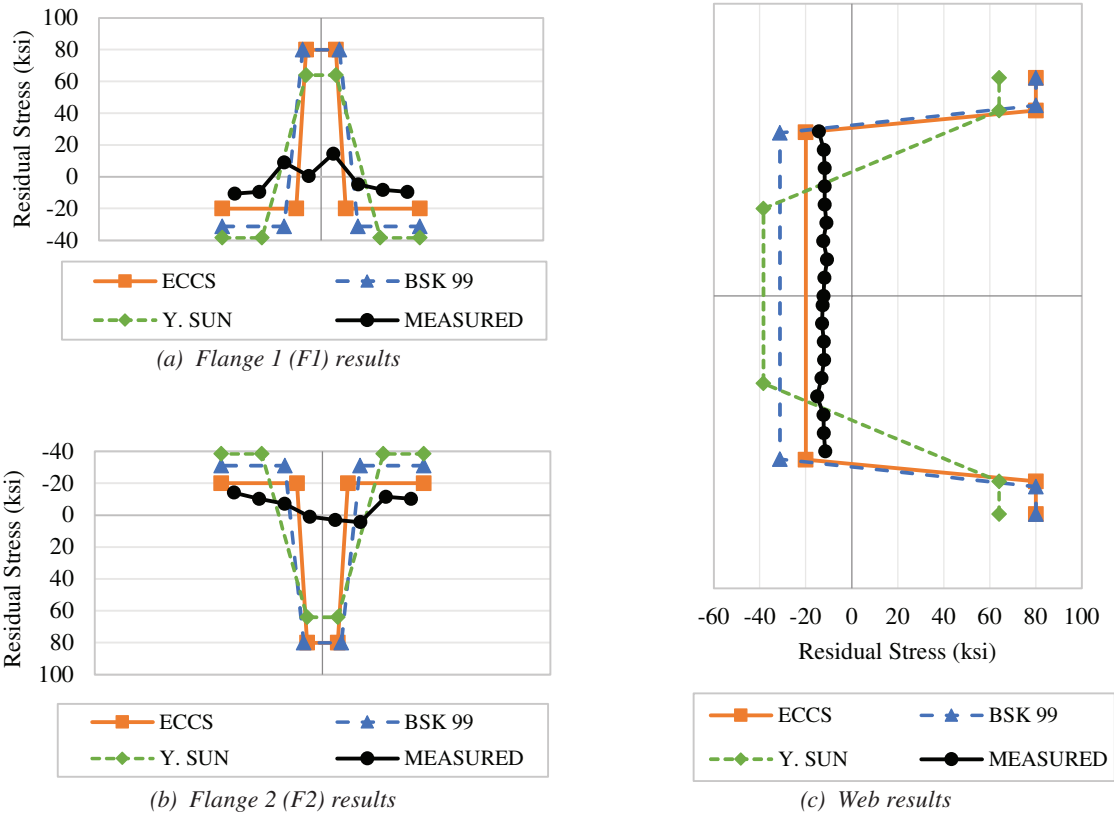
Fig. 14. Specimen I80-4-24R residual stress predictive model comparison.

(a) Flange 1 (F1) comparison

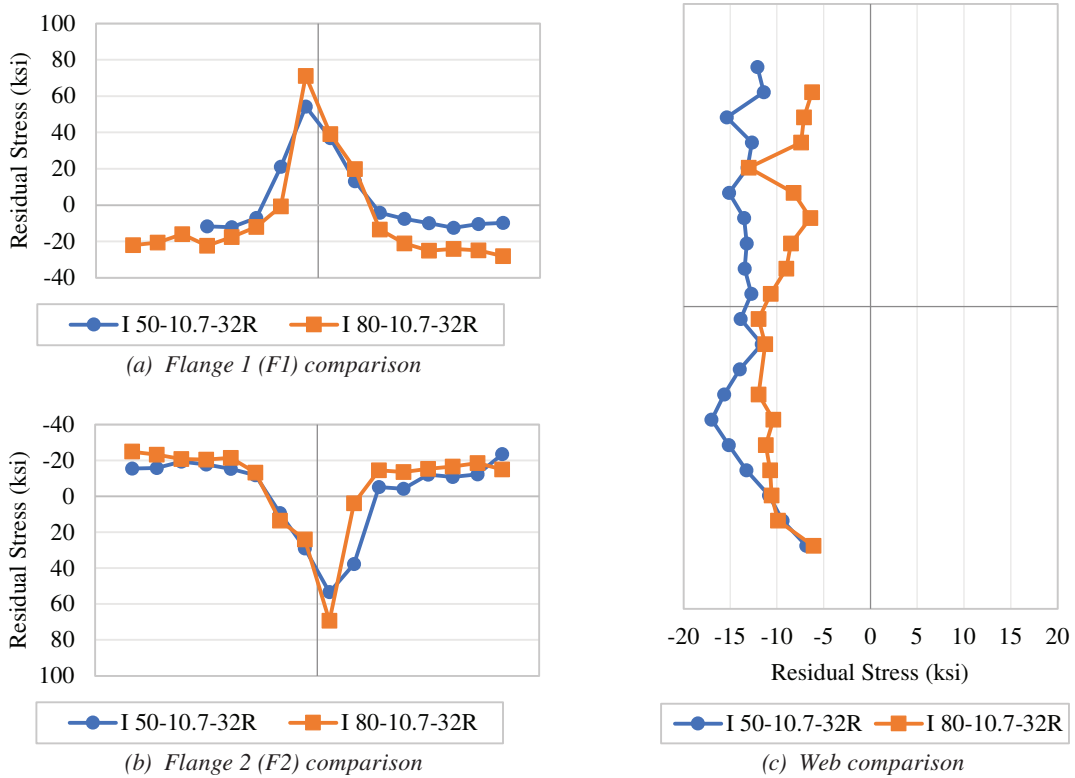(b) Flange 2 (F2) comparison

(c) Web comparison

Fig. 15. Specimen I80-10.7-32R and specimen I50-10.7-32R comparison.

stress, but are more influenced by cross-sectional geometry, as was determined in Schaper et al. (2022).

Results from this study found that the maximum tensile residual stress in the flanges was typically in the 0.75-1.0F_y range, for all specimens except I80-4-24R. The Schaper et al. (2022) study found, however, through a comparison of S460 (65 ksi) and S690 (100 ksi) steel, that the maximum tensile residual stress in the flanges was anywhere from 0.2-0.7F_y. It is worth noting that the specimens studied in the Schaper study were thermal cut, which resulted in tensile residual stresses at the flange tips and could be the cause of the reduced residual stresses at the flange/web interface.

SUMMARY AND CONCLUSIONS

Two different assessments were completed as part of this work using 50 and 80 ksi material—tensile coupon tests and residual stress measurements. Tensile coupon testing was performed on 48 dog bone coupons, and average stress-strain curves were generated for each of the plate materials and thicknesses. All coupons that were tested had a modulus of elasticity of approximately 29,000 ksi. The A572-50 material performed as expected with the curves for each plate thickness being almost identical, while the A656-80 material showed some unanticipated variation between the two thicknesses that can likely be attributed to their different material compositions and manufacturing process. The stress-strain curve for the A656-80 0.5 in. plate material showed almost no yield plateau and had a yield stress that was significantly lower than the A656-80 0.375 in. plate.

Six built-up I-sections underwent residual stress testing, and the results of these tests were compared to three previously published residual stress predictive models. Results showed that the ECCS model was the best predictor of residual stresses in the flanges of sections with larger b/t ratios ($b/t = 10.7$). The ECCS model also proved to be the best comparison for the 50 ksi material as well. For sections with slightly smaller b/t ratios ($b/t = 9.3$), the BSK99 model was the best predictor, while none of the models showed to be good predictors of sections with the smallest b/t ratios ($b/t = 5, 4.3$). A comparison of the Gr. 50 and Gr. 80 sections showed that residual stresses of built-up I-shapes are controlled more by cross-sectional geometry than by the nominal stress of the material.

Future Work

The specimens outlined in this work will be subjected to stub column testing in order to evaluate the cross-sectional slenderness limits and local buckling behavior of high-strength steel sections under compressive load. Additional residual stress studies using the 0.5 in. plate is warranted to understand the anomaly in results relative to the other test results. Further experimental testing and detailed analytical studies are needed for other material grades and larger cross sections to fully understand its behavior as compression members in buildings.

REFERENCES

AISC (2019), "Task Group Report on: High Strength Steel," prepared by the AISC Committee on Specifications Ad Hoc Task Group on High Strength Steel, December 19, American Institute of Steel Construction, Chicago, Ill.

AISC (2022), *Specification for Structural Steel Buildings*, ANSI/AISC 360-22, American Institute of Steel Construction, Chicago, Ill.

ArcelorMittal (2019), "High-Rise Building Brochure," ArcelorMittal Europe—Long Products, Sections and Merchant Bars, Luxembourg.

ASTM (2019), *Standard Specification for High-Strength Low-Alloy Steel Shapes of Structural Quality, Produced by Quenching and Self-Tempering Process (QST)*, ASTM A913/A913M, ASTM International, West Conshohocken, Pa.

ASTM (2020), *Standard Test Methods and Definitions for Mechanical Testing of Steel Products*, ASTM A370, ASTM International, West Conshohocken, Pa.

ASTM (2021), *Standard Specification for High-Strength Low-Alloy Columbium-Vanadium Structural Steel*, ASTM A572/A572M, ASTM International, West Conshohocken, Pa.

ASTM (2022), *Standard Specification for Structural Steel Shapes*, ASTM A992/A992M, ASTM International, West Conshohocken, Pa.

ASTM (2024), *Standard Specification for Hot-Rolled Structural Steel, High-Strength Low-Alloy Plate with Improved Formability*, ASTM A656/A656M, ASTM International, West Conshohocken, Pa.

Ban, H., Shi, G., Bai, Y., and Wang, Y. (2013), "Residual Stress of 460 MPa High Strength Steel Welded I Section: Experimental Investigation and Modeling," *International Journal of Steel Structures*, Vol. 13, No. 4, pp. 691–705.

Ban, H., Shi, G., Shi, Y., and Wang, Y. (2011), "Research Progress on the Mechanical Property of High Strength Structural Steels," *Advanced Materials Research*, Vol. 250–253, pp. 640−648. doi:10.4028/www.scientific.net/AMR.250-253.640

Beg, D. and Hladnik, L. (1996), "Slenderness Limit of Class 3 I Cross-Sections Made of High Strength Steel," *Journal of Constructional Steel Research*, Vol. 38, No. 3, pp. 201–217.

Boverket (2003), *Swedish Regulations for Steel Structures*, BSK 99, Boverket, Karlskrona, Sweden.

Clark, A. (2022), "Material Characterization of High Strength Structural Steel for Building Applications," MS Thesis, University of Cincinnati, Cincinnati, Ohio.

ECCS (1984), "Ultimate Limit State Calculation of Sway Frames with Rigid Joints," Technical Committee 8, Publication No. 33, European Convention for Constructional Steelwork, Brussels, Belgium.

Liu, X. (2017), "Structural Effects of Welding onto High Strength S690 Steel Plates and Welded Sections," PhD Thesis, Hong Kong Polytechnic University, Hong Kong.

NSC (2015), "High Strength Steel," Technical Paper, New Steel Construction, London, United Kingdom.

Rasmussen, K.J.R. and Hancock, G.J. (1995), "Tests of High Strength Steel Columns," *Journal of Constructional Steel Research*, Vol. 34, No. 1, pp. 27–52.

Sampath, K. (2006), "An Understanding of HSLA-65 Plate Steels," *Journal of Materials Engineering and Performance,* ASM International, Vol. 51, No. 1, pp. 32−40.

Schaper, L., Tankova, T., Simoes da Silva, L., and Knobloch, M. (2022), "A Novel Residual Stress Model for Welded I-Sections," *Journal of Constructional Steel Research*, Vol. 188.

Simoes da Silva, L., Tankova, T., and Rodrigues, F. (2021), "Research Report on the Results from the Experimental Programme on Members in HSS," STROnger Steels in the Built Environment (STROBE) Deliverable D3.1.

Sun, Y., Liang, Y., and Zhao, O. (2019), "Testing, Numerical Modelling and Design of S690 High Strength Steel Welded I-Section Stub Columns," *Journal of Constructional Steel Research*, Vol. 159, pp. 521–533.

Wang, K. (2018), "Study on Structural Behaviour of High Strength Steel S690 Welded H- and I-Sections," PhD Thesis, Hong Kong Polytechnic University, Hong Kong.

Wang, Y., Li, G., Chen, S., and Sun, F. (2012), "Experimental and Numerical Study on the Behavior of Axially Compressed High Strength Steel Columns with H-Section," *Engineering Structures*, Vol. 43, pp. 149−159.

Ziemian, R. (2010), *Guide to Stability Design Criteria for Metal Structures*, 6th Ed., Wiley, New York, N.Y.

Guide for Authors

Scope *Engineering Journal* is dedicated to the improvement and advancement of steel construction. Its pages are open to all who wish to report on new developments or techniques in steel design, research, the design and/or construction of new projects, steel fabrication methods, or new products of significance to the uses of steel in construction. Only original papers should be submitted.

General Papers intended for publication should be submitted by email Margaret Matthew, editor, at **matthew@aisc.org**.

The articles published in the *Engineering Journal* undergo peer review before publication for (1) originality of contribution; (2) technical value to the steel construction community; (3) proper credit to others working in the same area; (4) prior publication of the material; and (5) justification of the conclusion based on the report.

All papers within the scope outlined above will be reviewed by engineers selected from among AISC, industry, design firms, and universities. The standard review process includes outside review by an average of three reviewers, who are experts in their respective technical area, and volunteers in the program. Papers not accepted will not be returned to the author. Published papers become the property of the American Institute of Steel Construction and are protected by appropriate copyrights. No proofs will be sent to authors.

Manuscripts Manuscripts must be provided in Microsoft Word format. Include a PDF with your submittal so we may verify fonts, equations and figures. View our complete author guidelines at **aisc.org/ej**.